Icy moon plume simulator chamber

The design of a laboratory recreation of an icy moon plume

T.J. Becx

Delft University of Technology

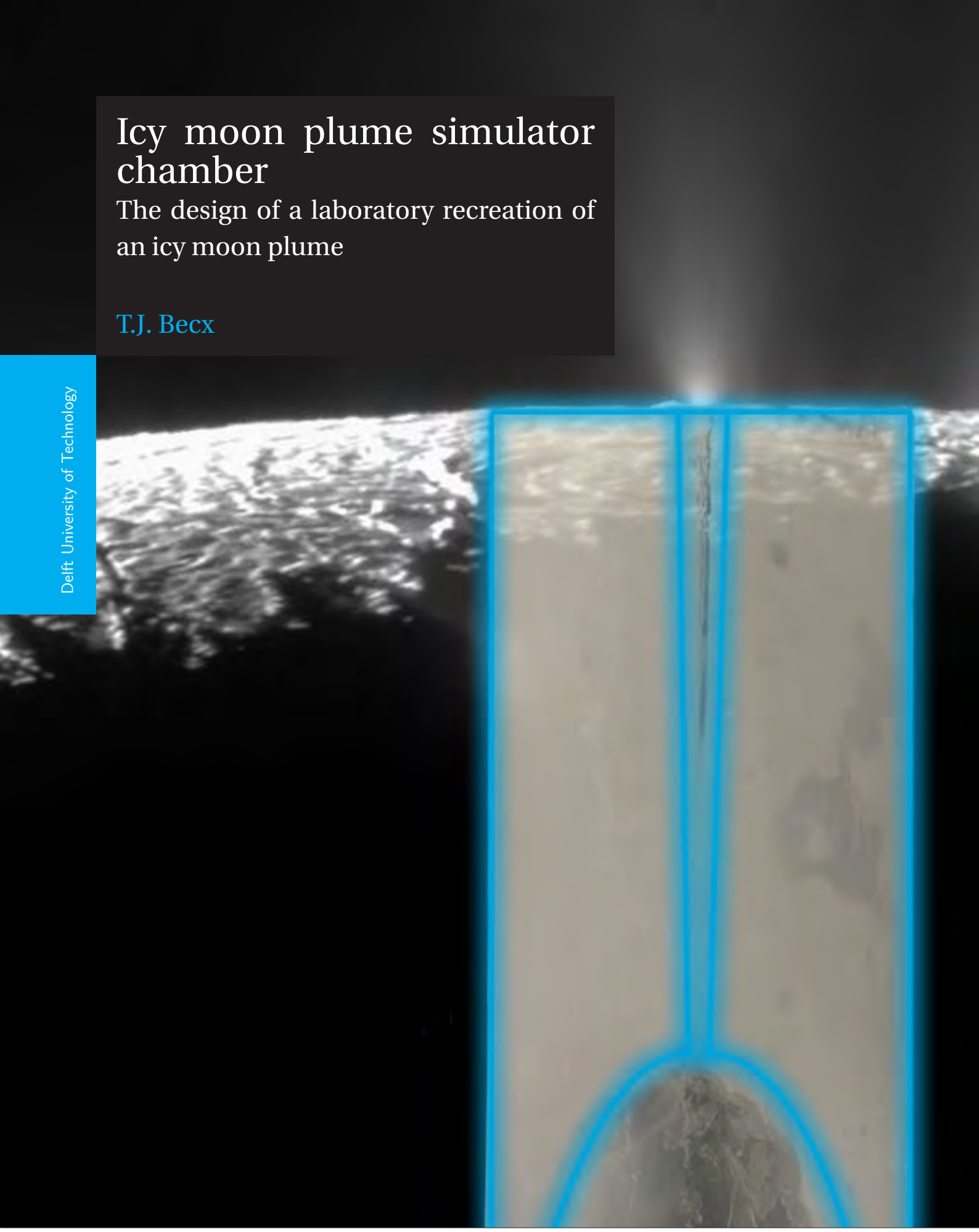

TU Delft Delft University of Technology

Challenge the future

ICY MOON PLUME SIMULATOR CHAMBER

THE DESIGN OF A LABORATORY RECREATION OF AN ICY MOON PLUME

by

T.J. Becx

in partial fulfilment of the requirements for the degree of

Master of Science
in Aerospace Engineering

at the Delft University of Technology,
to be defended publicly on Thursday Februari 21, 2019 at 17:00 PM.

Student number:	4062965	
Project duration:	June 26, 2018 – February 21, 2019	
Supervisor:	Dr. S. M. Cazaux	
Thesis committee:	Prof. dr. L. L. A. Vermeersen,	TU Delft
	Dr. ir. F. F. J. Schrijer,	TU Delft
	Dr. S. M. Cazaux,	TU Delft
	Prof. dr. ing. B. Dachwald,	FH Aachen
	F. Baader MSc.,	FH Aachen

This thesis is confidential and cannot be made public until February 21, 2019.

TU Delft Delft University of Technology

ACKNOWLEDGEMENTS

This is the Master Thesis report by T.J. Becx for the Masters Degree in Space Flight of Delft University of Technology. This master thesis has been performed from April 23rd to Februari 25th 2019 which includes a separate literature study report.

I would like to express my gratitude to my thesis supervisor Stéphanie Cazaux for making this master thesis possible. Special thanks also to Ferdinand Schrijer, Bert Vermeersen, Marc Rovira Navarro, François Dulieu, Hans Huybrighs, Frank Postberg, Fabian Baader and Bernd Dachwald for answering questions that arose during the study.

I would also like to thank the Aerospace Department and the DEMO department of the Delft University of Technology for their input, assistance and letting me use their facilities.

Further, I would like to thank Michael Manga (University of California, Berkeley), Atsushi Toramaru (Kyushu University, Higashiku), Atsuko Namiki (Hiroshima University, Higashi Hiroshima), Miki Nakajima (University of Rochester, Rochester New York) and Juergen Schmidt (University of Oulu, Finland) for permitting me to use figures from their published work in my thesis.

And finally I would like to thank my parents. They have always seen in me the potential to be an Aerospace Engineer even at times when I did not.

T.J. Becx, Faculty of Aerospace Engineering, Delft University of Technology, The Netherlands
February 5, 2019

ABSTRACT

In 2005 Cassini discovered plumes erupting from the surface of Saturn's moon Enceladus. In 2012 the Hubble Space Telescope took images of evidence of the existence of plumes erupting from the surface of Jupiter's moon Europa. Both these moons have an icy moon classification which means that both moons have a surface that is completely made out of ice. Below both surfaces there is a global liquid ocean consisting out of water and several trace elements. Most data on these plumes came from a combination of observations and computer simulations. It has not yet been attempted to recreate such an icy moon plume in a laboratory. Such a real-life recreation can assist in testing the current hypotheses on the mechanisms of icy moon plumes. But also assist in research on the content of the subsurface oceans by reverse engineering measurements of plume exhausts. Are the current hypotheses on the plume mechanism correct? What is the relation between the ocean and the plume? And what is the relation between the ice sheet and the plueme? This study proposes a design for a set-up that will make it possible to recreate an icy moon plume in a laboratory and perform these experiments. Since Cassini provided a lot more information on the Enceladus plumes than there is on Europa's plumes, Enceladus is taken as basis for this study.

Enceladus is a moon with a diameter of approximately 500 kilometer and due to its position and orbit around Saturn, it experiences tidal heating. This allows for enough heat to keep a liquid ocean below the frozen surface. At the south pole, the ice sheet is only a few kilometers thick. The south pole is covered with long rectangular cracks dubbed 'Tiger Stripes' where plumes are emanating from. Cassini measured mostly pure water coming from the plumes with small concentrations of ammonia and sodium-chloride (among various other trace elements). The velocity of the plumes are estimated to be supersonic and even hypersonic speeds and expel several tens of kilograms of vapour per second. According to computer simulations, those speeds and mass flows are best achieved if the cracks in the ice leading from the ocean to the surface have a rectangular supersonic converging-diverging nozzle like structure with a thin width and several kilometers in length. Next to the vapour in the exhaust, also grains and traces of organic molecules are detected. Since the grains have slower speeds than the vapour, they are most likely formed in the channel. And the organic molecules are most likely transported via gas bubbles rising from the ocean where they reside in a thin organic film on top of the ocean.

There are several mechanisms that could form a plume of which a crack in the ice sheet leading all the way to the ocean is the most likely one. The low pressures boil the exposed ocean whereafter the generated vapour is expelled through the crack in the ice (or crevasse). The design of a laboratory set-up requires a relation between the boiling ocean and the channel in the ice. The supersonic converging diverging nozzle structure involves a throat (smallest opening area) above the ocean leading to a wider surface opening (or vent). The ratio between this throat and vent areas determine the exhaust velocity. To get supersonic (or higher) speeds, the velocity at the throat must be Mach 1. A Mach 1 velocity requires a certain mass flow. This mass flow needs to be equal to the vapour mass flow that is generated by the boiling ocean. Combining Hertz, Knudsen and Langmuir evaporation with aerodynamic nozzle principles provides this needed relation that makes it possible to design the geometry of the set-up. This was combined in a model that has a design Mach number and vacuum chamber size as inputs and the geometry of the ice channel (throat and vent areas) as output.

This design requires a liquid ocean. The lowest temperature and pressure at which pure water can remain liquid is the triple point of water at $0.01°C$ and $612\ Pa$. At this point water can exist in the liquid, gas and ice phase at the same time. This is taken as a starting point for the design. The presence of small concentrations of ammonia and sodium-chloride in the water influences this minimum temperature and pressure. Both ammonia and sodium-chloride reduce the freezing temperature of pure water making it possible to have a liquid ocean below the freezing temperature of pure water. Though from experiments done in this study, combined with literature, it was found that the influence is small enough to not play a factor on the dimensions of the design. The design is therefore based on the characteristics of pure water. But, since this influence of ammonia and sodium-chloride on the design is small, it can also be used for ammonia and sodium-chloride oceans and ices.

The FH Aachen University of Applied Sciences expressed interrest in building this set-up for an icy moon plume with the equipement they have available. This set some boundaries for the design of the set-up such as the minimum achievable pressure and the size. It is also required that the set-up is easily removable to free the vacuum chamber for other experiments.
For this study a smaller version (one-third the size of the Aachen version) of the set-up was constructed at Delft University of Technology with the equipement available there to test the validity of the design and to tackle possible practical issues. The dimensions of the model were derived by downsizing what could be made at Aachen. The established model generated the geometry which was used to 3D print the mould parts. Those mould parts were placed in a tube and water was poured around it and then frozen. When the ice was formed, the mould parts were removed leaving an ice block with openings for the ocean (water reservoir) and channel (crevasse). The ice shape was placed in a see-through tube and closed with a cap at the bottom, the reservoir was filled with a layer of liquid water and temperature and pressure sensors were connected to the reservoir and vent locations. The entire set-up was then placed inside a vacuum chamber and the pressure was reduced. When the pressure was low enough the water started to boil starting the plume mechanism. But since the physical process of boiling takes away energy from the liquid, the water reservoir froze a few seconds after the triple point was reached. A redesigned version of the experiment included a heater in the cap below the water reservoir keeping the temperature of the water just above freezing so the plume could be maintained until all the water was boiled away. The equipement available in Delft was unable to lower the pressure in the vacuum chamber to the pressure needed to start a supersonic plume. The plume that was generated with the smaller version of the model was therefore subsonic.
The final design for Aachen is based on the same model that designed the small Delft model. But it also includes redesigned parts based on the practical knowledge gained from the small Delft model experiments. The use of a non-conducting material for the moulds made it difficult to remove the parts from the ice. Therefore, for the larger design it is proposed to use a conducting material that can be flash heated, melting the outer layer of the ice so the moulds can be removed more easily. The heating element will be placed in the reservoir instead of underneath it for more efficient heating. The thickness of the ice is doubled to prevent breaking. The height ratio of the channel and reservoir and the throat-vent ratio are kept the same, though the mould parts are modular and multiple mould parts can be interchanged to create multiple versions of the experiment.
Taking into account the need for metal mould parts, sensors and heater, the one time expenses to build the set-up for Aachen are ranging from €7000 to €15000 depending on the method of construction and volume. The operating costs per experiment run are expected to be around €345.

Though the smaller version of the model was not able to generate a supersonic plume, it did serve as a proof of concept. With a stronger pump it should technically be possible to generate a supersonic plume. With this set-up it should be possible to prove the current hypotheses on the plume mechanism. In the future, this set-up can answer more questions on plumes and icy moons by reverse engineering the measurements taken by Cassini on plume content such as elements, organic molecules and grains. But with some slight adaptions it can also be used to test other mechanisms for plumes by varying the length of the channel, the volume of the reservoir or even removing the reservoir all together and see if a plume can form without a liquid ocean. It can even serve as a testing facility for future landers.

Contents

List of Acronyms

Acronym	Description
CAPS	CAssini's Plasma Spectrometer
CDA	Cosmic Dust Analyser
CIRS	Cassini?s Composite Infrared Spectrometer
DSMC	Direct Simulation Monte Carlo
ESA	European Space Agency
FORMOLISM	FORmation of MOLecules in the InterStellar Medium
HST	Hubble Space Telescope
IMF	Interplanetary Magnetic Field
INMS	Ion and Neutral Mass Spectrometer
IRAM	Instituto de Radioastronomie Milimetrica
JPL	Jet Propulsion Laboratory
JUICE	JUpiter ICy moons Explorer
ML	MonoLayer
NASA	National Aeronautic and Space Administration
PID	Proportional-Integral-Derivative
QMS	Quadrupole Mass Spectrometer
RAIRS	Reflection Absorption InfraRed Spectroscopy
RPWS	Radio and Plasma Wave Science
US	United States (of America)
UVIS	UltraViolet Imaging Spectrograph
VIMS	Visible and Infrared Mapping Spectrometer

List of Symbols

Symbol	Description	Unit
α	Sticking coefficient	$[-]$
A	Area	$[m^2]$
a	Speed of sound	$[m/s]$
B	Magnetic field strength	$[T]$
c_p	Specific heat at constant pressure	$[J/kg/K]$
c_v	Specific heat at constant volume	$[J/kg/K]$
δ	Crack width	$[m]$
D	Crack depth*	$[m]$
D	Diameter*	$[m]$
E	Energy	$[eV]$
F	Force	$[N]$
γ	Specific heat ratio	$[-]$
I	Irradiance	$[W/m^2]$
L	Length	$[m]$
M	Mach number**	$[-]$
$\dot{m}$	Mass flow	$[kg/s]$
M_{molar}	Molar mass	$[kg/mole]$
N_A	Avogadro's number	$[mole^{-1}]$
N	Number of molecules	$[-]$
n	Number densities	$[m^{-3}]$
P	Pressure***	$[Pa]$ or $[bar]$
R_{sp}	Specific gas constant	$[J/kg/K]$
R	Universal gas constant	$[J/mole/K]$
r	Radius	$[m]$
ρ	Density	$[kg/m^3]$
s	Distance	$[m]$
T	Temperature****	$[K]$ or $[^\circ C]$
t	Time	$[s]$
U	Horizontal velocity	$[m/s]$
V	Velocity	$[m/s]$
v	Volume	$[m^3]$
W	Weight	$[kg]$

* *The symbol for Crack depth used in Nakajima and Ingersoll [1] and Diameter used in Yeoh* et al. *[2] are the same. This was unavoidable when citing these sources.*

** *The symbol for Mach number used in Yeoh* et al. *[2] is* Ma.

*** Pa *is used throughout this study as the standard unit for pressure while* bar *is used mostly in sources with* $1.00bar = 100,000Pa$.

**** *Both* K *and* $^\circ C$ *are used as temperature units when convenient with* $0.00^\circ C = 273.15K$.

List of Figures

List of Tables

1

INTRODUCTION

When Galileo Galilei discovered Jupiter's moon Europa in 1610 and William Herschel discovered Saturn's moon Enceladus in 1789, they could not have known how different those moon were from Earth's moon and what interesting phenomena they house. The surface is completely covered in ice giving them the name: 'icy moons'. Tidal heating due to the presence of their large parent gas giants allows both Europa and Enceladus to have liquid oceans below their frozen ice shells [13]. When Cassini flew by Enceladus in 2005 it was discovered that large volumes of water vapour and various trace elements were being shot in space from the ocean through the surface. This phenomena is called 'cryovolcanism' or simply 'plume'. Cassini's fly-by's and even fly-throughs provided a lot of data on this phenomenon [15]. The Hubble Space Telescope (HST) observed similar plumes in 2012 on Europa but without any direct measurements from flyby's, the data on Europa's plumes is limited [16].
The current knowledge of icy-moon plumes has come from measurements done by Cassini's during its flybys of Enceladus, observations of Europa and computer simulations. There have not been any real life laboratory recreations of the plumes. Such laboratory recreations could give insights in the mechanism of icy moon plumes that computer simulations cannot. A plume laboratory recreation could also assist in proving and expanding on current hypotheses on grain growth, ocean environment and organic material or serve as a testing ground for future landers. At the time of writing there are only two icy moons which are known to have plumes with reasonable certainty. But of those two moons, there is a lot more data on Enceladus' plumes compared to Europa, which is mostly due to Cassini. Therefore, the icy moon plume simulator design proposed in this study will be based mostly on Enceladus' plume mechanism. Europa's plume mechanism is expected to be similar, but the chemical composition of the ocean, ices and possible plumes might vary from Enceladus. The FH Aachen University of applied sciences expressed interest in a design for a laboratory set-up of an icy moon plume experiment for the facilities they currently have. *The research objective of this study is to provide a means of testing current icy moon plume hypotheses and future landers by designing a real life icy moon laboratory set-up specified for the facilities of the FH Aachen University of applied sciences.* There are several largely unanswered questions resulting from this that will be solvable with the proposed design in this study.

Do the current hypotheses on the plume mechanism explain the observations of Enceladus? This is the big question that this study attempts to solve by proposing a set-up for a laboratory version of the Enceladus plume.

What is the relation between plume and ocean? Cassini observed the plume content and discovered various elements in the vapour and even traces of large organic molecules. What do these plume observations say about the content of Enceladus' ocean? With a laboratory plume model like the one designed in this study, this might be reverse-engineered.

What is the relation between plume and ice wall? Cassini also detected the presence of grains in the plume. And both vapour and grains were expelled at different velocities. What does this say about the geometry of the ice channel walls? With the design proposed in this study this might be investigated in the future.

Can a plume only be created with a liquid ocean or can it form without an ocean? It is widely accepted that the plumes on Enceladus are formed by a direct connection between the surface and the subsurface ocean. But would it be possible to create such a plume without a liquid reservoir?

How long can a plume be sustained? Will plumes remain active for long periods of time? Or will the crevasses close up due to accretion of plume material on the channel walls? Letting the experiment designed in this study run for long periods of time and comparing the channel geometries before and after a run may give an indication of the longevity of plumes.

Not all these questions will be immediately solved in this study, but this study will propose a design for a set-up that will enable experimental research into these questions. To enable the design of such a set-up a few elementary questions will need answering. All the following practical questions are solved in this study and their answers form the basis for the proposed laboratory set-up.

What is known about plume mechanisms? What is known already from Cassini's observations and computer simulations?

Which mechanism will drive the design of this study? Which of the hypotheses on the plume mechanism proposed by the computer simulations of the previous question will drive this study?

Which facilities are available at the FH Aachen University of applied sciences? To make the design as cost efficient as possible, as much of the already present equipement as possible will be re-used for this set-up. What are the limitations of the equipement?

What should be the initial conditions of the design? What environmental conditions are expected on- and in Enceladus? What are the temperatures and pressures of the ocean and ice? What is the content of the ocean and ice?

What should be the geometry of the design based on the initial conditions? What is the lay-out needed for the mechanism to work? What is the influence of the temperatures, pressures and content of the ocean and ice on the design?

What is the final design proposed for the FH Aachen University of applied sciences? Based on all of the previous questions and some small scale testing done at Delft University of Technology, what will be the final design? What are the costs?

To answer these questions, this study is divided into several chapters. The background information on Enceladus and its plumes is given in Chapter 2. Chapter 3 explores some comparable laboratory experiments of which elements can be used in the design of this study. Chapter 4 gives restrictions to the design based on the available equipement and proposes a preliminary idea of what a feasible laboratory set-up of an icy moon plume could look like. Chapter 5 dives into the ocean content of Enceladus and explores the impacts of certain volatiles and salts on the design boundaries. This includes experimental parts. Chapter 6 sets up a relation between ocean evaporation rate and exhaust velocity which serves as a physical principle for the design of the laboratory icy-moon plume simulation set-up. This also includes an experimental part. Chapter 7 finally proposes a design for the icy-moon plume simulator based on the previous chapters. Chapter 8 estimates the costs of such an experimental set-up. Chapter 9 verifies all the calculations on which the model that drives the design is based and validates the whole design. Chapter 10 explores a few practical applications of this design and includes recommendations for future experiments. Chapter 11 concludes this study.

2

THE ICY MOON

To be able to recreate the Enceladus plume in a laboratory, the environmental conditions in which the Enceladus plumes reside and that allow for the plumes to form have to be recreated. Section 2.1 investigates the global structure of Enceladus including its core, ocean, surface and exosphere. Section 2.2 summarises what is known about the plumes from observations and computer models.

2.1. STRUCTURE

Enceladus has a fully differentiated inner structure. This means that Enceladus is comprised of separate layers that are made up of different materials. The denser the material, the closer they sink to the core [13]. Enceladus consists most likely of three separate layers, a silicate core, a liquid ocean and an ice surface. Based on the density of the moon, Enceladus most likely has a rocky core comprised of hydrated silicates. Those silicates were detected in Enceladus' plume [20]. The core has an estimated radius of 180 to 185 km [21] [22]. The fact that the silicates were detected in the plume also means that there is a direct contact between Enceladus' ocean and its core without a layer of ice in between. The content of Enceladus' ocean is easier to determine than for other icy moons since Enceladus' plume content was measured by Cassini's Ion and Neutral Mass Spectrometer (INMS). The ocean composition consists mostly of H_2O, a smaller amount of CO_2 and various trace elements such as Ar, CO, NH_3, N_2 CH_4 and many more. The full list is shown in Table 2.1. One of these trace elements, ammonia (NH_3), will server as an antifreeze allowing the ocean to remain liquid with lower temperatures [14]. The estimated concentration of ammonia in Enceladus' ocean has a range of 0.8% to 4.8% of which the lower concentrations are favoured [14] [12]. The ocean layer of Enceladus is estimated to be 34 to 42 km on average, but this can vary more at locations where the ice shell is very thin [21] [22].

Table 2.1: INMS measurements of Enceladus plume content measured on 09-10-2008. Data obtained from [14].

Molecule	Volume mixing ratio
H_2O	0.90 ± 0.01
CO_2	0.053 ± 0.001
H_2CO	$(3.1 \pm 1) \cdot 10^{-3}$
CH_3OH	$(1.5 \pm 0.6) \cdot 10^{-4}$
C_2H_4O	$< 7.0 \cdot 10^{-4}$
C_2H_6O	$< 3.0 \cdot 10^{-4}$
H_2S	$(2.1 \pm 1) \cdot 10^{-5}$
^{40}Ar	$(3.1 \pm 0.3) \cdot 10^{-4}$
NH_3	$(8.2 \pm 0.2) \cdot 10^{-3}$
N_2	< 0.011
HCN	$< 7.4 \cdot 10^{-3}$
CH_4	$(9.1 \pm 0.5) \cdot 10^{-3}$
C_2H_2	$(3.3 \pm 2) \cdot 10^{-3}$
C_2H_4	< 0.012
C_2H_6	$< 1.7 \cdot 10^{-3}$
C_3H_4	$< 1.1 \cdot 10^{-4}$
C_3H_6	$(1.4 \pm 0.3) \cdot 10^{-3}$
C_3H_8	$< 1.4 \cdot 10^{-3}$
C_4H_2	$(3.7 \pm 0.8) \cdot 10^{-5}$
C_4H_4	$(1.5 \pm 0.6) \cdot 10^{-5}$
C_4H_6	$(5.7 \pm 3) \cdot 10^{-5}$
C_4H_8	$(2.3 \pm 0.3) \cdot 10^{-4}$
C_4H_{10}	$< 7.2 \cdot 10^{-4}$
C_5H_6	$< 2.7 \cdot 10^{-6}$
C_5H_{12}	$< 6.2 \cdot 10^{-5}$
C_6H_6	$(8.1 \pm 1) \cdot 10^{-5}$

Ground based telescope observations by the Lowell Observatory have indicated partially crystalline water (H_2O) ice on the surface of Enceladus and very small absorption lines indicating ammonia (NH_3). The small NH_3 absorption lines account for global 2% ammonia deposits on the surface [23] [24]. Later observations done by Cassini's Visible and Infrared Mapping Spectrometer (VIMS) point out that the surface of Enceladus is mostly covered by crystalline water ice [23]. The most abundant ice on the Enceladus surface is type I hexagonal crystalline (I_h) ice, but there are small variations detected that indicate the presence of smaller quantities of other ice types [24]. Type I_h ice is the most common form of type I ice in which the lattice has an hexagonal form (see Figure 2.1 for the different ice type latices). The other form of type I ice has a cubic lattice (type I_c) which had a diamond form and is produced at temperatures ranging between 130 and 220 K. It can be kept stable to 240 K before transforming to hexagonal type I_h [25]. Other ice types that can be expected on icy moons are type III, type V and type VI crystallised ice. These ice types can exist around the triple point temperature but at differente pressures [26]. Type III tetragonal crystalline ice can be formed by cooling down water at 300 MPa to 250 K and is denser than liquid water. Type V ice is formed by cooling down liquid water at 500 MPa to 253 K. Type VI ice is formed by cooling down liquid water at 1.1 GPa to 270 K [25]. The visual observations of the Enceladus surface show that amorphous ice is also present which is formed when water vapour is deposited at temperatures below 100 K. Looking only at the south pole, crystallised ice is present in the tiger stripes while amorphous ice dominates the regions outside the tiger stripes. When this amorphous ice's temperature is increased to about 150 K the ice crystallises. This proces can take as short as minutes to only hours [23]. The other way around, crystalline ice can convert to amorphous ice when bombarded with highly energetic particles from the radiation belt in which Enceladus resides at temperatures below 100 K [27]. Due to the high reflectivity of Enceladus' surface, the surface temperature can be as low as 75 K [28]. On the other hand, Enceladus is internally heated due to tidal friction. The closer a body is to its parent, the stronger the gravitational pull is. A spherical satellite will form tidal bulges in de direction of the parent

planet and since the bodies are not completely rigid, they can change in shape. Since Enceladus' eccentricity is non-zero, the distance between Saturnus and Enceladus varies along its orbit which causes variations in the gravitational attractions. Variations in these so called tidal forces (and thus the shapes of the bodies) lead to internal heating of Enceladus. This internal heating is one of the possible mechanisms that allow for liquid oceans below the iced surface of to exist [13]. Taking into account the radiation belt in which Enceladus is located, the low estimated surface temperature and the fact that Enceladus is geologically active, the exact origin of the different ice types is difficult to predict. The ice at the surface is expected to have a density of 925 kg/m^3 and is expected to be 18 to 22 km thick on average. The ice shell is thickest around the equator and drops to 5 km around the south pole [22]. The outer radii of the ice surface of Enceladus are 257 x 251 x 248 km[1] which are respectively the equatorial radius, the equatorial radius and the polar radius.

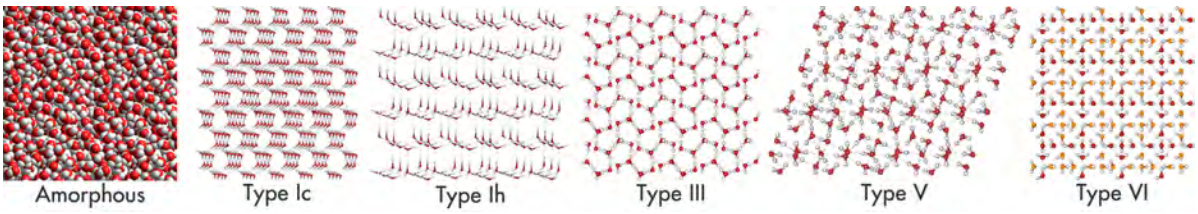

Figure 2.1: Crystalline structure of type I_c, I_h, III, V, VI and amorphous ices. (Images credits M. Chaplin distributed under a CC BY-SA 2.0 license)

As explained above, the temperature of the ice surface is observed and having a liquid ocean sets restrictions on the temperature of the ocean. But the exact temperature gradient of the ice layer is not known in great detail. Roberts and Nimmo [3] modelled the temperature gradient ranging from 75 K on the surface and 273 K at the ocean based on convection heating (circulating currents in the ocean) and shear heating (friction between moving ice sheets). The results are shown in Figure 2.2 in which $T' = 0$ corresponds to $T = 75\ K$ and $T' = 1$ corresponds to $T = 273\ K$. It can be seen that while the most part of the ice shell has a gradual temperature transition from the ocean to the surface, the ice at the south pole remains close to 273 K and only the very outer layer of ice drops to 75 K.

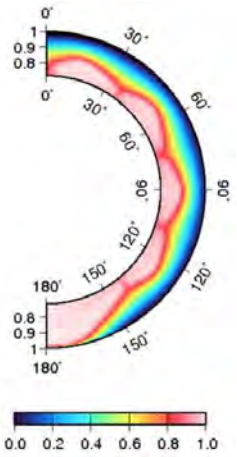

Figure 2.2: Internal temperature gradient of Enceladus' ice shell including convection and shear heating. T'=0 corresponds to T=75 K and T'=1 corresponds to T=273 K (Image taken from Roberts and Nimmo [3])

The exosphere of Enceladus has a surface pressure ranging between 10^{-10} and 10^{-13} bar [29]. Since the moon is relatively small, it does not generate enough gravity to possess an exosphere for very long before it dissipates [29]. The exosphere is therefore be assumed to be resupplied by a continuous source which in the case of Enceladus is its plumes (see Chapter 2.2). The content of the exosphere of Enceladus was therefore assumed to be comparable to the content of the plumes with H_2O, CO_2, CH_4 and other trace elements as shown in Table 2.1. However, the content of Enceladus' exosphere is not exactly the same as the content of the plumes. Observations made at Instituto de Radioastronomie Milimetrica (IRAM) indicated the presence of methanol

[1] https://nssdc.gsfc.nasa.gov/planetary/factsheet/saturniansatfact.html, last checked on 08-09-2018

(CH_3OH) in Enceladus' orbit. The presence of methanol in the Enceladus orbit is much higher than the presence around the Enceladus plume vents. This lead to the conclusion that methanol is a byproduct of chemical interactions occurring outside of Enceladus' plumes [30]. The structure of Enceladus is summarised in Table 2.2 and Figure 2.3. Due to the lack of precise data of the interior structure, it is here assumed here that the silicate core is a perfect sphere and the ocean is a perfect ellipsoid. The plumes, which are discussed in Section 2.2 are already included in this figure at the southern pole.

Table 2.2: Sizes of the structure of Enceladus (the varying significant digits are due to the varying precision of the available data and models)

Silicate core radius [km]	182.5 ± 2.5
Ocean thickness [km]	38 ± 4
Ice-shell thickness [km]	20 ± 2 x 5
Outer radius [km]	257 x 251 x 248

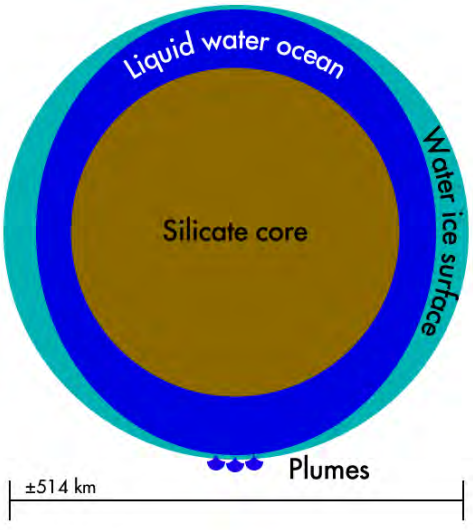

Figure 2.3: Structure Enceladus to scale (except for the size of the plumes).

2.2. PLUMES

On July 14th 2005 Cassini flew over Enceladus within 175 km from its surface. The Ion and Neutral Mass Spectrometer (INMS) on board detected a plume of mostly water with a few trace elements emanating from the southern pole [29] [31]. The exact content is listed in Table 2.1 of Section 2.1. Due to the distinct striped pattern of that region of Enceladus' surface, the area at the south pole where the plumes originate got dubbed the Tiger Stripes (see bottom left of Figure 2.4 A). Cassini's Composite Infrared Spectrometer (CIRS) measured an increase in temperature when flying over one of those stripes (see Figure 2.4 B). The mean surface temperature of Enceladus is around 70 K, whereas the measured temperatures directly above one of the plume vents are more than 145 K [15]. Figure 2.4 C shows a photograph taken by Cassini in which the sun lights up the plumes, making them clearly visible.

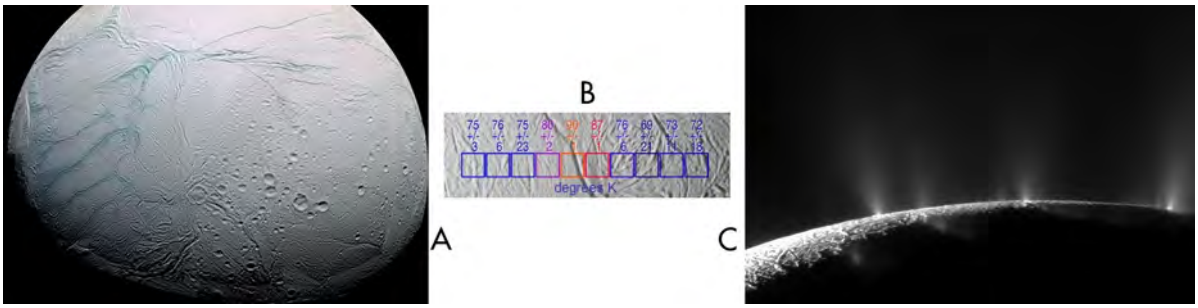

Figure 2.4: A: the Tiger Stripes on Enceladus' southern pole (bottom left corner). B: the increased temperature measurement over a Tiger Stripe. C: a photograph taken by Cassini where the sun lights up Enceladus' plumes. (all three image credits: NASA/JPL)

2.2.1. EXHAUST

Tian *et al.* [32] esitmated an exhaust velocity from Enceladus' Tiger Stripes in the range of 300 to 500 m/s in 2007. These velocities are around the sonic conditions. A few years later this velocity was expected to be higher, within the supersonic region. Dong *et al.* [33] expected an exhaust velocity of 550 to 750 m/s. The most recent models of Schmidt *et al.* [6], Tucker *et al.* [34], Yeoh *et al.* [2], Yeoh *et al.* [5] estimate even higher velocities (in the supersonic to hypersonic regions) of 780 to 902 m/s. There are also variations in the reported mass flow rate of the ejected vapour from Enceladus's plumes. Tian *et al.* [32] estimates a mass flow rate of 120 to 180 kg/s whereas Saur *et al.* [35] mentions a mass flow rate of 200 to 1600 kg/s. Nakajima and Ingersoll [1] uses an intermediate mass flow rate of 200 kg/s as aim for their model.

2.2.2. COMPUTER MODELS

Since the discovery of the plumes there have been several analytical and computational models describing the observed characteristics of Enceladus' cold water geysers. In these models, it is generally assumed that the temperature and pressure of Enceladus' ocean is around the triple point of water. The triple point of water is the combination of temperature and pressure where water can exist in its frozen phase, in its liquid phase and in its gas phase. This is a logical assumption since at the bottom of a crack in the ice, water and vapour are all present. For pure H_2O water the temperature is 273.16 K (or 0.01°C) and the pressure is 611.657 Pa (or about 6 $mbar$) [25]. The presence of salts in the ocean of Enceladus will change this triple point so that water will remain liquid at lower temperatures (like the low percentage of ammonia as mentioned in Chapter 2). This is not been incorporated into the models described here as they assume the triple point of pure H_2O water. In 2016 Nakajima and Ingersoll [1] proposed a crack in the ice of uniform width that extends from the surface to the subsurface ocean, which is several kilometers deep (modelled here between 1.7 to 3.2 km). They found that a crack width of 0.05 to 0.075 m wide and 850 km in length explains the observed mass flow rate due to evaporation at the triple point. Figure 2.5 shows the schematic view of their uniform crack width model in which δ is the crack width, D is the crack depth. A tapered crack with the same surface opening produces similar results. In the companion article by Ingersoll and Nakajima [36] it was investigated that the ocean surfaces from which the water can evaporate can be small. There is not necessarily a need for large vapour reservoirs.

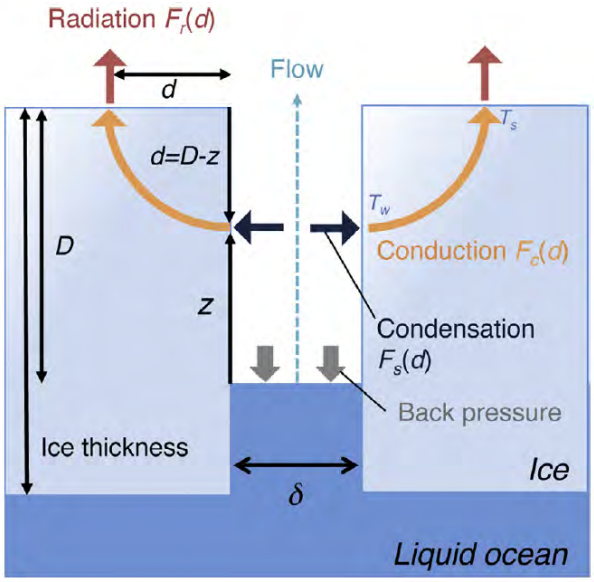

Figure 2.5: Schematic view of a straight column crack model at the triple point. D is the depth and δ is the width of the crack. (Image taken from [1])

A slightly different approach was taken by Yeoh *et al.* [2] in 2015 where they did not assume a long straight column but a nozzle structure in the ice. This converging-diverging nozzle structure works based on an aerodynamic principle in which a gas at subsonic velocities in a reservoir (when it just evaporated from the ocean) is accelerated to Mach 1 at the narrowest point (the throat) and accelerated to supersonic and hypersonic velocities at the wider surface opening (or vent) [37]. This mechanism works when the pressure at the ocean is much higher than the pressure the the surface. Since the pressure at the ocean is expected to be the triple point pressure of water (612 pa) and the pressure at the surface is more or less vacuum, this mechanism seems plausible. It does however require a very specific shape of the crack in the ice layer. While Nakajima and Ingersoll [1] seemed to have focussed more on reproducing the observed mass flow rate, Yeoh *et al.* [2] has modelled the observed exhaust velocity. They designed their model with the triple point temperature and pressure of water in the reservoir, a lower surface pressure and an exhaust velocity of Mach 3 and 5 in mind. Figure 2.6 shows the schematic view of their model. Table 2.3 lists all the important characteristics of this model and the results. It can be seen that the mass flow rate of one such nozzle-like crack is a lot lower than one 850 km wide crack. It would take multiple nozzle-like cracks to produce the observed mass flow rate.

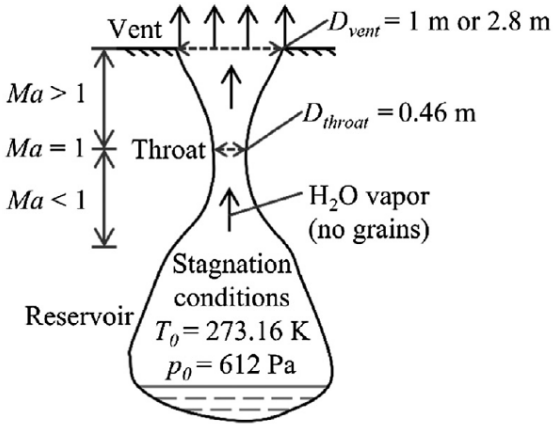

Figure 2.6: Schematic view of a nozzle crack model at the triple point. D is the diameter and Ma is the local Mach number. (Image taken from [2])

Table 2.3: List of conditions at the vent of a single throat model for Mach 3 and Mach 5 exhaust velocities. (taken from [2])

Properties	Mach 3	Mach 5
Vent-to-throat area ratio	4.8	36.6
D_{throat} $[m]$	0.46	0.46
D_{vent} $[m]$	1	2.8
Density $[kg/m^3]$	$3.1 \cdot 10^{-4}$	$3.5 \cdot 10^{-5}$
Velocity $[m/s]$	780	902
Temperature $[K]$	110	53
Pressure $[Pa]$	15.8	0.9
Mean free path $[m]$	$1.4 \cdot 10^{-4}$	$1.2 \cdot 10^{-3}$
Mass flow rate $[kg/s]$	0.2	0.2

A continuation on this work was published in 2016. Yeoh *et al.* [5] proposed that narrower jets resulted in better fits with the observed data. Narrower jets implies higher mach numbers (Mach 5 and higher) and those higher Mach numbers can only be a result of large vent-throat ratio's. This means that the channels leading from the ocean to the surface have large variations in width and are most likely not straight channels as suggested earlier. Figure 2.7 shows this updated model. The dimensions of the first throat and the vent are the same as in the previous model's Mach 5 setup (Figure 2.6), the total length of the channel $L_{channel}$ is 45 m and the wall temperature T_{wall} is 230 K. The conditions in the reservoir are again chosen to be at the triple point. The first throat has the smallest diameter resulting in sonic conditions (Mach 1) in that throat (See Figure 2.7 C for all the throat details). In Figure 2.7 B the distributions of gas (B1) and grains (B2) over the vent's cross section are shown in which n and n_{grain} are the gas and grain number densities respectively, V and V_{grain} are the vertical velocities of the gas and grains respectively in m/s, Ma is the Mach number of the gas, U and U_{grain} are the horizontal velocities of the gas and grains respectively in m/s and T_{rot}, T_{tr} and T_{grain} are the rotational, translational temperatures of the gas and the grain temperature respectively in K.

2.2.3. GRAINS

Next to gas, the plumes also release icy grains. This was already shown in Figure 2.7. These are ice particles in the solid phase that are a lot heavier and larger than the gas particles. These icy grains are formed by collisions. The average velocity of the icy grains at the vent is with 240 m/s a lot less than the velocity of the released gas at the vent (300-900 m/s). This is also lower than the escape velocity of Enceladus. Grain formation in space after leaving the vent does not explain this velocity. The gas is more or less collision free in space. The velocity can be explained with an explosion-like event inside the ice layer of Enceladus where lots of collisions occur, the grains coagulate and loose velocity. It is therefore more logical for the ice grains to have condensed from the water vapour after leaving the ocean, and grown in the channels leading from the ocean to the surface by colliding with each other and the walls [6]. See Figure 2.8 in which a schematic view of such a channel is given as wel as temperature-, velocity-, mass- and size variations over the length of the channel.

The observed ice grains leaving the vents (but not necessarily Enceladus due to their velocity often being slower than the escape velocity) have estimated sizes of less than 1 nm to more than 1 μm. The different sizes of the grains will be accelerated to different velocities. The larger micron sized grains may only be accelerated to 80 to 160 m/s which is much lower than Enceladus' escape velocity [38]. It is not entirely clear if the expelled grains from the plumes are made of crystallised ice or amorphous ice. Both ice types have been detected on the surface around the plume vents in the tiger stripes and have (at least partially) been deposited by the plumes [23]. The formation of the different ice types depends on the pressure, temperature and nucleation sites present inside and outside the plumes [25]. Three types of ice grains have been observed by Cassini. Those grain types (not to be confused with ice types) have been divided in type-1 (pure H_2O ice grains), type 2 (organic enriched grains) and type-3 (salt enriched grains). Figure 2.9 shows Cassini's E17 approach at the right hand side in black and the location of the Tiger Stripes in blue and the detection of these three grain types while crossing over a Tiger Stripe at the left hand side. It can be seen that when passing over the Tiger Stripes, the percentage pure H_2O grains degreases and the percentage organic- and salt enriched grains increase [7].

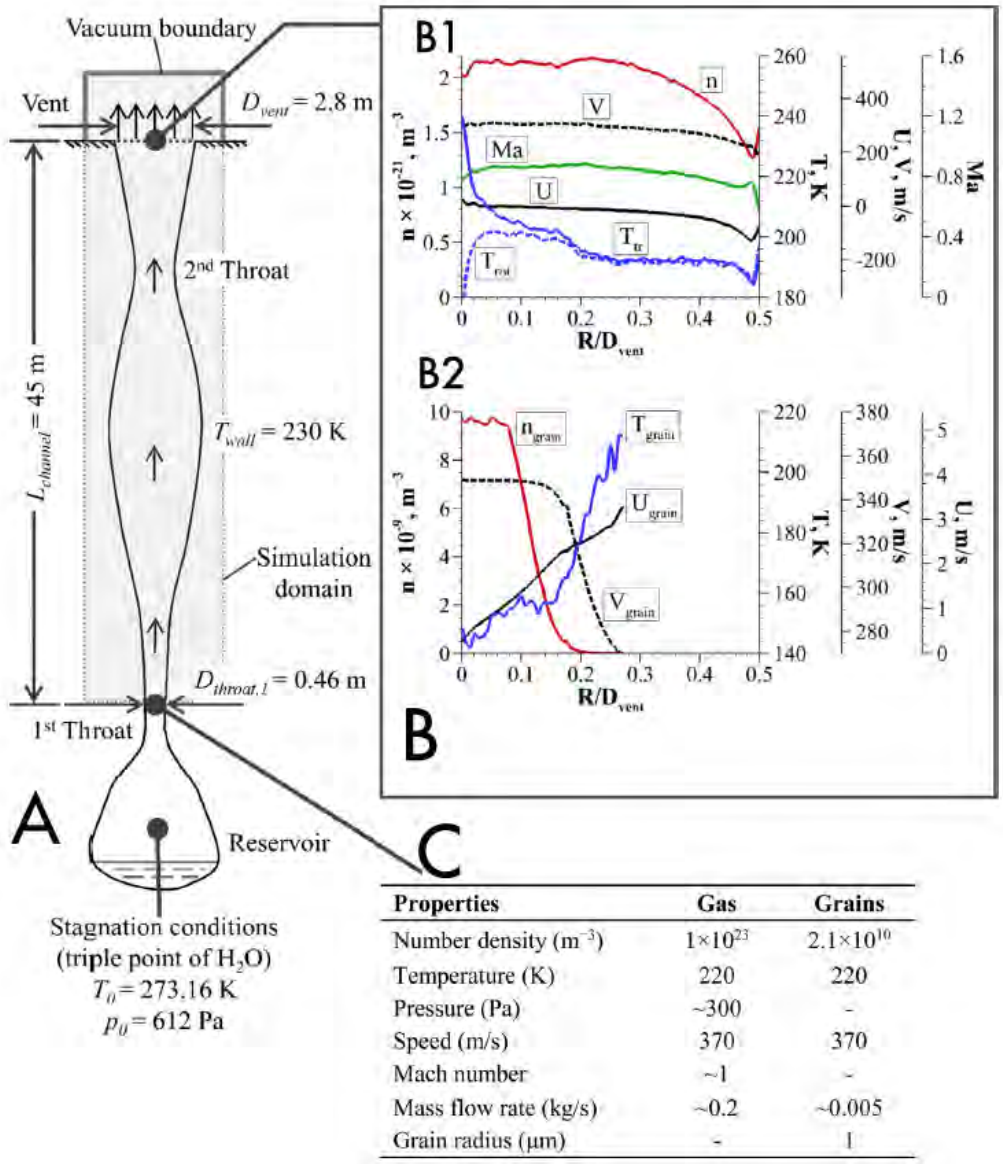

Properties	Gas	Grains
Number density (m^{-3})	1×10^{23}	2.1×10^{10}
Temperature (K)	220	220
Pressure (Pa)	~300	-
Speed (m/s)	370	370
Mach number	~1	-
Mass flow rate (kg/s)	~0.2	~0.005
Grain radius (μm)	-	1

Figure 2.7: Update of the model presented in Figure 2.6. A: Schematic view of the updated model. B: properties of the gas (B1) and the grains (B2) across the vent. C: properties of the throat. (Image taken from [5])

2.2.4. ORGANIC MOLECULES

In 2018 Postberg *et al.* [4] found evidence for the presence of macromolecular organic molecules in the plume of Enceladus. The molecular masses found to be above 200 atomic mass units can have several interpretations of which the presence of large organic molecules is the most likely one. It is suggested that there exists a thin film of this organic-rich material on top of the ocean inside a plume channel (more about the structure of a plume channel can be read in Chapter 2.2). Gas bubbles in the ocean transport these organics to the top of the ocean where they are expelled with the plumes. Figure 2.10 shows this process in which blue indicates pure water and orange indicates organic material.

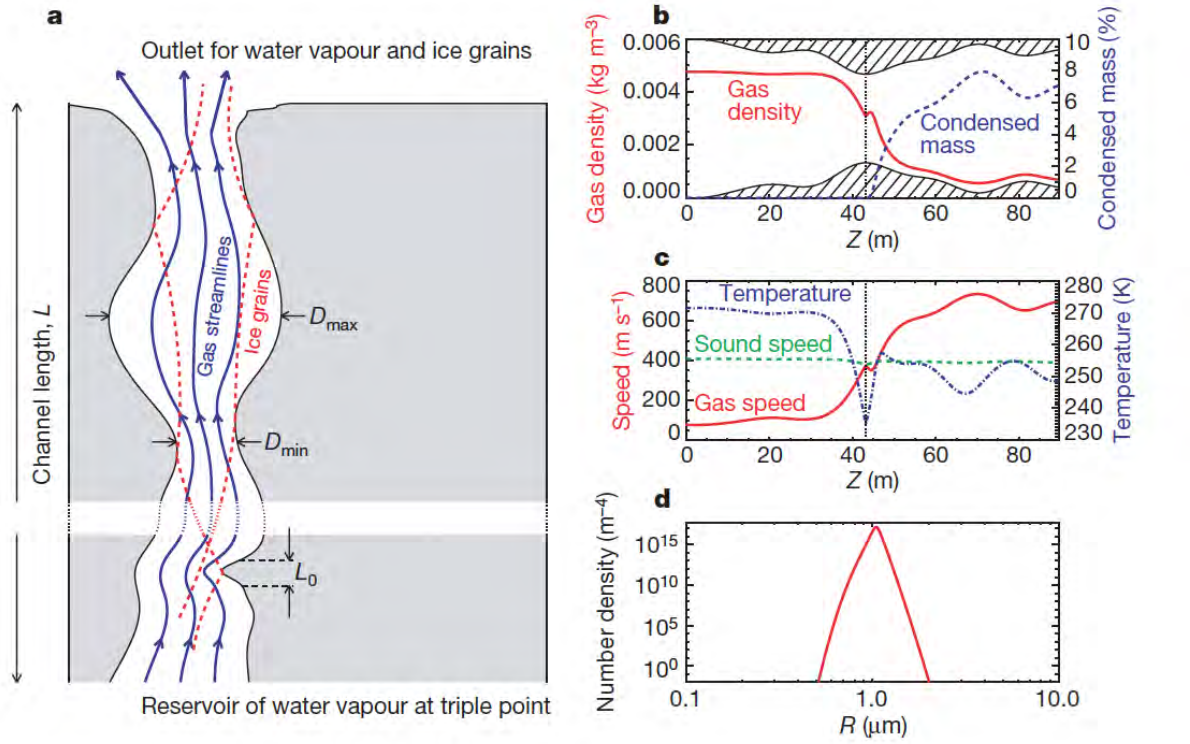

Figure 2.8: Model based on grain formation from vapour condensation. A: a schematic view of a plume channel in which the paths of the vapour and grains are shown. B: the variation of gas density and grain mass fraction along the length of the channel. C: the variation of gas speed and temperature over the length of the channel with a throat located just over 40 m. D: Particle number density per particle radius. (image taken from [6])

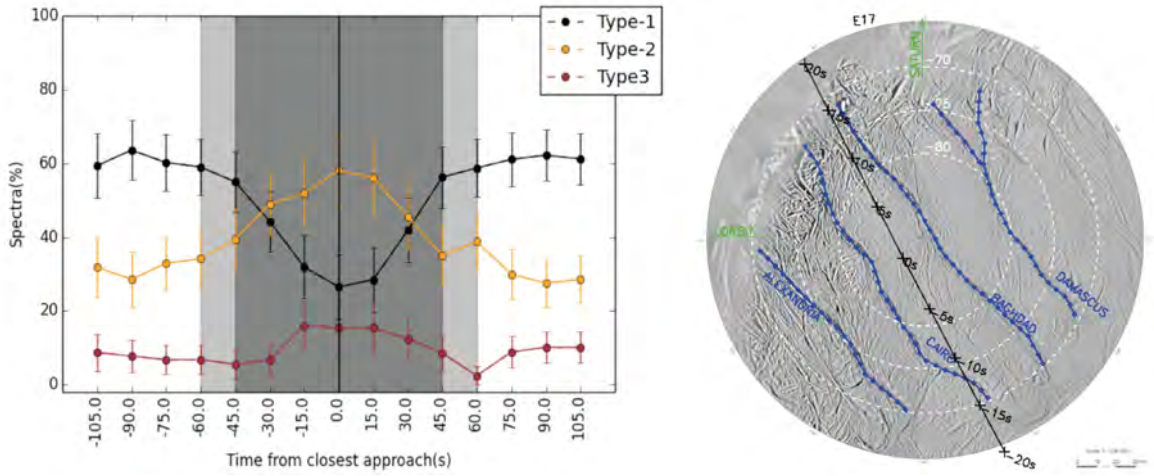

Figure 2.9: Spectra of pure water ice grains (type-1), salt rich ice grains (type-3) and organic rich ice grains (type-2) during Cassini's E17 approach of Enceladus' Tiger Stripes (image taken from [7])

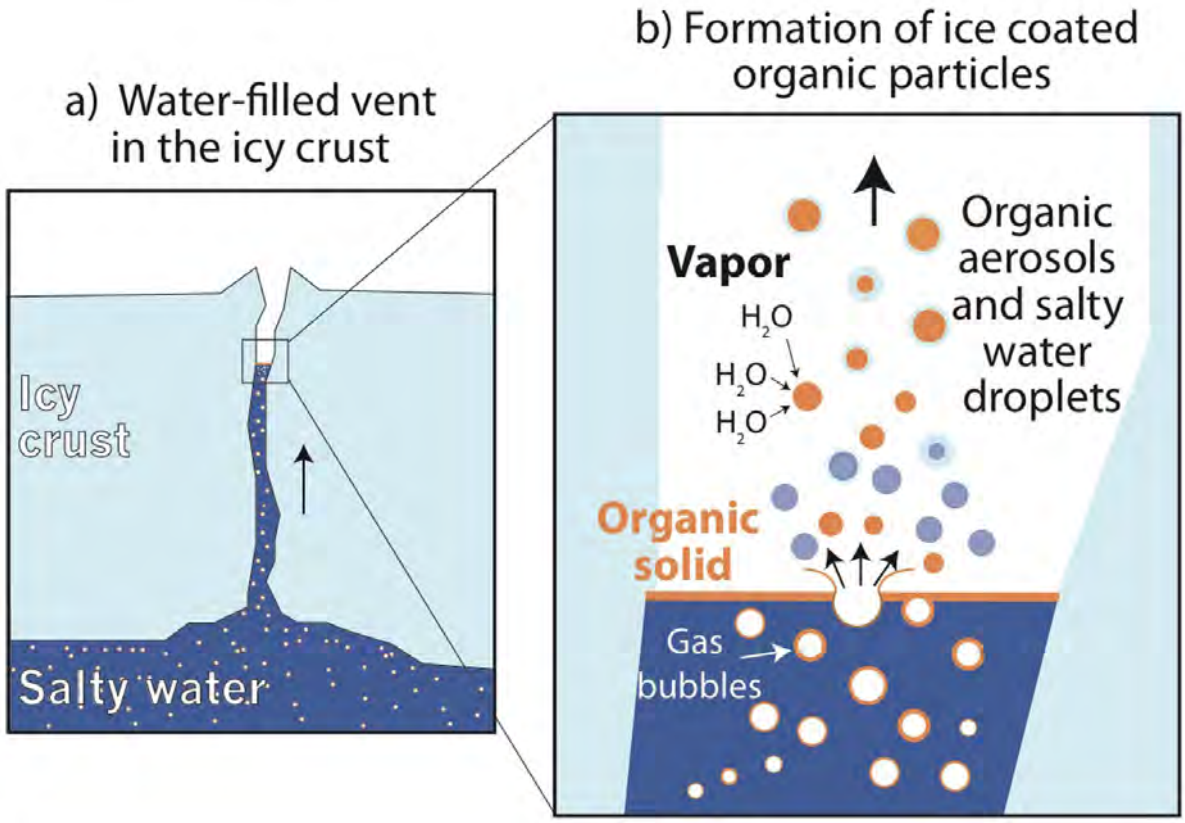

Figure 2.10: Mechanism for the creation of detected macromolecular organic molecules in which A shows the organic material being carried to the top of the ocean with gas bubbles and B shows the thin organic film on top of the ocean and the expulsion of molecular material into the plume. (Image taken from Postberg *et al.* [4])

3

COMPARABLE EXPERIMENTAL SET-UPS

This chapter lists previously done laboratory experiments that, in part, have similar aspects as the set-up that is proposed later in this study. This is to review what has been done experimentally and how similar experiments have been designed. Section 3.1 describes recent laboratory set-ups that model Earth geysers. Section 3.2 reports on previous experiments that dealt with ice deposition in simulations.

3.1. LABORATORY MODELS ON EARTH GEYSERS

Although icy moon plumes have only recently been discovered and models of plumes have only been developed after the discovery of the Enceladus plumes in 2015, studies on geysers on Earth have been documented from 1902. The Earth geysers are a result of volcanic activity. Heat released in these volcanic active areas heats up the groundwater. Pressure increased due to the steam build up will cause periodic eruptions of water and steam. This is for example the case in Yellowstone National Park (United States) [13].

Laboratory set-ups of Earth geysers found in publications go back as far as 1902. Anderson *et al.* [39] documented a working set-up after various attempts which used four Bunsen burners to vaporise steady dripping water (1800 ml/h) through iron pipes. This simple lecture table geyser model was able to automatically produce 180 cm high eruptions at periodic intervals.

Toramaru and Maeda [9] studied the predictability of the periodic eruptions of geysers like the ones in Yellowstone National Park by recreating a simplified version of a geyser in a laboratory. Their set-up consisted out of a glass flask with liquid water at the bottom that served as a liquid water reservoir (see Figure 3.1 B). The heat released by the volcanic activity was simulated by an As-one hotplate under the reservoir. The channel leading from the reservoir to the vent was constructed out of a straight 2 mm thick, 1 m long and 10 mm diameter glass cylindrical tube (which was also the diameter of the vent). The vent existed in an inverted glass flask with a tube leading to a tank that collected and weighed the expelled water. The temperature of the hotplate was varied between 260 $^{\circ}C$ and 340 $^{\circ}C$ in different versions of the experiment in which they also used either tap water (containing minerals and byproducts) and distilled water. Extra water was added as needed to the heated water reservoir at the bottom by an external cooler water tank. This was a different tank than the one that collected the expelled water and therefore the system was not closed. They measured the temperature at the heated water reservoir at the bottom with a T-type thermocouple (an electrical device that produces temperature dependent voltages). The pressure in the heated water reservoir and at the vent was measured by a Kisler pressure sensor. The expelled water mass was measured with a Sartorius electronic balance and the flow of the water between the cooler water tank and the heated water reservoir was measured by a Coriolis flow meter every 0.8 seconds.

Adelstein *et al.* [8] proposed and build a geyser model in 2014 to study the effect of a certain geometry on the eruption intervals and styles (continuous stream or sputtering). The set-up from Adelstein *et al.* [8] can be seen in Figure 3.1 A. Contrary to Toramaru's model above, Adelstein's model was a closed system consisting of a water reservoir at the bottom, pipes leading upward with a diameter of 1 cm with an S-shaped curve, rotated about 45 degrees counterclockwise and ending in a converging vent. The S-shaped curve was added

to create a bubble trap at the upwards facing part of the bend to collect gas. Similar structures have been seen in nature and account in part for the periodic eruptions. A collecting reservoir was placed over the vent at the top with a valve leading back to the bottom of the reservoir. The water reservoir at the bottom was heated with a Cole-Parmer hotplate till 170 $^{\circ}C$ - 185 $^{\circ}C$. The temperature in the top and bottom reservoirs was measured with a K-type thermocouple from the outside via cavities in the reservoirs. The pressure is not measured. The vent resided in sea-level conditions. The entire structure was made out of glass and is 24 cm in height with a total pipe-length of 34 cm.

Namiki *et al.* [10] investigated the differences in geyser eruption styles and intervals as well, also by using varying geometries (see Figure 3.1 C). They focussed additionally on the heat loss between the channel walls and the effect of that heat loss on the discharge styles. They used a flask at the bottom on top of a 220 W hotplate as a hot water reservoir (T1 of Figure 3.1 C). This was connected to a Teflon vent with an inner diameter of either 1 mm or 3 mm. The vent was connected to a reservoir again to collect the expelled water (T4 of Figure 3.1 C). They had two set-ups in which they varied the length, diameter and the the amount of branches connected to the system via side ports to investigate the effect of branches on the pressure, temperature and interaction with external water sources (T5 and T8 of Figure 3.1 C). The first set-up had a combined conduit length of 80 mm and the second set-up had a length of 160 mm (T1 to T4 of Figure 3.1 C). The temperature was measured with a K-type thermocouples in the reservoir, at the connection between the reservoir and the channel, in the middle of the channel and at the vent. It is not specifically mentioned to what temperature the water reservoir was heated. The pressure was measured in the channel by a Measurement Specialties sensor. The environmental conditions had a temperature of 15 $^{\circ}C$ to 29 $^{\circ}C$ and a pressure of 10^5 Pa.

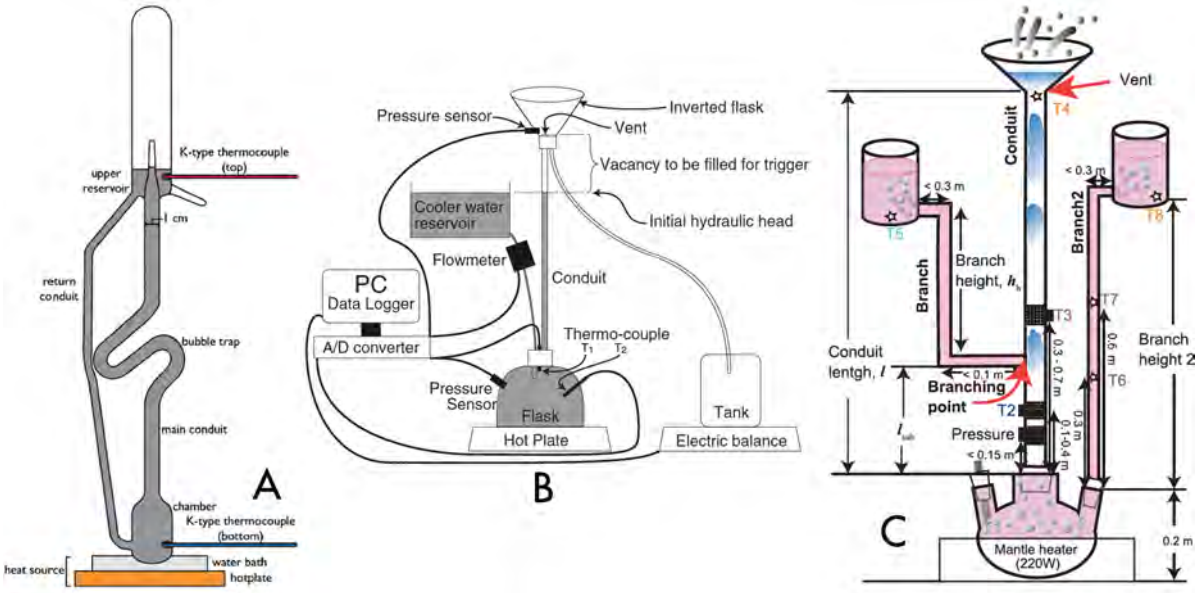

Figure 3.1: Different laboratory geyser set-ups. A: Set-up used by Adelstein *et al.* [8] (Image taken from [8]). B: Set-up used by Toramaru and Maeda [9] (Image taken from [9]). C: Set-up used by Namiki *et al.* [10]) (Image taken from [10])

Although the underlying mechanisms appear comparable, the biggest difference between the geysers on Earth and the plumes on Enceladus and Europa is the environment. This is reflected in the laboratory set-ups for Earth geysers. The geysers on Earth have a temperature at the vent of about 273 K and a pressure of about 1 bar, while the pressures and temperatures at the vents of Enceladus and Europa plumes are considerably lower since they end up in more or less the vacuum of space. For Europa the expected surface temperature is 125 K and the expected surface pressure is $1 \cdot 10^{-12}$ bar [40] [41]. For Enceladus the expected surface temperature is even lower at 75 K and the surface pressure is expected to be 10^{-10} to 10^{-13} bar [29] [28]. For the mechanism to work, an overpressure and higher temperature is needed in the liquid water reservoir which - if put side by side - results in much higher reservoir pressures and temperatures for the Earth geyser models than for the Enceladus- and Europa plume models. Furthermore, the laboratory experiments are done in Earth environmental conditions (sea level surrounding temperatures and pressures). Next to that, the walls

of the channels of Earth geysers are composed of rocky materials (glass and plastics in the lab experiments) while the Enceladus- and Europa plume channel walls are assumed to be water ice. This might seem trivial, but this interaction between water ice, liquid water and water vapour is especially important for grain growth [6] (see Chapter 2.2 for a clearer explanation of grain growth). Lastly, there is a gravity difference. The surface gravitational acceleration on Enceladus is 0.113 m/s^2 while on Earth this is 9.807 m/s^2 [13]. That is almost a factor 100 difference which has to be accounted for. The icy moon plumes are often referred to as 'cryo-volcano's' or 'cryo-geysers' implying similar mechanisms as Earth volcano's and geysers but with much colder liquids [13]. Therefore, even though the environmental conditions are quite different, these replicated Earth geyser laboratory models can serve as a basis for the mechanism for the icy moon plume laboratory model that is developed in this study. Examples are using a heating element (or lessen the cryo-cooling element) at the bottom of the water reservoir, whether or not to use a closed system, and obtaining the temperature and pressure gradient by performing measurements at multiple intervals.

3.2. LABORATORY MODELS ON WATER DEPOSITION

As mentioned above, the main differences between those set-ups and the set-up needed for a plume simulator are the temperature and pressure. The icy moon plumes reside in near vacuum environmental conditions and therefore the water (either in solid form, liquid form or gaseous form) needs to be deposited in these extremely low temperatures and pressures. There have been previous experiments. The goals of these experiments were different from this study, but the method of how the water was deposited is of interest here. One such set-up is the FORMOLISM set-up (FORmation of MOLecules in the InterStellar Medium) which is located in the physics department of the Université de Cergy-Pontoise (France). This set-up consists of an ultra-high vacuum chamber that can reduce the inside pressure to less than 10^{-10} mbar and the temperature to a minimum of 8 K [42]. The device reaches these pressures by a turbo molecular pump and these temperatures by a Gifford-McMahon refrigerator cycle based two stage cryocooler [43]. In the 2013 set-up by Accolla *et al.* [43] the main chamber housed a sample holder constructed of highly conducting copper and a microchannel doser equiped leak valve (with an estimated flux of $9 \cdot 10^{12}$ $molecules\ cm^{-2}\ s^{-1}$ [44]). This leak valve - once opened - diffused water vapour onto the sample holder. This method allowed for the production of 0.8 $monolayer$ (ML) of interstellar ice after opening the valve for 30 seconds (1 ML = 10^{15} $molecules/cm^2$ [42]) at a temperature of 15 K and heated to 30 K afterwards. Water in the gas phase was measured by a Quadrupole Mass Spectrometer (QMS) and resultant interstellar ice was measured via Reflection Absorption InfraRed Spectroscopy (RAIRS). The angle at which the water is deposited has an effect on the resultant amorphous ice layer and its detection. Dohnálek *et al.* [45] deposited pure water at 22 K for 50 ML and used laser optical interferometry to detect differences in indexes of refraction when the deposition occurred at different angles. When no angle is introduced, the index of refraction of the amorphous ice was 1.285 at an assumed density of 0.94 g/cm^3. The larger the incidence angle, the lower the refractive index and the density became. Although these set-ups resulted in a very precise method to recreate interstellar, porous, amorphous ice, the scale was very small compared to the cm to m scale icy moon surface model proposed in this study. It is, however, expected that the most part of icy moon surface ice consists out of hexagonal type-I ice instead of amorphous ice. Only small portions of the surface and grains formed in the plumes are expected to contain amorphous porous ice (as explained in Chapter 2.2). In Chapter 2 and 2.2 it is mentioned that the temperature and pressure of the surface ice are expected to be around the triple point of water (237 K and 6.12 $mbar$). This is higher than the temperatures and pressures used in the FORMULISM set-up.

Experiments on water deposition under Martian conditions resemble the temperatures and pressures on Enceladus more closely. Hudson *et al.* [46] and Siegler *et al.* [47] designed and build a Mars environment chamber (30 cm diameter by 40 cm in height) with a pressure of 6 $mbar$ and a temperature range between < 220 K at the bottom and 268 K at the top of the chamber (which is just below the triple point temperature of water). The Mars environment chamber was cooled from the bottom with a cold plate which was chilled by liquid methanol to around 212 K and heated by a halogen lamp at the top to reach a top temperature of 268 K [47]. The environment chamber was continuously evacuated by a vacuum pump to keep the pressure at 6 $mbar$ even after adding material to the chamber (this could be adjusted manually when needed) [46]. Inside the chamber a porous medium was used to simulate the Martian surface and the atmosphere was simulated by CO_2 gas. When the required temperature and pressure conditions were reached, water vapour was introduced to the atmosphere. The environmental temperature, pressure and water vapour pressure were individually controlled by Proportional-Integral-Derivative (PID) control loops. The temperature was measured by 11 T-type thermocouples at different heights in the chamber. The atmospheric pressure was mea-

sured by a manometer. Hudson *et al.* [46] demonstrated ice deposition below the surface from atmospheric water vapour in Martian conditions. Siegler *et al.* [47] investigated icy regolith on Mars on thermal conductivity, thermal diffusivity and heat capacity. Both experiments had a different goal from this study and both the atmosphere- and surface content on Mars are different from Enceladus, but the environmental pressures and temperatures at which water deposition took place are similar to what is expected on Enceladus and therefore similar to what is required in this study.
For the design of an Enceladus simulator chamber a controlled temperature gradient is important. The Mars environment chamber has achieved this by cryo-cooling from below and heating from above. This part of the set-up can be inversely applied to this study where the top should be colder than the bottom. Especially the method of cryo-cooling used in the Martian environment chamber is of interest. Using standard refrigerators will only allow for a small temperature difference with respect to the environment. Using liquid methanol (or a similar substance like liquid nitrogen) will allow for the much colder temperatures required. But applying it directly into the chamber would be unpredictable, therefore, to have a closed system where the liquid methanol can be circulated around, absorbing heat from the Enceladus chamber while still being separated from the Enceladus chamber would be ideal. The use of a vacuum pomp at the top combined with a manometer in the Mars environment chamber to control the pressure can be applied to this study as well. The use of optical sensors like in the FORMULISM set-up and Cassini itself can be used to measure different types of ices that are introduced or have formed.

4

PRELIMINARY DESIGN

This chapter forms a first draft for the design of the Enceladus plume laboratory set-up. Section 4.1 shows what has already been done with the refurbished vacuum chamber of the FH Aachen university of applied sciences where the Enceladus plume will be simulated. The use of that vacuum chamber will impose some restrictions on the design. These restrictions are summarised in Section 4.2. With the Cassini measurements on the plume exhaust (Chapter 2), the Enceladus plume computer models on the mechanism (Chapter 2.2), the comparable laboratory set-ups and the vacuum chamber in Aachen in mind, a preliminary design is formed in Section 4.3. In the end, this first draft raised some questions which will be answered in the coming chapters.

4.1. ABOUT THE REFURBISHED VACUUM CHAMBER

In this study, the focus is to design an experimental set-up that can be operated with the equipement already available. This experiment and subsequent experiments based on this study will be done by a cooperation of the Delft University of Technology (The Netherlands) and the FH Aachen University of Applied Sciences (Germany). The large scale experiments will be carried out in the large vacuum chamber available in Aachen. The refurbished vacuum chamber at the FH Aachen university of applied sciences has a diameter of 1.0 m and a height of 1.9 m. Depending on the vacuum pump used, the internal pressure can be reduced to 8 Pa without gas ballast and 70 Pa with gas ballast which it will reach after about 10 minutes with the connected Leybold SV 630B 50Hz pump. Figure 4.1 shows the pump characteristic graphs for a 1 m^3 volume taken from the manufacturer's brochure. This volume is less than the volume of the vacuum chamber, therefore the pumping times will be higher to get the same pressures. Figure 4.2 shows the vacuum chamber located in Aachen from the outside and the inside.

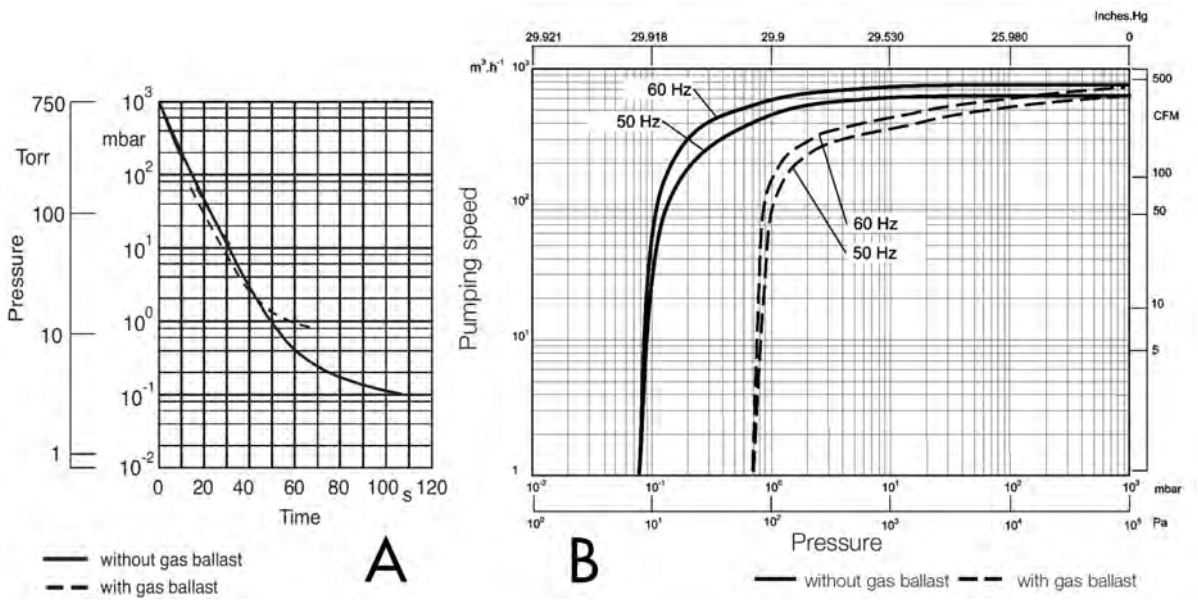

Figure 4.1: Pump characteristic graphs. A: Pumping time to reach specific pressures for a 1000 liter container. B: Pumping time and limits. (Taken from the Laybold SOGEVAC SV 630 B(F) - 750 B(F) Single-stage, oil-sealed Rotary Vane Vacuum Pumps Brochure)

The operational volume is less due to equipement and tubes in the chamber (as can be seen in Figure 4.2 B). The previous experiments used a smaller ice tank that can be placed inside the vacuum chamber. This smaller tank has an inner diameter of about 29 cm and a length of about 1.0 m.

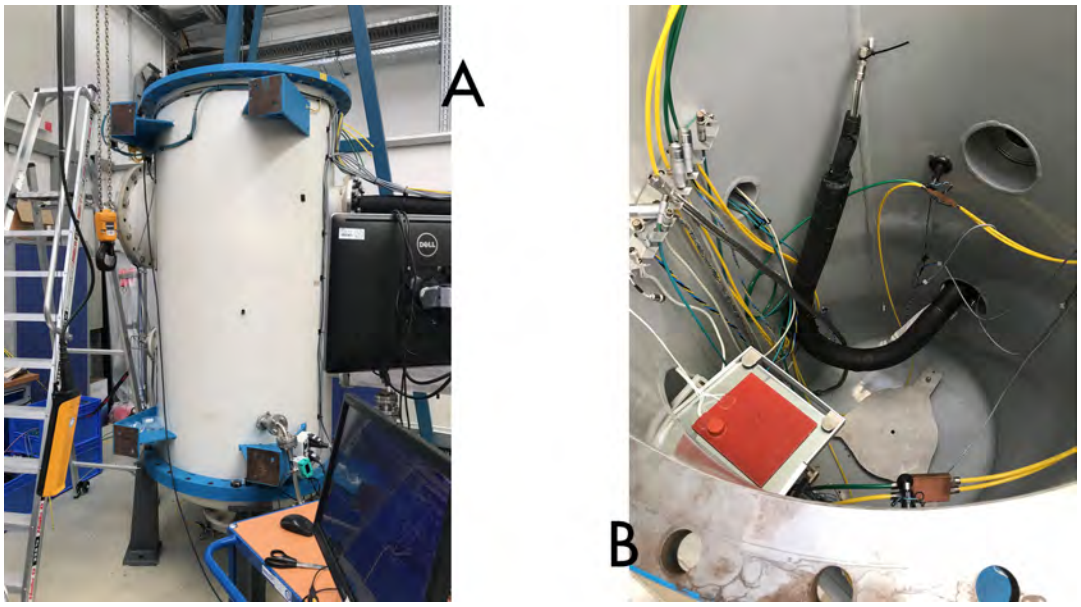

Figure 4.2: The large scale vacuum chamber at the FH University of Aachen (Germany) from A: the outside and B: the inside

Currently, water is frozen in a container outside the vacuum chamber to a temperature of $-180°$ C or about 93 K by a liquid nitrogen coolant (the theoretical minimum achievable temperature is $-196°$ C or 77 K). The ice block is smaller than the vacuum chamber interior. Before the experiment, the ice cylinder is moved into the testing case (on which a camera is mounted) to move the ice block in to the vacuum chamber. The entire combination of ice cilinder and case is moved into the vacuum chamber for the experiment. While inside the chamber, the temperature is measured, but not controlled.

The goal of this set-up is to recreate an icy moon plume which can be used to gain valuable scientific insights

on the plumes and might also provide a testing environment for icy moon landers like the EnEx-nExT[1]. This is a probe which uses heating element and a drill to manoeuvre itself trough layers of ice. This ice mole is designed for probing the ice of Europa.

4.2. RESTRICTIONS ON THE ENCELADUS PLUME SET-UP

Based on the specifications of the vacuum pump, the space environment pressure is limited to a minimum 70 Pa instead of the approximate $1 \cdot 10^{-5}$ Pa the Enceladus plume exhaust is exposed to (see Chapter 2). This will have an influence on the plume exhaust speed and mass flow rate. There are no restrictions on the required temperature since the temperature of the ice and liquid reservoir should be around the triple point of the used liquid. For pure water this is 0.01 $°C$. When an ammonia water solution of a few percent is used (which is expected to be on Enceladus), the required temperature is likely to be slightly lower. Since the cooling system used for experiments with the vacuum chamber are able to reach temperatures far below the freezing point of water, no adaptions need to be made. To reuse as much of the already available equipment, the dimensions of the smaller ice tank will be used as the dimensions for Enceladus plume set-up. This will allow the use of this already available tank which is known to fit in the vacuum chamber with all the necessary equipment. The maximum volume available for the Enceladus plume set-up is therefore a cilinder with an inner diameter of 29 cm and a length of 1.0 m.

The data from Cassini together with the plume computer models detailed in Chapter 2 suggest the use of the triple point temperature at the location of the ocean. This temperature is known for pure water, but this needs to be determined for water with different ammonia concentrations. The same holds for the triple point pressure of the used solution. To create the velocity and mass flow rate measured by Cassini, the geometry of the crack in the surface ice needs to resemble a nozzle as proposed by Yeoh *et al.* [2]. But at the same time it needs to be considered that the Tiger Stripes on Enceladus are long horizontal cracks in the ice resembling crevasses as proposed by Nakajima and Ingersoll [1]. Both geometries need to be combined to form a laboratory set-up with a thin, long and deep crack in the ice which has a nozzle-like structure (see Figure 4.3). This specific ice structure needs to be designed to fulfil all the above requirements and in such a way that it is easily repeatable without too many variations in the ice sculptures.

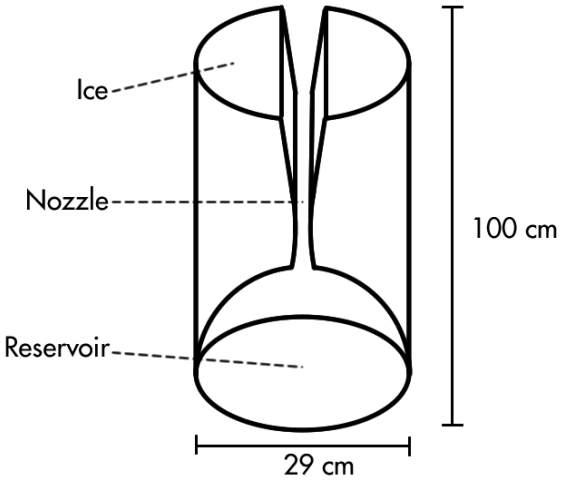

Figure 4.3: The Enceladus plume laboratory model requirements combined in a simplified preliminary first draft

[1] https://www.youtube.com/watch?v=AyPoseYkI1Q&frags=pl%2Cwn, last visited on 24-07-2018

4.3. REQUIREMENTS FOR THE ENCELADUS PLUME SET-UP DESIGN

This section summarises the above mentioned items in a list of restrictions. First there are physical parameters that restrict the design. Those are listed below.

Res-1. The design shall mimic Enceladus' liquid ocean content.

Res-2. The design shall mimic Enceladus' ocean temperature.

Res-3. The design shall mimic Enceladus' ocean pressure.

Res-4. The design shall mimic Enceladus' ice layer.

Res-5. The design shall mimic Enceladus' surface geometry.

Res-6. The set-up shall be able to produce a supersonic plume via a converging diverging nozzle structure.

Next tot the physical restrictions there are a few requirements requested from Aachen for the design. Those are listed below.

Req-1. The set-up shall fit inside the existing test cilinder and therefore shall have a diameter of 29 cm and a height of 100 cm.

Req-2. The design shall not need a vacuum chamber pressure lower than 70 Pa.

Req-3. The set-up shall be removable from the vacuum chamber.

Req-4. The set-up shall be designed to use freezing equipement present in Aachen.

Req-5. The set-up shall be reusable.

Req-6. The experiment shall be repeatable.

5

TEMPERATURE AND PRESSURE OF THE RESERVOIR

In chapter 2 it was determined that Enceladus' liquid water and ice is not constituted by pure H_2O water but contains all sorts of molecules that have been detected in the ice and in the plumes. From chapter 2 it is expected that Enceladus' ocean has a 0.8% to 4.8% ammonia concentration and a 0.5% to 4.0% sodium-chloride concentration. Ammonia is most likely closer to the lower end of this limit while sodium-chloride is most likely closer to the upper limit [52]. Having saline water allows for a lower freezing temperature which influences the triple point temperature on which the design of the plume simulator chamber is based. It is therefore important to determine the triple point for Enceladus' ocean. 5.1 lists what is known about the effect of ammonia on the freezing and boiling points of water and determines what still has to be determined for this study. Section 5.2 describes the experiments designed and performed to acquire the missing information and Section 5.3 shows the results of this experiment.

5.1. VOLATILES AND SALINITY

The influence of small ammonia and salt concentrations on liquid water and water ice and their connections to icy moons have been studied before. This section gives a theoretical basis of the influence of ammonia and salt on the vapour and freezing points of Enceladus' ocean and ice. This section also shows the limit of theoretical knowledge which will be experimentally determined in the next section.

5.1.1. AMMONIA

Studies that go back as far as 1909 have experimentally determined the phases of ammonia water in different concentrations at atmospheric pressure [48]. In this study the lowest ammonia level was 4.1% which had a freezing temperature of -2.9°C. More recent studies have linked the ammonia water to icy satellites and a number of older studies have been combined in Kargel [11] to form a more complete overview of the behaviour of ammonia water in different concentrations at atmospheric pressure (see Figure 5.1). It was found that ammonia water can exist in various solid and liquid phases at the same temperature and pressure. Ammonia dihydrate ($NH_3 \cdot 2H_2O$) can be present together with both liquid and ice when lower concentrations of ammonia are present. Ammonia monohydrate ($NH_3 \cdot H_2O$) occurs with higher concentrations of ammonia. The most relevant for this study is that up to a concentration of about 33%, the higher the concentration of ammonia, the lower the freezing point temperature.

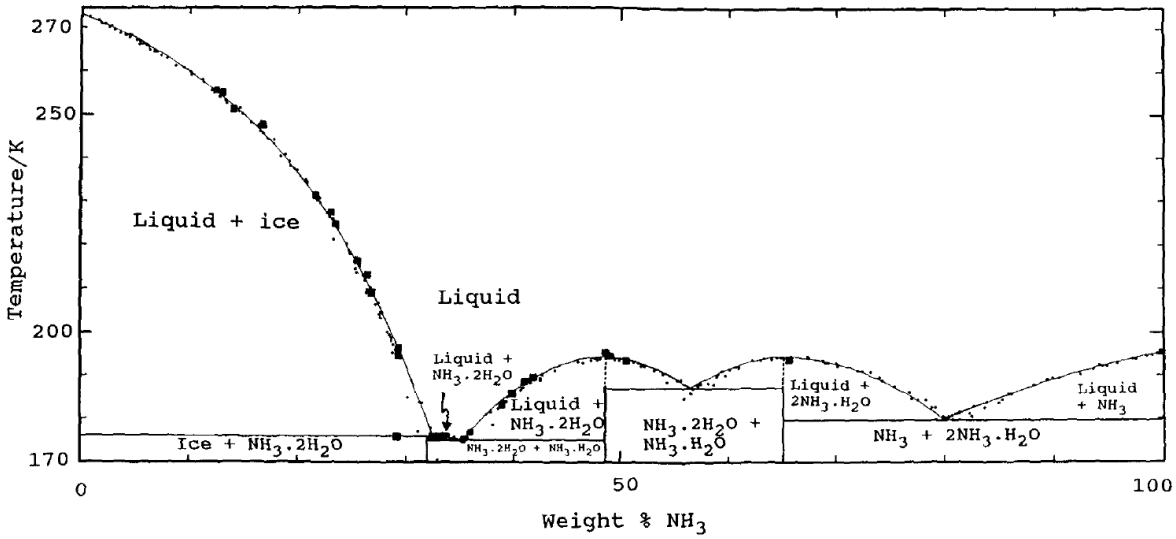

Figure 5.1: Ammonia water phases for different temperatures at atmospheric pressure for different ammonia concentrations. The solution can (depending on the ammonia concentration and the temperature) be in liquid or ice state together with ammonia monohydrate ($NH_3 \cdot H_2O$) and ammonia dihydrate ($NH_3 \cdot 2H_2O$) (Image taken from Kargel [11])

Other studies have extended the ammonia water phase diagram to include higher pressures than atmospheric pressure [49] [50] [51]. The most extensive work on this was done by Johnson and Nicol [12] in which the phases of ammonia water were experimentally found for different ammonia concentrations at different temperatures under pressures up to 5 GPa. It is most likely that the ammonia concentration is only a few percent (as explained in Chapter 2 and assumed by Spohn and Schubert [49] Grasset and Sotin [50] Leliwa-Kopystyński *et al.* [51] in which 5% is used). Figure 5.2 shows the phase diagram for pure water (the thick lines) and the adapted phase diagram for 4.8% ammonia water (the thin lines) as determined by Johnson and Nicol [12]. The diagram includes the different states of the ammonia water substance as explained by the different circles and letters where L stands for liquid, D for ammonia dihydrate and M for ammonia monohidrate. It can be seen that for the same pressures, the freezing points of the 4.8% ammonia water is lower than for pure water. It can again also be seen that there is an area in the diagram in which both liquid and solid phases occur. The ammonia concentration was created with aqueous ammonia and distilled water and checked with titration. The different phases of the substance were determined by visual inspections.

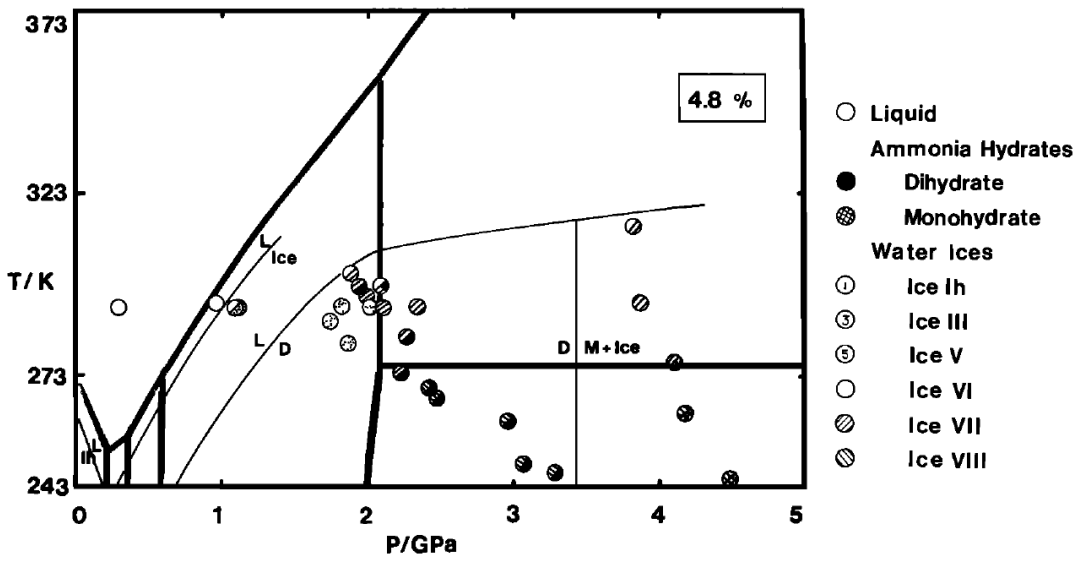

Figure 5.2: Ammonia water phases for different temperatures and different pressures for an ammonia concentration of 4.8%. The thick lines indicate the phase changes of pure water. The thin lines indicate the changed phase transitions due to the 4.8% ammonia. L is Liquid, D is ammonia dihydrate, M is ammonia monohidrate. (Image taken from Johnson and Nicol [12])

Although it has been shown that there have been a lot of studies of ammonia water solutions linked to icy moons, they have been performed at atmospheric pressures and higher. While for the Enceladus plume mechanism of this study to work, the pressure has to be around the gas-liquid-solid triple point of the substance.
Because of the higher pressures, the above phase diagrams show only the liquid and gas phase of ammonia. A theoretical phase diagram of pure water and pure ammonia is shown in Figure 5.3 (the data for this figure was obtained from The Engineering Toolbox[1] [2]). It can be seen that pure ammonia freezes around 195.5 K and vaporises at much higher pressures. Logically, a combination of water and ammonia will result in a phase diagram that lies between these two limits.

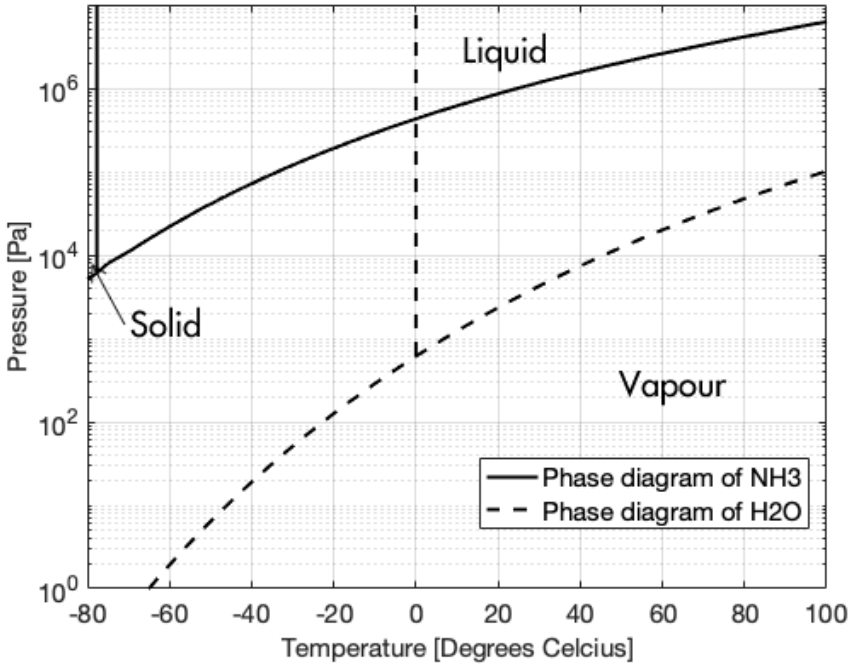

Figure 5.3: Theoretical phase diagram of pure water (dashed line) and pure ammonia (solid line)

The behaviour of a low concentration ammonia water solution at low pressures - or more precisely, the triple point of this ammonia water - has therefore to be determined for a more accurate experimental Enceladus plume set-up than one with pure water. The experiment to determine this and the results are explained in Section 5.2.

5.1.2. SODIUM-CHLORIDE

Besides from volatiles, of which ammonia is most abundant, the presence of salt also influences the minimum temperature at which the ocean can remain liquid. The most abundant salt in Enceladus' ocean is sodium-chloride ($NaCl$ or simple table-salt found in Earth's ocean's as well). The expected concentration ranges between 0.5% and 4.0% [20] [52]. The effect of small concentration of sodium-chloride on water has been studied more than the effects of small concentrations of ammonia. Figure 5.4 shows the freezing point of water with different concentrations of sodium-chloride (the data for this figure was obtained from The Engineering Toolbox[3]). Pure sodium-chloride 'freezes' below 801°. It can be seen that the freezing point temperature decreases with increasing concentrations of sodium-chloride down to -21.12° Celsius with a concentration of 23.31%. This is the eutectic point (the point where the combination of the two substances has a lower freezing point then the individual substances). Increasing the concentration of sodium-chloride

[1] https://www.engineeringtoolbox.com/water-evacuation-pressure-temperature-d_1686.html, last checked on 06-12-2018
[2] https://www.engineeringtoolbox.com/ammonia-gas-liquid-equilibrium-condition-properties-temperature-pressure-boiling-curve-d_2013.html, last checked on 06-12-2018
[3] https://www.engineeringtoolbox.com/sodium-chloride-water-d_1187.html, last checked on 07-12-18

will increase the freezing point again. At the expected concentrations of 0.5% to 4.0% the freezing point is lowered by -0.3° to -2.41°. For a complete phase diagram of a sodium chloride solution, the altered vapour pressure line (the pressures at which the solution vaporises at set temperatures) needs to be known.

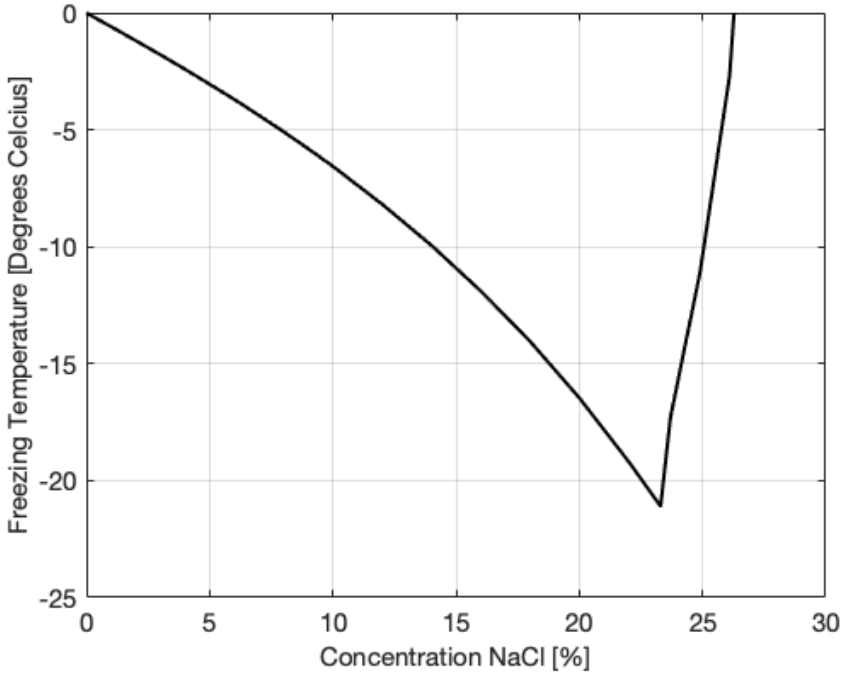

Figure 5.4: Freezing point temperature of different concentrations of sodium-chloride in water

5.2. EXPERIMENT

The right panel of Figure 5.5 shows the graphical representation of the set-up for this experiment and a photo of the actual setup on the left. It consist out of a vacuum chamber connected to a vacuum pomp which is able to handle chemical vapours. Inside the vacuum chamber a see-trough beaker and the to-be-tested fluid is present. The boiling chips inside the container help to reduce splashing during boiling and provide nucleation sites for the other two phases. A K-type thermocouple is present inside the container at the top of the liquid. A relative pressure sensor is present at the valve of the container and an absolute pressure sensor is present at the vacuum pump.

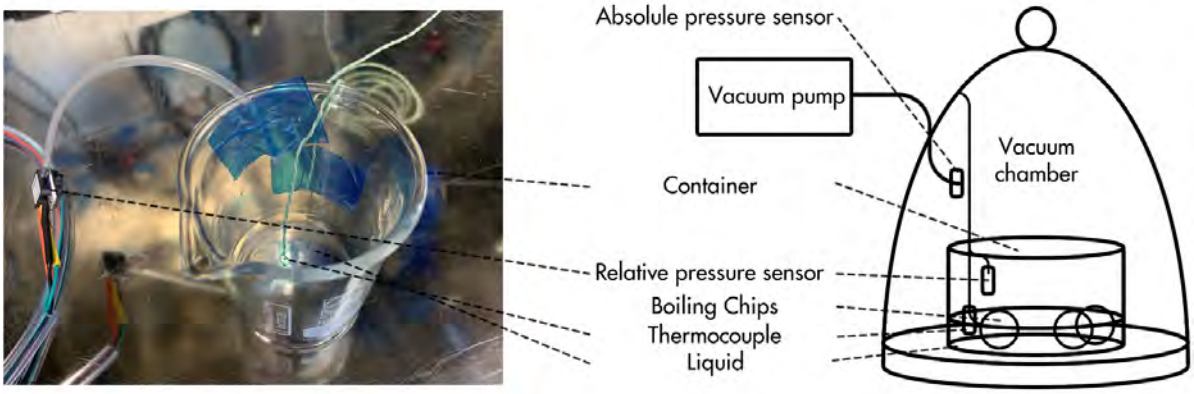

Figure 5.5: Set-up for the measurement of the triple point of a fluid

Pressure control The pressure should be decreased from a room pressure of approximately 100,000 Pa to the triple point pressure of 611.657 Pa [25] and lower with the use of the vacuum pomp. Two vacuum pumps

are available for this experiment. A Vacuubrand RZ6 and a Vacuubrand MD1. The RZ6 is quicker and can reach lower pressures but can only handle pure water. The MD1 can handle water mixed with ammonia concentrations but is slower and will not be able to achieve triple point pressures with gas ballast. Therefore, only the triple point of pure water can therefore be determined with this experiment. The triple points of different ammonia concentrations will be a combination of measurements and extrapolations (this is be discussed later). The pressure is measured at the vacuum pump inlet (or outlet) by an absolute pressure sensor, but this is not the exact pressure close to the liquid. Placing a relative pressure sensor close to the water and comparing the measurements with the absolute pressure sensor at the vacuum pump allows for more precise pressure measurements.

Temperature control In this first experiment, the temperature of the substance will not be controlled. It will only be measured. The to-be-tested substance will be entered into the vacuum chamber at room temperature. This is about $20 \pm 2°C$. Controlling the temperature inside the vacuum chamber would require a much more complex set-up which, for this preliminary experiment, is not yet necessary. The boiling process (the chemical phase change from liquid to gas) of a substance requires energy which will be taken from the remaining substance. This means that when part of the substance starts to boil, the remaining substance looses energy (or heat) and will therefore cool down on its own [53]. The temperature inside the vacuum chamber should be measured by a K-type thermocouple inside the liquid.

Preparing the substance For the experiments with pure water, the substance does not need to be prepared. Distilled water can be used. But the experiments with ammonia water need preparation. Aqueous ammonia needs to be added to pure water to form the desired solution by the use of titration [12]. The available aqueous ammonia contains 25% ammonia which means it needs to be diluted. Table 5.1 shows the needed volume of pure water and 25% aqueous ammonia to get a 10 ml solution with different concentrations.

Table 5.1: Required volumes of distilled water and 25% aqueous ammonia to get different concentrations of 10 ml

Desired ammonia concentration	0%	1%	2%	3%	4%	5%
Water volume	10 ml	9.6 ml	9.2 ml	8.8 ml	8.4 ml	8.0 ml
25% aqueous ammonia volume	0 ml	0.4 ml	0.8 ml	1.2 ml	1.6 ml	2.0 ml

Performing the experiment This experiment should be repeated multiple times for each concentration of ammonia. The first attempt will be to reach the triple point of pure H_2O water without ammonia to calibrate the experiment. This temperature and pressure are well known and performing this experiment first will show if the triple point can be reached with this set up and if the measuring equipement is working correctly. The determination of the conditions at which the triple point is reached will be made by visual observation. It should be clearly visible when part of the substance simultaneously boils, freezes and remains liquid. The experiment will be activated by depressurising the vacuum chamber to the desired triple point pressure. When the experimental results and literature matches, part two of the experiment can start. This time the ammonia water solutions will be put in the vacuum chamber which has been prepared earlier by titration. Since only the MD1 pump is rated for the use of chemicals other than pure water, that pump has to be used for this part. Pure water is expected to follow the existing phase diagram lines. Concentrations of ammonia mixed with water are expected to boil and freeze at lower temperatures (when the pressures are kept the same). A camera set-up outside the vacuum chamber records each run.
Since the Vacuubrand MD1 vacuum pump is not able to decrease the pressure below the freezing point, only part of the phase diagram can be obtained. It is limited to moving from room temperature and room pressure to a pressure of about 880 Pa and varying temperatures (based on the amount of ammonia present). The freezing point of the different ammonia concentrations has to be reached from the other side. The different ammonia concentrations are prepared and frozen to about -20 degrees Celsius in a freezer. A thermocouple is suspended in the liquid and therefore frozen as well. When the different ammonia concentrations are frozen, they are removed from the freezer and then put at room temperature and room pressure to melt. A second thermocouple is placed on the top of the frozen substance. Both thermocouples are monitored

and the temperature is recorded when both thermocouples are surrounded by liquid and therefore no more frozen in. This is done by visual observations.

Required materials

- Vacuum chamber
- Vacuubrand MD1 vacuum pump
- Vacuubrand RZ6 vacuum pump
- A glass beaker
- About 0.1 liter of distilled water
- About 0.1 liter of 25% aqueous ammonia
- A measuring pipette
- An absolute pressure sensor
- A relative pressure sensor (HCLA12X5DU, First sensor, 0-12.5 $mbar \pm 0.016\ mbar$)
- A K-type thermocouples
- A camera
- A freezer
- Boiling chips
- Connected computer with LabVIEW

5.3. RESULTS

The experiment has two sets of results. The pure water phase diagram was created using the RZ6 vacuum pump which has enough pressure range to recreate the entire phase diagram needed. The ammonia experiments were done with the MD1 vacuum pump that is able to handle other chemicals than water. This pump cannot reach the triple point due to its limited pressure range. This will require some extrapolation.

5.3.1. PURE WATER

The full phase diagram of pure water is shown in Figure 5.6 with the pressure on the y-axis and the temperature on the x-axis. The time diagrams are shown in Figure 5.7 with temperatures and pressures plotted on the y-axis and the time plotted on the x-axis. The pure water experiment has been repeated five times with different starting temperatures and with and without boiling chips. These figures were created with the third experiment's results since this experiment showed the triple point the most clear compared to the other runs. This experiment began at room temperature and did not contain boiling chips. It can be seen from the irregular liquid-vapour line that the boiling was quite violent and did not follow the theoretical line. Experiments with boiling chips boiled less violently and followed the theoretical vapour line more closely (this is shown with the ammonia experiments in Figure 5.8). But with the boiling chips, the transition between liquid and solid was rather fast, not showing the triple point for very long. The violent boiling allows for longer triple point times. In this third experiment, the triple point (water in liquid, solid and gas phase) was shown for several seconds before freezing completely. The reason it always freezes eventually is that the pump continuously decreases the pressure and does not hold the triple point pressure.

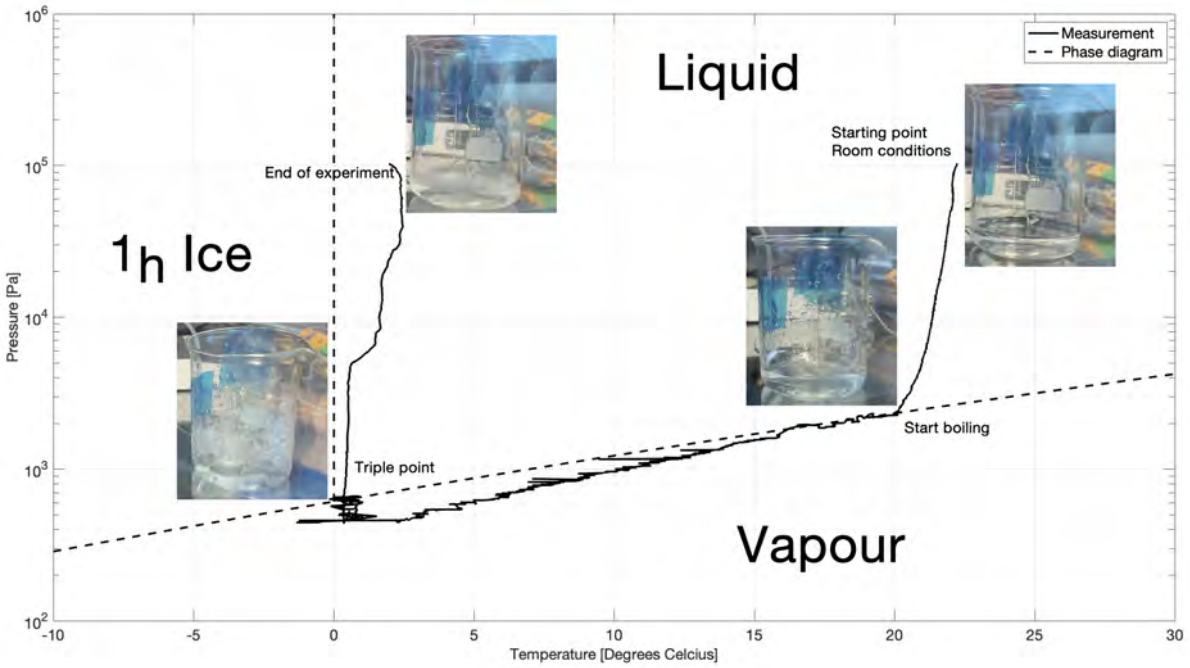

Figure 5.6: Results of experimental phase diagram of water (solid line) and the theoretical phase diagram (dashed line)

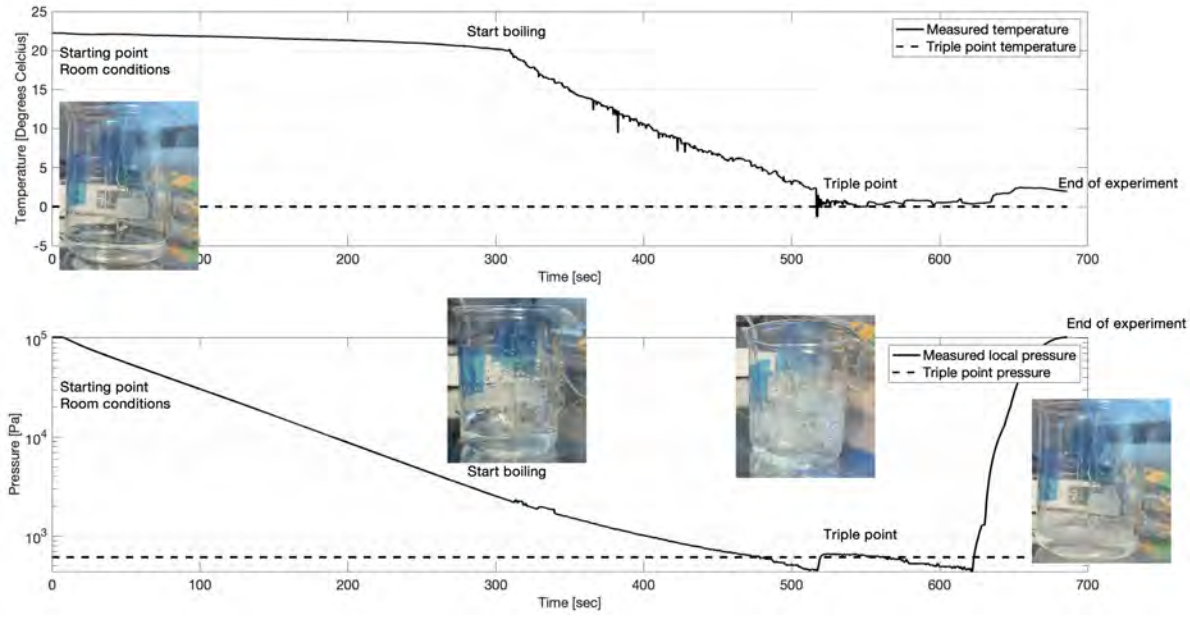

Figure 5.7: Results of experimental phase diagram of water (solid line) and the theoretical triple point (dashed line)

5.3.2. AMMONIA WATER

Since the solid-vapour transition for both pure ammonia and pure water is more or less a straight vertical line (ranging from atmospheric pressure to vapour pressure the temperature only varies by 0.01°), this line can be extrapolated by knowing the freezing point of the substance at atmospheric pressure. The liquid-vapour line can be extrapolated from a combination of the known water phase diagram and the measured ammonia water data. This together results in Figure 5.8 with pressure on the y-axis and temperature on the x-axis. The dashed lines are the theoretical phase changes of pure water. The dark blue lines are the measured phase changes of pure water and the light blue, red and green lines are the measured and extrapolated phase changes of different ammonia water concentrations. It can be seen that the pure water curve follows the

theoretical liquid-vapour line. The different percentages of ammonia water follow the expectations. The more ammonia present, the higher the vapour pressures are at similar temperatures and the lower the freezing points are. The estimated triple points of the different percentarges of ammonia water have, as expected, lower pressures and temperatures and are shown in Table 5.2.

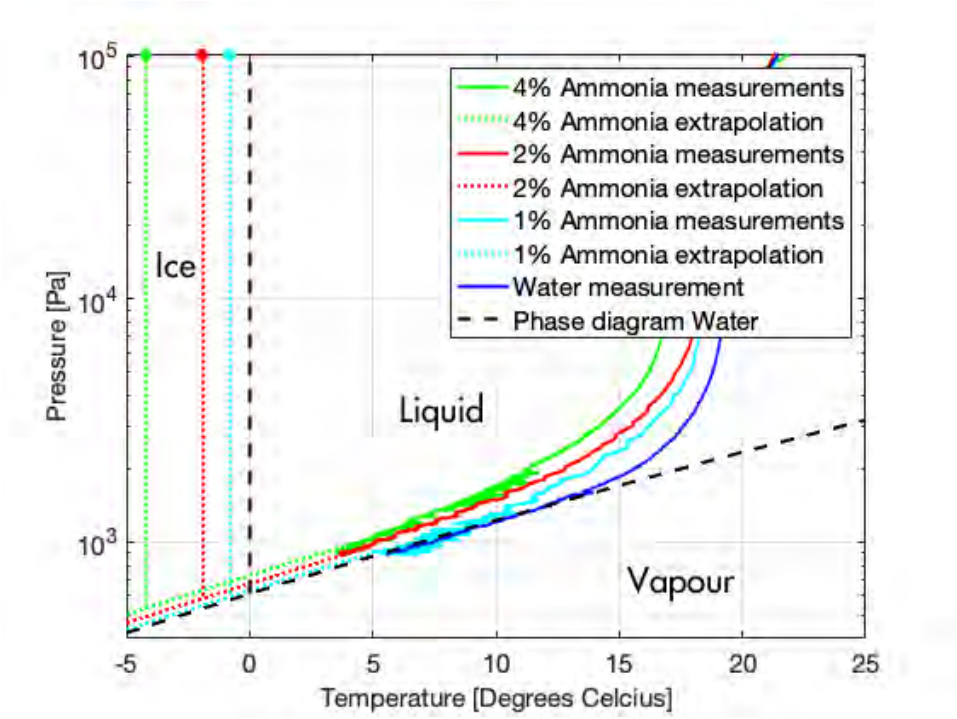

Figure 5.8: Results of experimental phase diagram of water and ammonia water (coloured solid lines and points), extrapolated phase diagram lines (coloured dashed lines) and the theoretical phase diagram of pure water (black dashed line)

Table 5.2: Expected triple points of different percentages of ammonia water

Ammonia concentration	0%	1%	2%	4%
Temperature [degrees Celcius]	0.0 ± 0.1	-0.8 ± 0.1	-1.9 ± 0.1	-4.2 ± 0.1
Pressure [Pa]	≈ 612	≈ 590	≈ 580	≈ 530

5.3.3. SODIUM-CHLORIDE WATER

In contrast with ammonia, which remains in a gaseous form when aqueous ammonia is vaporised, sodium-chloride leaves a residue in the form of salt crystals when aqueous sodium-chloride is vaporised. Due to the risk of damaging the vacuum chamber equipement and pump when these salt crystals are spread around by violent boiling, the experiments done to determine the phase diagram of ammonia water solutions was not repeated for sodium-chloride water solutions. Therefore, only the freezing temperatures or triple point temperatures of sodium-chloride are known and this incomplete phase diagram is shown in Figure 5.9 (the data for this figure was obtained from The Engineering Toolbox[4]). It is assumed that, as with ammonia, the influence of small concentrations of sodium-chloride on the triple point pressures are present, but very small.

[4] https://www.engineeringtoolbox.com/sodium-chloride-water-d_1187.html, last checked on 07-12-18

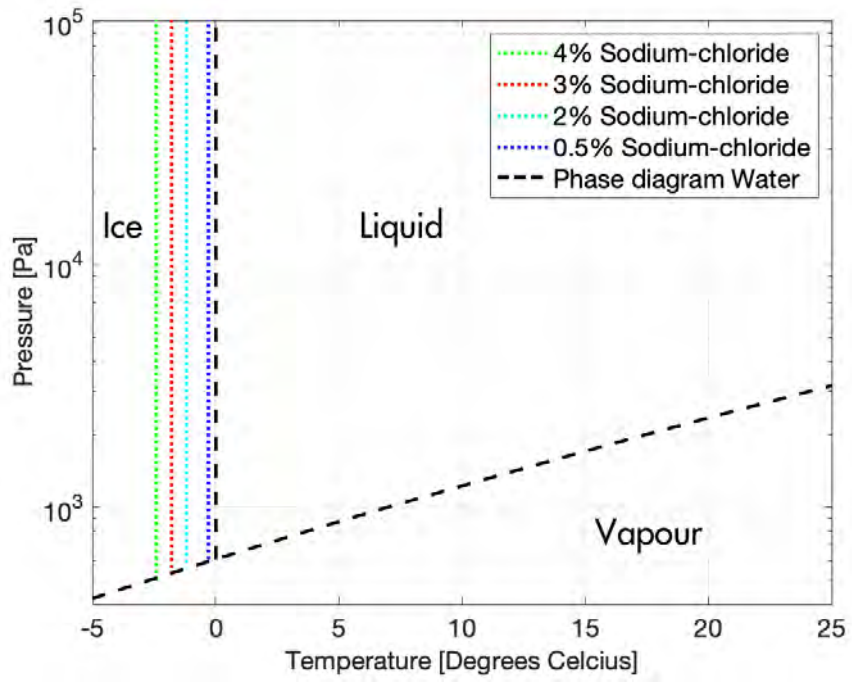

Figure 5.9: Partial phase diagram of sodium-chloride water (coloured dotted lines) and the theoretical phase diagram of pure water (black dashed line)

5.4. CONCLUSION

The effects of the two influencing factors on the to be designed model - ammonia and sodium-chloride - which are both present in Enceladus' ocean, have been investigated in this chapter. These will influence the design starting temperature and pressure in the next chapter. Ammonia and sodium-chloride are the most common elements besides pure water in Enceladus' ocean. The effects of small concentrations of ammonia had not yet been documented. It can be seen that both ammonia and sodium-chloride affect the triple point of the water. The triple point temperature and pressure both decrease, but only slightly. The triple point pressure of sodium-chloride water is assumed since that experiment could not be performed without risk of damaging the equipement. In the next chapter the model geometry will be designed which uses the triple point as a basis. Firstly based on pure water and afterwards based on the lowered possible triple points calculated here. The true effects of the lowered triple points will therefore be best visible at the end of the next chapter.

6

CHANNEL DESIGN

The design of the ice channel that allows for a plume to exist is a balance between observations of natural phenomena on Enceladus, the laws of physics and practical availabilities of equipement. This chapter explores this balance and finally comes to a design of the Enceladus plume replica ice crack. Section 6.1 gives some background information on natural occurring crevasses in ice. Section 6.2 explains how the supersonic plume can be realised, what the physical relations are and how to calculate the channel geometry. Section 6.3 links the evaporation of liquid in the ocean/reservoir to the area of the opening of the ice crack. Section 6.4 shows two methods of bringing the calculated ice shaped of the previous sections to a physical design. Section 6.5 brings all of the previous sections' results together in a design for a small test model of the Enceladus plume laboratory replica. Section 6.6 documents a first small scale experiment recreating the Enceladus plume based on this chapter. Section 6.7 draws some conclusions based on the design and experiment and proposes suggestions for the final design in Chapter 7.

6.1. CREVASSE

The fractures in the surface ice of Enceladus do not have perfectly nozzle shaped geometries. As such fractures are a result of moving ice layers and the resultant shear stresses due to this movement. When the combined normal and/or tensile stress on the ice sheet is higher than the tensile strength of the ice sheet, the ice forms a crack or crevasse (not to be confused with crevice which is a crack in a rock) in the direction of maximum tension [54]. These crevasses often have almost vertical walls, are much longer than their width and can be very deep. This is seen on Earth in crevasses in the ice sheets on the poles and on glaciers (see Figure 6.1). The depth of a crevasse depends on the stresses it is subjected to, but also on the temperature of the ice sheet. The yield strength of the ice increases with lower temperatures. On Earth it can indeed be seen that deeper crevasses occur in the colder polar regions [55]. While the tensile and normal stresses on the ice sheet tend to open a crevasse, the weight of the ice sheets tend to close it again [56]. The exact process that forms the crevasses on Enceladus is not yet fully understood but it is expected to be related to the tidal normal stresses[57] [58]. For this study it is not necessarily relevant to know this exact mechanism. It can be assumed that the fractures that allow for the existence of the Enceladus plumes are formed similarly and therefore have similar resultant shapes (long, deep and narrow). At some points the crevasse will reach all the way to the subsurface ocean creating a channel from the ocean to the surface. The shape will be highly random. The nozzle effect described in Section 6.2 is realised by taking into account the maximum and minimum openings along such a crevasse. A theoretical perfect nozzle shape is shown in Figure 6.2. In reality, a crevasse will not have perfect even slopes but it will have a more random ribbed structure.

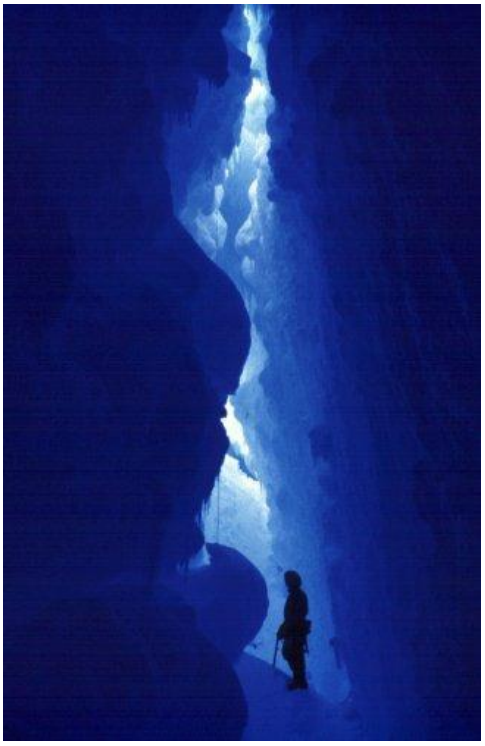

Figure 6.1: A cross section of a crevasse on Antarctica (Image credit Mtpaley. distributed under a CC BY-SA 2.5 license).

6.2. SUPERSONIC NOZZLE STRUCTURE

The design of the channel must be partially based on a supersonic nozzle mechanism with a horizontal flow direction (although Cassini measured plume exhaust velocities of Mach 3 to 5[2], due to the minimum achievable pressure of the available vacuum chamber, hypersonic velocities are not reachable. This is explained in more detail later in this chapter). The reservoir is connected to the global subsurface ocean of Enceladus and the channel is the crack trough the surface ice leading to the vent at the surface itself. A requirement for the design of the channel wall is that there need to be two fixed points: the smallest opening area close to the reservoir (or throat) and the largest opening area at the surface (or vent). The schematic design is shown in Figure 6.2.

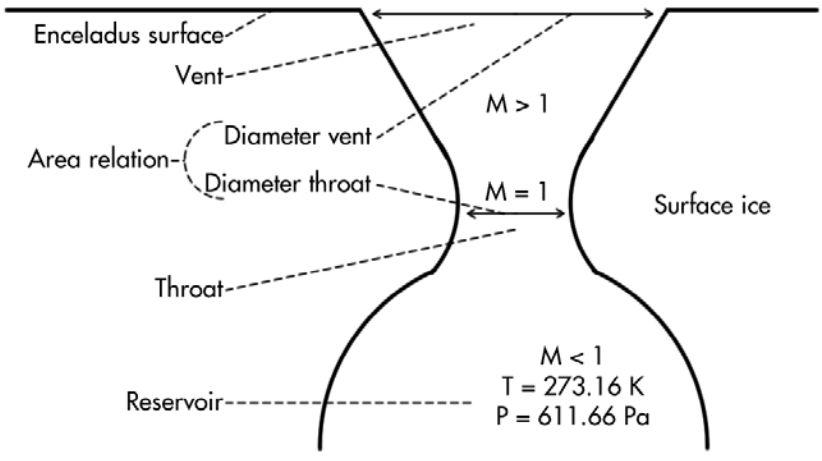

Figure 6.2: Schematic design for a subsurface converging-diverging Enceladus plume nozzle

The conditions at the reservoir require that liquid water, frozen water ice and water vapour are all present which is only possible at the triple point. For this first design it is assumed that the Enceladus surface and ocean consist of pure water (H_2O). However, in reality, it is expected that Enceladus water contains an ammo-

nia (NH_3) solution [23]. The presence of saltwater alters the triple point conditions [26]. But for this section pure H_2O is assumed. The conditions of the triple point of water are a temperature of 273.16 K and a pressure of 611.657 Pa [59] which are therefore also the conditions at the reservoir.

The design is required to accelerate slow moving water vapour from the reservoir to supersonic exhaust velocities based on known temperatures, pressures and physical characteristics of water vapour. It is assumed that this is an isentropic process (a reversible process where no heat is added or removed) or constant entropy process. The change in entropy (s) is given by equations 6.1 and 6.2 which, since entropy is constant, are equal to 0. P is pressure in Pa, T is temperature in K, R_{sp} is the specific gas constant in $\frac{J}{kg \cdot K}$, c_v is the specific heat at constant volume and c_p is the specific heat at constant pressure [37]. In these equations γ is the specific heat ratio: $\left(\gamma = \frac{c_p}{c_v}\right)$, the ratio of specific heat at constant pressure and constant volume which are related to the specific gas constant R_{sp}. v is volume and since volume is depending on density ρ, the volume ratio is equal to the density ratio.

$$\begin{aligned} s_2 - s_1 &= c_p \cdot ln\left(\frac{T_2}{T_1}\right) - R_{sp} \cdot ln\left(\frac{P_2}{P_1}\right) \\ 0 &= c_p \cdot ln\left(\frac{T_2}{T_1}\right) - R_{sp} \cdot ln\left(\frac{P_2}{P_1}\right) \\ \frac{P_2}{P_1} &= \frac{T_2}{T_1}^{\frac{cp}{Rsp}} \; with \; \frac{c_p}{R_{sp}} = \frac{\gamma}{\gamma - 1} \\ \frac{P_2}{P_1} &= \left(\frac{T_2}{T_1}\right)^{\frac{\gamma}{\gamma-1}} \end{aligned} \tag{6.1}$$

$$\begin{aligned} s_2 - s_1 &= c_v \cdot ln\left(\frac{T_2}{T_1}\right) + R_{sp} \cdot ln\left(\frac{v_2}{v_1}\right) \\ 0 &= c_v \cdot ln\left(\frac{T_2}{T_1}\right) + R_{sp} \cdot ln\left(\frac{v_2}{v_1}\right) \\ \frac{v_2}{v_1} = \frac{\rho_1}{\rho_2} &= \frac{T_2}{T_1}^{\frac{-c_v}{R_{sp}}} \; with \; \frac{c_v}{R_{sp}} = \frac{1}{\gamma - 1} \\ \frac{\rho_2}{\rho_1} &= \left(\frac{T_2}{T_1}\right)^{\frac{1}{\gamma-1}} \end{aligned} \tag{6.2}$$

Combing equations 6.1 and 6.2 results in the isentropic flow relations of equation 6.3 for an incompressible gas (subsonic flow) [37].

$$\frac{P_2}{P_1} = \left(\frac{\rho_2}{\rho_1}\right)^{\gamma} = \left(\frac{T_2}{T_1}\right)^{\frac{\gamma}{\gamma-1}} \tag{6.3}$$

Since the required velocities are supersonic, the flow of vapour will become compressible. The energy equation for frictionless flow where no heat it added or removed (based on the first law of thermodynamics) is given in equation 6.4 [37]. Here the subscript 1 denotes the situation at the reservoir and the subscript 2 denotes the situation at the vent. Since the velocity of the flow in the reservoir is 0, the equation can be reduced. This can then be put in a temperature ratio based on Mach numbers in which $a = \sqrt{\gamma R_{sp} T}$ is the speed of sound in m/s [37].

$$
\begin{aligned}
c_p T_1 + \frac{V_1^2}{2} &= c_p T_2 + \frac{V_2^2}{2} \\
c_p T_{reservoir} &= c_p T_{vent} + \frac{V_{vent}^2}{2} \\
\frac{T_{reservoir}}{T_{vent}} &= 1 + \frac{V_{vent}^2}{2 c_p T_{vent}} \\
\frac{T_{reservoir}}{T_{vent}} &= 1 + \frac{V_{vent}^2}{2\gamma R_{sp} T_{vent}/(\gamma-1)} \\
\frac{T_{reservoir}}{T_{vent}} &= 1 + \frac{V_{vent}^2}{2a^2/(\gamma-1)} \\
\frac{T_{reservoir}}{T_{vent}} &= 1 + \frac{\gamma-1}{2}\left(\frac{V_{vent}}{a}\right)^2
\end{aligned} \tag{6.4}
$$

This makes it possible to link the situation in the reservoir (zero velocity) and the vent (supersonic velocity). Filling in the Mach-velocity relation defined in equation 6.5 into equation reftotal results in the temperature relation based on the Mach number and specific heat ratio of equation 6.6 [37].

$$V = M \cdot \sqrt{\gamma R_{sp} T} = M \cdot a \tag{6.5}$$

$$\frac{T_{reservoir}}{T_{vent}} = 1 + \frac{\gamma-1}{2} M^2 \tag{6.6}$$

Filling in equation 6.6 in equation 6.3 results in equations 6.7 and 6.8.

$$\frac{P_{reservoir}}{P_{vent}} = \left(1 + \frac{\gamma-1}{2} M^2\right)^{\frac{\gamma}{\gamma-1}} \tag{6.7}$$

$$\frac{\rho_{reservoir}}{\rho_{vent}} = \left(1 + \frac{\gamma-1}{2} M^2\right)^{\frac{1}{\gamma-1}} \tag{6.8}$$

The geometry of such a channel is based on a converging-diverging nozzle where the pressure difference between the reservoir and the conditions at the vent, the gas is accelerated to Mach 1 converging at the throat and higher Mach-numbers at the diverging nozzle (vent)[37]. This is the case on Enceladus where the pressure in the reservoir is at the triple point pressure (relatively high pressure) and the conditions at the vent are close to the vacuum of space (relatively low pressure). Since the conditions (temperature and pressure) in the reservoir are known and the exhaust velocity in terms of Mach-numbers (M) are chosen, the temperature at the vent can be calculated with the relation shown in Equation 6.6, the pressure at the vent can be calculated with the relation shown in Equation 6.7, the density (ρ in $\frac{kg}{m^3}$) along the channel can be calculated with equation 6.8 and the exhaust velocity (V in $\frac{m}{s}$) can be calculated with equation 6.5[37]. The mass flow ($\dot{m}$ in $\frac{kg}{s}$) through such a nozzle is given by equation 6.9 and is the same at every point along the nozzle or channel.

$$\dot{m} = \rho_{throat} \cdot V_{throat} \cdot A_{throat} = \rho_{vent} \cdot V_{vent} \cdot A_{vent} \tag{6.9}$$

Rewriting equation 6.9 into a vent-to-throat area relation, squaring it and taking into account the velocity at the throat is Mach 1 which is the speed of sound in the throat a_{throat} results in equation 6.10 [37].

$$
\begin{aligned}
\frac{A_{vent}}{A_{throat}} &= \frac{\rho_{throat} \cdot a_{throat}}{\rho_{vent} \cdot V_{vent}} = \frac{\rho_{throat} \cdot \rho_{reservoir} \cdot a_{throat}}{\rho_{reservoir} \cdot \rho_{vent} \cdot V_{vent}} \\
\left(\frac{A_{vent}}{A_{throat}}\right)^2 &= \left(\frac{\rho_{throat}}{\rho_{reservoir}}\right)^2 \left(\frac{\rho_{reservoir}}{\rho_{vent}}\right)^2 \left(\frac{a_{throat}}{V_{vent}}\right)^2
\end{aligned} \tag{6.10}
$$

In equation 6.10 $\left(\frac{\rho_{reservoir}}{\rho_{vent}}\right)^2$ can be taken from equation 6.8 and $\left(\frac{\rho_{throat}}{\rho_{reservoir}}\right)^2$ can also be taken from equation 6.8 by filling in $M = 1$ and inverting it. $\left(\frac{a_{throat}}{V_{vent}}\right)^2$ comes from the first line of equation 6.4 but since this time

the left hand side does not show the situation at the reservoir but at the throat, the velocity is not zero but Mach 1 (or a_{throat}) [37].

$$\begin{aligned} c_p T_{throat} + \frac{V_{throat}^2}{2} &= c_p T_{vent} + \frac{V_{vent}^2}{2} \\ & \quad with \;\; c_p = \frac{R_{sp}\gamma}{\gamma - 1} \\ \frac{\gamma R_{sp} T_{throat}}{\gamma - 1} + \frac{V_{throat}^2}{2} &= \frac{\gamma R_{sp} T_{vent}}{\gamma - 1} + \frac{V_{vent}^2}{2} \\ & \quad with \;\; a = \sqrt{\gamma R_{sp} T} \\ \frac{\gamma + 1}{2(\gamma - 1)} a_{throat}^2 &= \frac{a_{vent}^2}{\gamma - 1} + \frac{V_{vent}^2}{2} \\ \left(\frac{V_{vent}}{a_{throat}}\right)^2 &= \frac{[(\gamma + 1)/2]M^2}{1 + [(\gamma - 1)/2]M^2} \end{aligned} \tag{6.11}$$

Combining all this will result in equation 6.12, the relation between the area of the throat and the area of the vent depending on the Mach number and specific heat ratio [37].

$$\left(\frac{A_{vent}}{A_{throat}}\right)^2 = \frac{1}{M^2}\left(\frac{2}{\gamma + 1}\left(1 + \frac{\gamma - 1}{2}M^2\right)\right)^{\frac{\gamma+1}{\gamma-1}} \tag{6.12}$$

The specific heat ratio γ is dependent on the environmental conditions but it is not known for all conditions. White [59] gave the specific heat ratio for pure water at a number of temperatures which are given in Table 6.1.

Table 6.1: Specific heat ratio for pure water at different temperatures

Temperature [$^\circ C$]	γ [-]
20°	1.330
100°	1.324
200°	1.310

In this study an estimate will be provided by extrapolating the specific heat ratio to the triple point temperature of 0.01$^\circ C$. This results in a specific heat ratio of 1.331.

6.3. EVAPORATION RATE

In Section 6.1 it was set that the shape of the crack in the ice should be rectangular and in Section 6.2 the relation between the throat and vent areas has been found. Now the actual size of the throat (and therefore the vent) have to be estimated. To achieve the supersonic flow at the vent, a certain mass flow through the throat should be reached that is required for a Mach 1 velocity in the throat [37]. Equation 6.13 shows the closed-form for the mass flow of a choked nozzle (the limiting situation where the mass flow rate will not increase when the exit pressure is further reduced). This occurs when the velocity in the throat is Mach 1 [37]) in which $\dot{m}$ is the mass flow in kg/s, $T_{reservoir}$ is the temperature in the reservoir in K, $P_{reservoir}$ is the pressure in the reservoir in Pa, R_{sp} is the specific gas constant in $\frac{J}{kg \cdot K}$ and A_{throat} is the area of the throat in m^2. This relation is found by filling in a velocity of Mach 1 (the speed of sound of equation 6.5), the equation of state $\left(\rho = \frac{P}{R_{sp}T}\right)$ and isentropic flow equation 6.3 in the mass flow equation of 6.9.

$$\dot{m} = \frac{P_{reservoir} A_{throat}}{\sqrt{T_{reservoir}}} \sqrt{\frac{\gamma}{R_{sp}}\left(\frac{2}{\gamma + 1}\right)^{\frac{\gamma+1}{\gamma-1}}} \tag{6.13}$$

To now calculate the optimal throat area, the achievable mass flow needs to be known. The mass flow should be equal to the water vapour per second that is evaporating in the reservoir. This can be estimated by the

evaporation formula from Hertz, Knudsen & Langmuir in equation 6.14. P_{vapour} is the vapour pressure of the evaporating liquid in Pa, $P_{ambient}$ is the ambient pressure in the reservoir, M_{molar} is the molar mass of the evaporating liquid in $\frac{kg}{mole}$, R is the universal gas constant in $\frac{J}{mole \cdot K}$, $T_{ambient}$ is the ambient temperature of the reservoir in K, N are the number of evaporating particles, N_A is Avogadro's constant, t is time in seconds and $A_{evaporation}$ is the evaporation area which is the area of the liquid that is exposed to the lower pressure of the reservoir in m^2 and α is the sticking coefficient (ratio of absorption rate to the number of collisions) of the evaporation liquid. [53].

$$\frac{1}{A_{evaporation}} \frac{dN}{dt} = \alpha (P_{vapour} - P_{ambient}) \frac{N_A}{\sqrt{2\pi M_{molar} R T_{ambient}}} \tag{6.14}$$

Equation 6.14 is rewritten to a mass flow form in equation 6.15 in which also the molar mass and the universal gas constant are replaced with the specific gas constant.

$$\begin{aligned}
\frac{1}{A_{evaporation}} \frac{dN}{dt} &= \alpha (P_{vapour} - P_{reservoir}) \frac{N_A}{\sqrt{2\pi M_{molar} R T_{reservoir}}} \\
\frac{dN \cdot M_{molar}}{dt \cdot N_A} &= \alpha (P_{vapour} - P_{reservoir}) \frac{M_{molar}}{\sqrt{2\pi M_{molar} R T_{reservoir}}} \cdot A_{evaporation} \\
\dot{m} &= \alpha (P_{vapour} - P_{reservoir}) \sqrt{\frac{M_{molar}}{2\pi R T_{reservoir}}} \cdot A_{evaporation} \\
\dot{m} &= \alpha (P_{vapour} - P_{reservoir}) \sqrt{\frac{1}{2\pi R_{sp} T_{reservoir}}} \cdot A_{evaporation}
\end{aligned} \tag{6.15}$$

Combining equations 6.13 and 6.15 results in equation 6.16 which relates the evaporating reservoir area to the choked throat area. It can be seen that $T_{reservoir}$ and R_{sp} cancel out. The area of the throat is therefore only dependant on the area of the reservoir, the specific heat ratio of the liquid in the reservoir and the ratio of vapour pressure and reservoir pressure (which can be calculated with the inverse of equation 6.7 with the Mach number set to 1). The area vent (equation 6.12) only depends on the design Mach number, throat area and specific heat ratio and is therefore also independent of the temperature in the reservoir.

$$\begin{aligned}
\dot{m} = \alpha (P_{vapour} - P_{reservoir}) \sqrt{\frac{1}{2\pi R_{sp} T_{reservoir}}} \cdot A_{evaporation} &= \frac{P_{reservoir} A_{throat}}{\sqrt{T_{reservoir}}} \sqrt{\frac{\gamma}{R_{sp}} \left(\frac{2}{\gamma + 1} \right)^{\frac{\gamma+1}{\gamma-1}}} \\
\alpha \left(\frac{P_{vapour}}{P_{reservoir}} - 1 \right) \sqrt{\frac{1}{2\pi}} \cdot A_{evaporation} &= A_{throat} \sqrt{\gamma \left(\frac{2}{\gamma + 1} \right)^{\frac{\gamma+1}{\gamma-1}}} \\
A_{throat} &= \frac{\alpha \left(\frac{P_{vapour}}{P_{reservoir}} - 1 \right) \sqrt{\frac{1}{2\pi}}}{\sqrt{\gamma \left(\frac{2}{\gamma+1} \right)^{\frac{\gamma+1}{\gamma-1}}}} \cdot A_{reservoir}
\end{aligned} \tag{6.16}$$

The area of the reservoir, the reservoir pressure and the Mach number are design choices. The sticking coefficient, specific heat ratios and vapour pressures are physical constants. The specific heat ratios and vapour pressures of pure water and pure ammonia are 1.331 and 1.310 respectively and therefore very similar [59]. The vapour pressure of different ammonia water concentrations was determined in Chapter 5. The specific heat ratio and vapour pressure of sodium-chloride solutions are unknown, but as is the case with ammonia, the small concentrations are assumed to have little effect on the overal vapour pressure and specific heat ratio of the liquid reservoir. The sticking coefficient ranges from 0 to 1 and therefore can be a very large influencing factor. The estimated sticking factor for water around the triple point is 0.7 [60].
The area of the reservoir should be taken as large as possible to get as much mass flow as possible. And since this area is limited to the maximum diameter of the testing-case of the vacuum chamber, all the dimensions of the crevasse will follow from this limit. With the relation developed above an equilibrium situation can be designed where the mass flow generated by the evaporation is equal to the mass flow needed in the choked

nozzle to get supersonic speeds. As long as there is an evaporating liquid in the reservoir, the plume should keep erupting. It can be seen that to have an evaporating liquid, the pressure in the reservoir should be lower than the vapour pressure of this liquid. The triple point is the lowest combination of temperature and pressure where water can remain liquid. But at the exact triple point, the vapour pressure is equal tot the triple point pressure. Looking at Equation 6.15 both pressures will cancel out and there will be no mass flow theoretically. To prevent the reservoir from freezing completely, the reservoir temperature needs to be equal or higher than the triple point temperature. It is assumed here that the reservoir temperature will remain the triple point temperature to mimic the expected conditions of Enceladus. To have evaporation, the reservoir pressure needs to be lower than the vapour pressure and therefore lower than the triple point pressure. The lower the reservoir pressure is when compared to the vapour pressure, the faster the liquid will evaporate and therefore the higher the mass flow will be. But at the same time, with a lower reservoir pressure, the difference between reservoir pressure and vent pressure (which is limited by the minimal achievable pressure of the equipement) becomes smaller. And with a smaller difference between reservoir and vent pressure, the velocity increase will be smaller as well. A compromise has to be found here. This is a design choice.
It should be noted that the calculations above are the theoretical best case scenario of the maximum mass flow. In reality due to the unpredictability of situations around the triple point, the mass flow will most likely be less than estimated with the relations above. This implies that the resultant throat and vent areas based on these relations are maxima.

6.4. MOULD

With the ability to calculate the throat and vent opening areas of the crevasse, a method has to be found to make this ice-shape. The dimensions are quite specific and require a small error margine (the smaller the set-up, the smaller the error is allowed to be since the area ratio needs to be kept). Otherwise the desired effect will not be reached. To make the experiment repeatable, the ice should preferably have the same shape every time the experiment is performed. Therefore a mould will be used to force the ice to have the same shape every time. Two mould options are investigated in this section which are the inverse of each other. The first mould has the shape of the ice and the second option has the shape of the crevasse.

6.4.1. MOULD OPTION 1: DEPOSITION OF WATER FROM AIR ON COOLED MOULD

In this first option, the mould will have the shape of the crevasse. The mould is cooled to the desired temperature and then exposed to (humid) air. The water vapour in the air will freeze on the mould and create a small ice layer. The minimum requirement for this experiment are that the outer layer of the crevasse is made of ice. This mould option complies with this requirement. The material of the mould should be highly conductive to be able to let water freeze onto it. Plastic is not ideal for this and therefore the mould should be made out of metal. To cool the mould (more precisely the surface of the mould), channels in the mould are created through which a coolant can flow. Figure 6.3 shows a schematic view of this design.

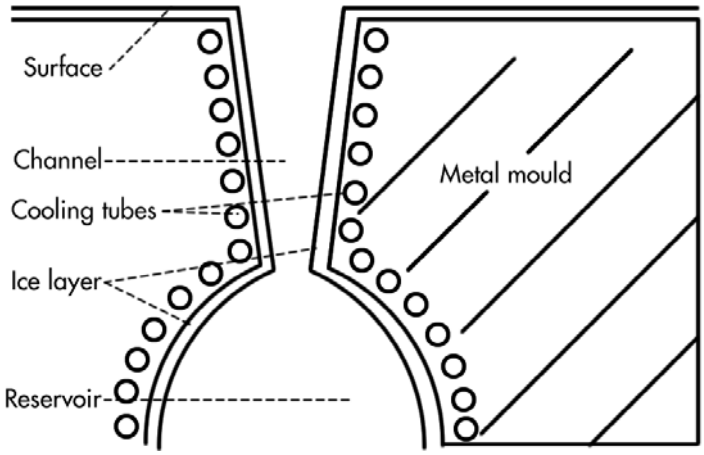

Figure 6.3: Schematic overview for mould option 1: Deposition of water from air on frozen mould

The benefit of this model is that the use of coolant ducts through the mould throughout the experiment keeps the ice layer at a constant temperature. A coolant flow connection in the vacuum chamber can be used

to keep cooling the model during the experiment. In a small model, the temperature will be uniform, but in a larger (longer) version of this model a temperature gradient might occur. This has to be managed.

The disadvantage of this option is that the deposited ice on the mould is difficult to control. There exist multiple models that can estimate the growth of ice on a cold flat metal surface based on parameters as air temperature, metal surface temperature, air velocity and air humidity, but ice rarely grows uniformly [61]. The layer thickness varies along the surface which makes it difficult to prepare the crevasse exactly as calculated. Moreover, the crevasse will change with every experiment (albeit slightly) depending on the conditions of the air present ar the day of the experiment. Another drawback is that since there is only a little ice-layer present, other future experiments (that for example try to drill a probe in the channel) are not possible with this design. Only experiments with the plume itself can be performed.

6.4.2. MOULD OPTION 2: FREEZE WATER IN ICE CUBE SHAPE AND REMOVE MOULD WHEN FROZEN

In this second option, the mould will have the shape of the crevasse. The mould is placed inside a tube and the water (or ammonia-solution) is poured around it. The tube, mould and water are then cooled. When the water is frozen, the mould pieces are removed creating an ice-cube with a crevasse in it. Due to the shape, the mould has to consist of two parts that are removed from the top and bottom. The material chosen for this mould should be able to withstand cold temperatures without becoming too brittle and should not float in (ammonia) water solutions. Plastics are therefore again not desirable and metals are preferred. This schematic view of the design is shown in Figure 6.4.

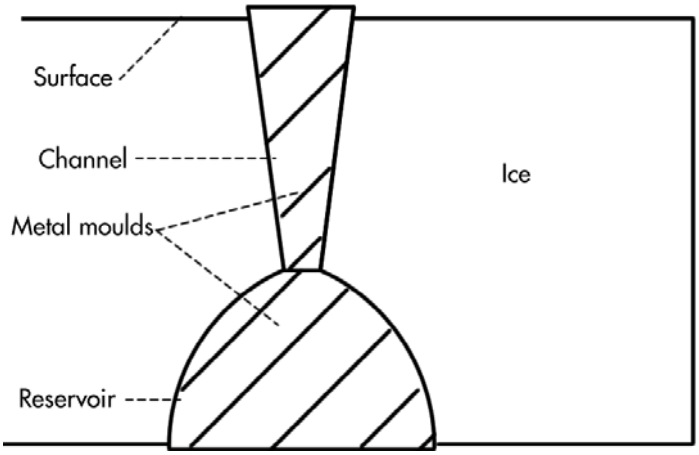

Figure 6.4: Schematic overview for mould option 2: Freeze water in ice cube shape and remove when frozen

The benefits of this model is that the crevasse will have the determined dimensions and will have the same dimensions from one experiment to another. The design is also not dependant on the consistency of the air. Therefore other solutions like ammonia water can also be used to make the ice shape (which is more true to nature). With this design it is possible to perform other future experiments that probe the ice near a plume, making this design multi purpose. It can also be adaptable. The exhaust velocity is dependant on the area ratio of the vent and throat. The top mould part can be interchanged for different top mould parts with the same throat area but different vent area's that will result in different exhaust velocities depending on the nature of the experiments.

A drawback of this design is that the ice is not kept at a constant temperature during the experiment. Furthermore, since the top plate will be quite thin (in the range of a few millimetres) there is a risk of breaking the mould, especially if it has to be removed from its frozen water position with a little force.

6.4.3. FINAL MOULD OPTION

Based on all the advantages and disadvantages mentioned above, the preference has been given to design option 2. This option will result in a higher accuracy of the channel shape, a higher repeatability accuracy and is a more multi purpose design than option 1 as can be seen in Table 6.2.

Table 6.2: Selection table for both design options

	Geometry precision	Temperature control	Pressure control	Ease of use	Ease of manufacturing	Reusability	Use for future experiments	Total
Option 1	-	++	0	+	-	++	-	2
Option 2	+	0	0	0	+	+	++	5

6.5. CREVASSE DESIGN

As shown above, there are a few physical restrictions that influence the design such as the relation between evaporation area, throat area and vent area. Next to that there are a few practical restrictions to the design. The south polar crevasses on Enceladus are a few kilometers deep and therefore, to make the design as accurate as possible, the laboratory crevasse should be as long as possible. Furthermore, there is approximately a 1 to 3 ratio between the diameter and the length of the test cylinder available at the FH University of applied sciences in Aachen (as shown in Section 4.2). The preferred case will be to use the full available diameter as crevasse width. But that would result in two loose ice blocks facing each other. There needs to be a connection between the ice blocks otherwise the required throat and vent area will be impossible to control. Next to that, it may be preferred that there is a view of the cut of the crevasse. Therefore, the crevasse will be 'open' on one side, but closed by ice on the opposite side for support (see the horizontal ice cuts column in Figure 6.5). The ice form will be created by placing the two inverse mould-pieces in a tube which, when filled with liquid, will create the required crevasse cut-out when removed from the frozen substance. The two pieces are the bottom, hollowing out the reservoir to the throat, and the top. hollowing out the throat to the vent (see the right column of Figure 6.5). The ice model will be placed inside a see-through tube. To make sure one side is pressed against the wall of the tube, a bottom plate is added with the maximum diameter of the tube forcing the open end of the crevasse to form against the tube wall. The bottom area of the reservoir needs to be as large as possible to have the largest possible mass flow generation.

6.5.1. EFFECTS OF DIFFERENT TRIPLE POINTS ON CREVASSE DESIGN

As discussed in Section 5.4 the effects of ammonia and sodium-chloride that lowered the triple points on the crevasse dimensions have to be investigated. Also the difference specific heat ratios have been taken into account here. These results are summarised and compared to the pure water scenario in Table 6.3. Since the effects of sodium-chloride on the triple point pressures are not known, only the triple point temperatures are taken into effect and the triple point pressure is assumed to be unaltered from pure water. Table 6.3 shows the slid-widths of the throat and the vent for both a first design of the large scale version for Aachen and the smaller one-third version to be used in the facilities in Delft (this is explained more in the next section). It can be seen that the influence of lowering the triple point pressure and temperature due to the addition of ammonia has some effect on the widths of the throat and vent ranging from 4% to 15%. Since the expected concentration of ammonia is closer to the lower end of this range, such a resulting 4% change in throat and vent widths is considered negligible since those are also the expected error margins of producing the mould. Therefore, the same model can be used for both pure water experiments and ammonia water experiments. With the lack of vapour pressure data of sodium-chloride solutions, the effect of sodium-chloride on the design cannot be determined. Though it is expected that the effects of sodium-chloride are similar to those of ammonia based on the comparable freezing temperatures for comparable concentrations. But this will require further study. Based on the data above a design will be proposed for a pure water version of the experiment which can also be used for low concentrations of ammonia water and most likely also for low concentrations of sodium-chloride water.

Table 6.3: Comparative throat and vent slid-widths due to varying triple points by using ammonia

		Pure water	Ammonia		
			1%	2%	4%
Small Delft version	Throat [mm]	3.893	4.055	4.135	4.586
	Vent [mm]	5.840	6.083	6.203	6.879
Large Aachen version	Throat [mm]	12.54	13.06	13.32	14.78
	Vent [mm]	18.81	19.59	19.98	22.17

6.5.2. SMALL CREVASSE MODEL DESIGN SPECIFICATIONS

To perform a test with a small model at Delft University of Technology before creating the larger model for the FH University of applied sciences in Aachen, the maximum printable area of the 3D printer sets a practical limit on the smaller test model. The maximum diameter is 10 cm. Which together with the 1 to 3 ratio set by the facilities in Aachen results in a 30 cm long test model. All the design choices and results are shown in Figure 6.5. A margin of 1.00 cm is chosen for both the back connecting ice and the bottom plate. This results in a crevasse length and reservoir diameter of 9 cm.

As discussed in Section 6.3, a compromise needs to be made between the maximum achievable plume velocity and the achievable mass flow due to evaporation. The reservoir pressure needs to be below the vapour pressure but the lower the reservoir pressure, the lower the maximum achievable exit velocity can be. This design choice is made here. Using equation 6.7 with the minimum achievable pressure of 70 Pa (see Chapter 4) a maximum achievable Mach number of 2.00 can be achieved with a reservoir pressure of 540 Pa (about 72 Pa less than the vapour pressure). This is the starting point for the design. The Mach number at the vent in the design needs to be above 1.00 and below 2.00. Choosing a Mach number close to the upper limit is not practical since there may be all sorts of unforeseen circumstances that will increase this limit. A Mach number at the vent of 1.826 is chosen which results in a practical 1.50 vent-to-throat area ratio. The length of the rectangular throat and vent openings were set to be 9 cm by the evaporating area. All of these inputs for equations 6.12 and 6.16 results in a throat width of 3.9 mm and a vent width of 5.8 mm. Based on the mass flow from equation 6.15 and the volume of the liquid in the reservoir based on a 9 cm diameter and 1 cm height, a Mach 1.83 plume can theoretically be sustained for 177 seconds under perfect conditions (note that the starting-up phase would affect this since there will be partial boiling before the required conditions are reached). A small hole is made in the plastic tube at the hight of the reservoir. During freezing the mould is placed such that the mould covers the hole. When the mould is removed, the hole opens right in the reservoir. The hole serves as an opening to pour in the liquid water before the experiment and as a connection port for the temperature and pressure sensors since both sensors cannot handle long periods of being frozen and therefore have to be placed right before the experiment begins. The pressure sensor has an opening of 3 mm in diameter, the temperature sensor has a connecting cable of 1 mm in diameter. Therefore the hole needs to be 4 mm in diameter. The hole should be plugged when the sensors are placed during the experiment to prevent loss of pressure in the reservoir through this hole.

Figure 6.6 shows the supersonic nozzle specifications in which the available Mach number range is displayed (Mach 1.00 to Mach 2.00) and the design Mach number with its effects. The top graph shows the vent-to-throat ratio, the second graph shows the temperature at the exit, the third graph shows the velocity at the exit and the bottom graph shows the pressure at the exit. This figure is independent of set-up size and can be used to obtain the necessary exit pressure, the resultant exit velocities and temperature for all design Mach numbers between 1.00 and 2.00.

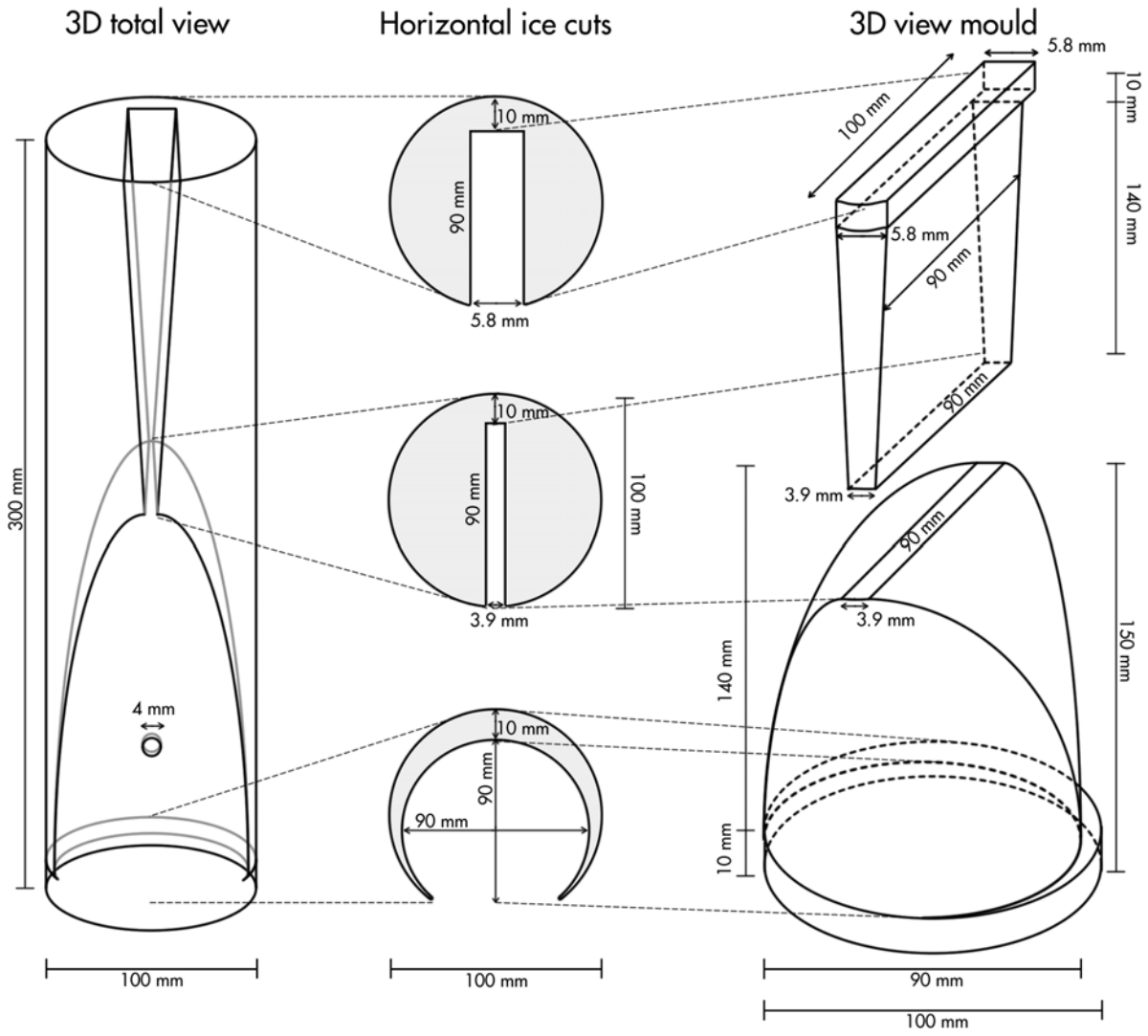

Figure 6.5: Design specifications of the small model

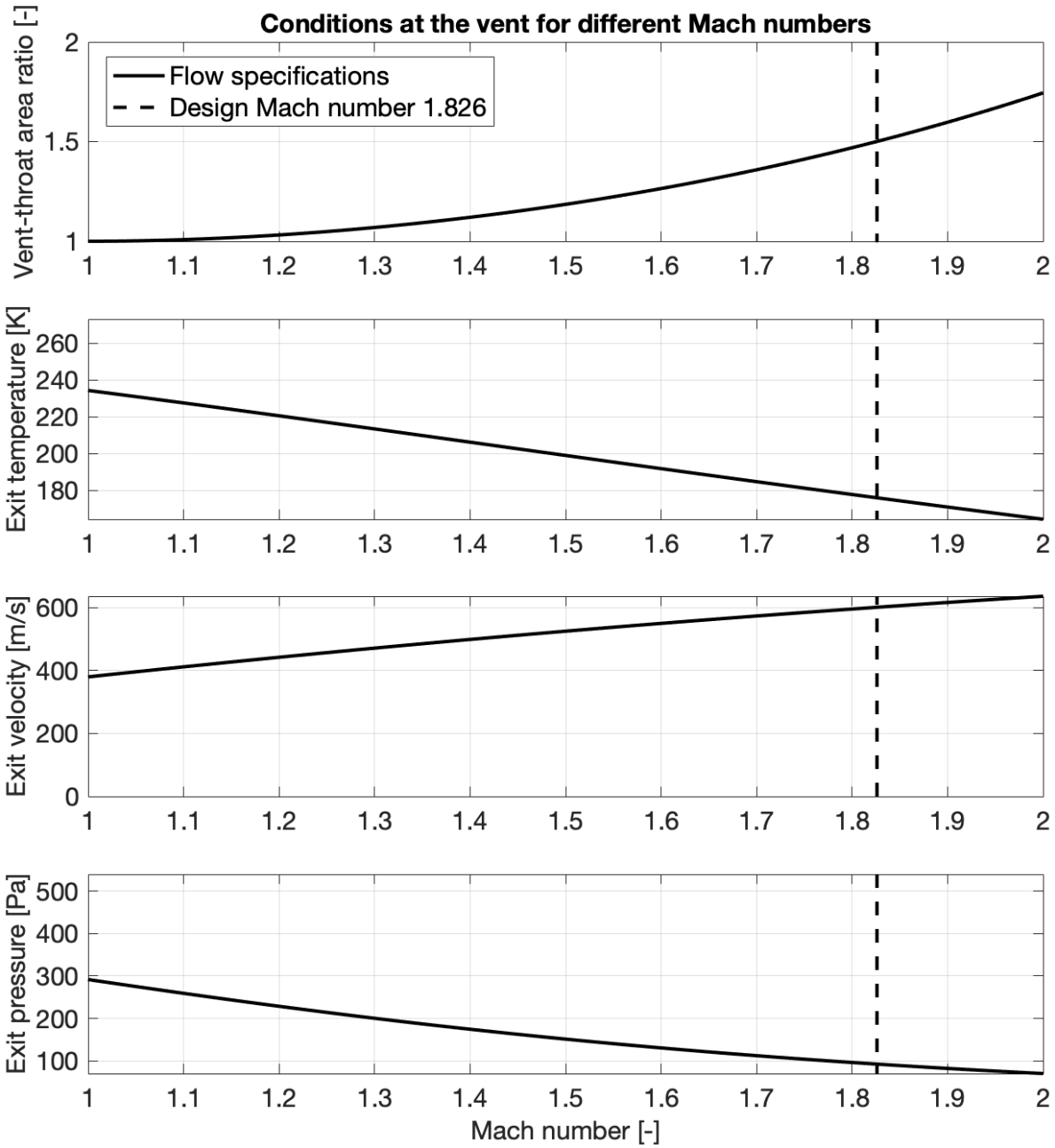

Figure 6.6: Supersonic nozzle specifications with throat-vent area ratio, temperature, exhaust velocity and pressure for an achievable interval of Mach 1 to Mach 2

6.6. EXPERIMENT

The purpose of this experiment is to test the validity and feasibility of a large scale Enceladus plume experimental set-up by creating first a small scale version. This has the that several parts of the full size laboratory set up can be tried out at relatively low cost and unforeseen practical issues can be discovered. The right panel of Figure 6.7 shows the graphical representation of the set-up for this experiment. It consists out of a vacuum chamber connected to a vacuum pomp (in a simple graphical representation). Inside the vacuum chamber the tube with the ice shape is present. The bottom of the reservoir is filled with liquid water. Due to the limitations of the available chemical Vacuubrand MD1 vacuum pump, a pure water version of this experiment is performed which allows the use of the more efficient Vacuubrand RZ6 pump. The pressure control, the temperature control and the preparation of the liquid are similar to the experiment performed in Section 5.2.

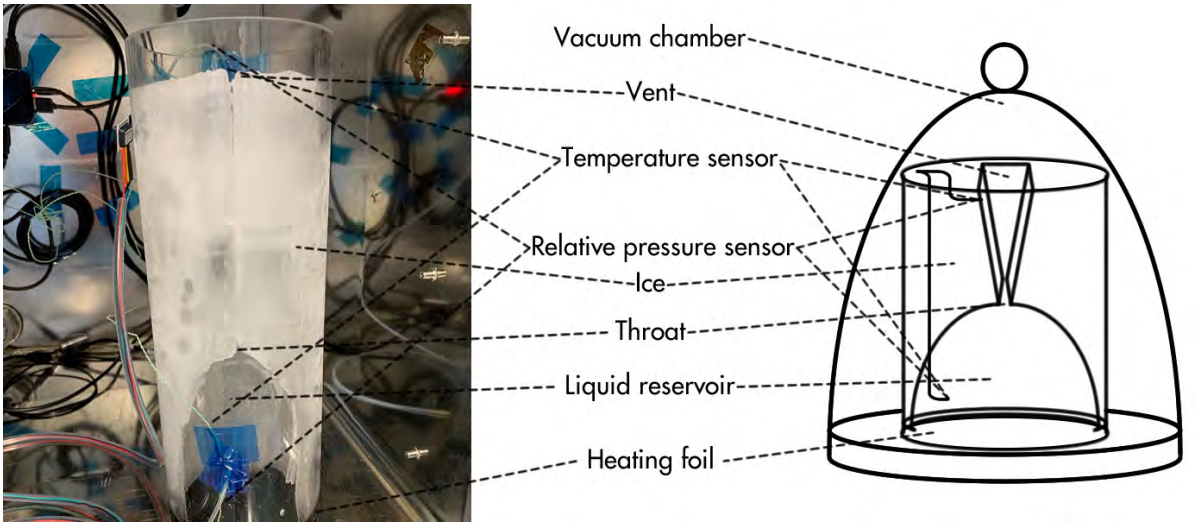

Figure 6.7: Set-up for the mini plume simulator. The right shows a graphical representation of the set-up (not to scale) and the left shows a photograph of the actual mini plume simulator in the vacuum chamber with all the sensors connected.

Preparing the ice The steps to prepare the ice are shown in the serie of photographs in Figure 6.8.

(A) The two mould pieces (right column of Figure 6.5) are placed inside the see-through plastic tube.

(B) To make the plastic mould pieces easily removable when covered in ice, a plastic layer is put around the two mould pieces. (In the photo it seems like the plastic is rather loose around the mould pieces. But the weight of the water will press the plastic layer against the mould pieces).

(C) The water is poured around the mould pieces and filled to the top of the mould (not the top of the tube since frozen water expands). The filled tube it placed in the freezer until the liquid is completely frozen. (for freezing without internal cracks, this can be done in multiple layers, slowly filling the tube).

(D) The tube is taken out of the freezer for about half an hour so the sides melt a little making it easier to remove the bottom mould piece from the tube.

(E) The top mould part is then removed including all the remaining plastic layers and a cap is placed on the bottom of the tube, closing the reservoir. Special attention has to be given making sure that the hole in the tube lines up with the open part of the reservoir. The finished ice is placed back in the freezer until the experiment starts.

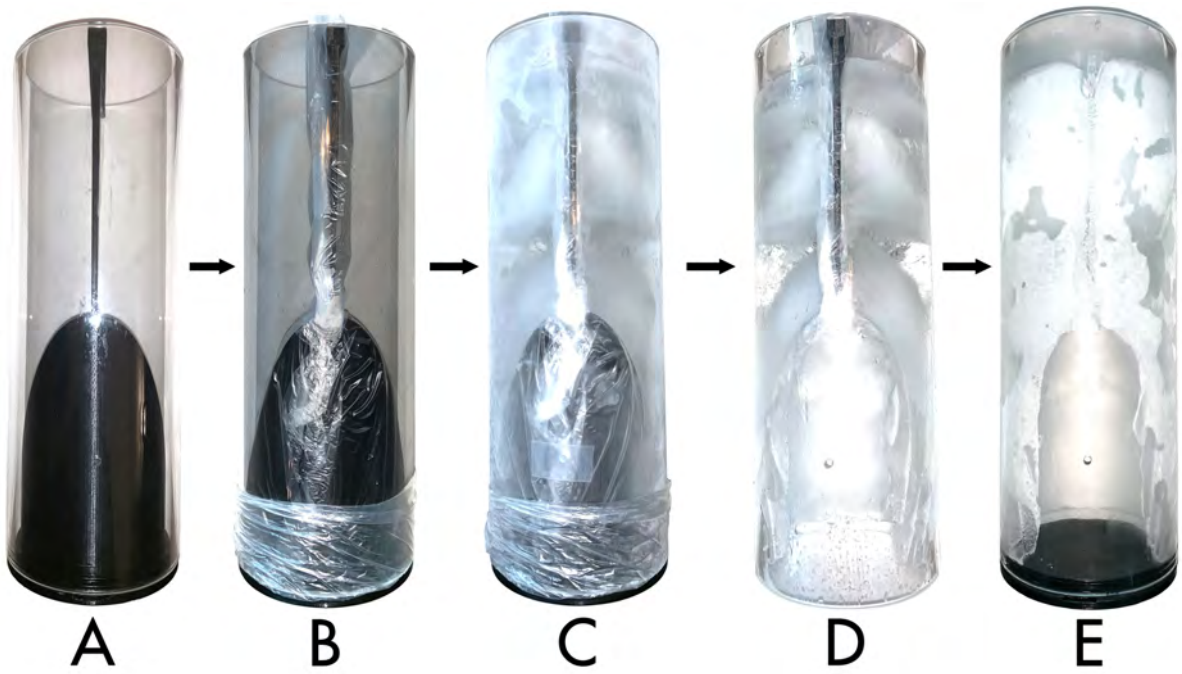

Figure 6.8: Experiment preparation. A: tube and two mould pieces. B: cover mould pieces in plastic layer. C: Pour water in tube and freeze. D: Remove bottom mould piece. E: remove top mould piece, plastic layers and place bottom cap.

Before the experiment, the ice is removed from the freezer. A layer of liquid water of about 1 cm high is poured through the reservoir hole in the reservoir. The thermocouple and high pressure port tube of the pressure sensor are placed inside the reservoir hole and the hole is closed off with tape so no vapour can escape through the hole. The other thermocouple and high pressure port tube of the pressure sensor are placed at the vent of the ice. See left of Figure 6.7. A heating foil is placed in a hollowed out version of the bottom cap that closes the bottom side of the see-through tube (see Figure 6.9). Earlier versions of this experiment did not contain this heating foil. Since the physical process of boiling takes away energy from the liquid water, the reservoir froze over completely a few seconds after the triple point was reached. This heating foil allows the temperature of the reservoir to be controlled so the reservoir stays liquid until all the liquid has boiled away.

Figure 6.9: Bottom view of the bottom cap of the see-through tube. This cap is hollowed out and a heating foil is placed close to the surface allowing to control the temperature in the reservoir without the risk of short circuiting since no water comes in to contact with the electronics

Performing the experiment The prepared tube with ice and liquid is placed in the vacuum chamber (with the visible channel opening facing towards the window) and the sensors are connected. The heating foil under the bottom cap is connected to the power supply and turned on. The pressure in the vacuum chamber is lowered until the triple point of the liquid in the reservoir is reached. When the liquid starts to boil, vapour will build up in the reservoir and there should be a pressure difference between the reservoir and the rest of the vacuum chamber. This starts the plume mechanism. When the pressure difference between reservoir and vent is high enough, the plume becomes supersonic. A camera set-up outside the vacuum chamber records each run.

Required materials

- Vacuum chamber
- Vacuubrand RZ6 vacuum pump
- The plastic see-through tube
- About 2 liter of distilled H_2O water
- 2x K-type thermocouple
- 2x HCLAI2X5DU relative pressure sensors
- An absolute pressure sensor
- The two part mould
- A bottom cap with 12v heating foil
- A camera
- A connected computer with LabVIEW

Results Figure 6.10 shows the total set-up of the experiment with on the right the mini moon in the vacuum chamber, in the middle the power supply and on the left the computer registering the temperatures and pressures.

As stated before, the earlier versions of the experiment did not contain a heating foil to control the temperature in the reservoir. As a result of the physical process of boiling taking away energy from the liquid, the entire reservoir froze a few seconds after the triple point was reached (Figure 6.12 shows the set-up of the earlier experiments without heating foil and frozen reservoir after a run). The use of non-conducting material for the 3D printed bottom cap makes it more difficult to heat up. The heatingfoil can not touch the water without the risk of short circuiting. The heating foil needs to be close to the surface of the bottom cap otherwise the cap insulates too much. But the cap cannot be too thin since it needs to carry the entire set-up without breaking. A cap thickness of 2.5 mm has been selected. The heat from the heating foil can be regulated by increasing or lowering the voltage between 0 and 12 volts. Figure 6.11 shows the temperature difference between the top of the cap and the room temperature for different voltages through the heatingfoil.

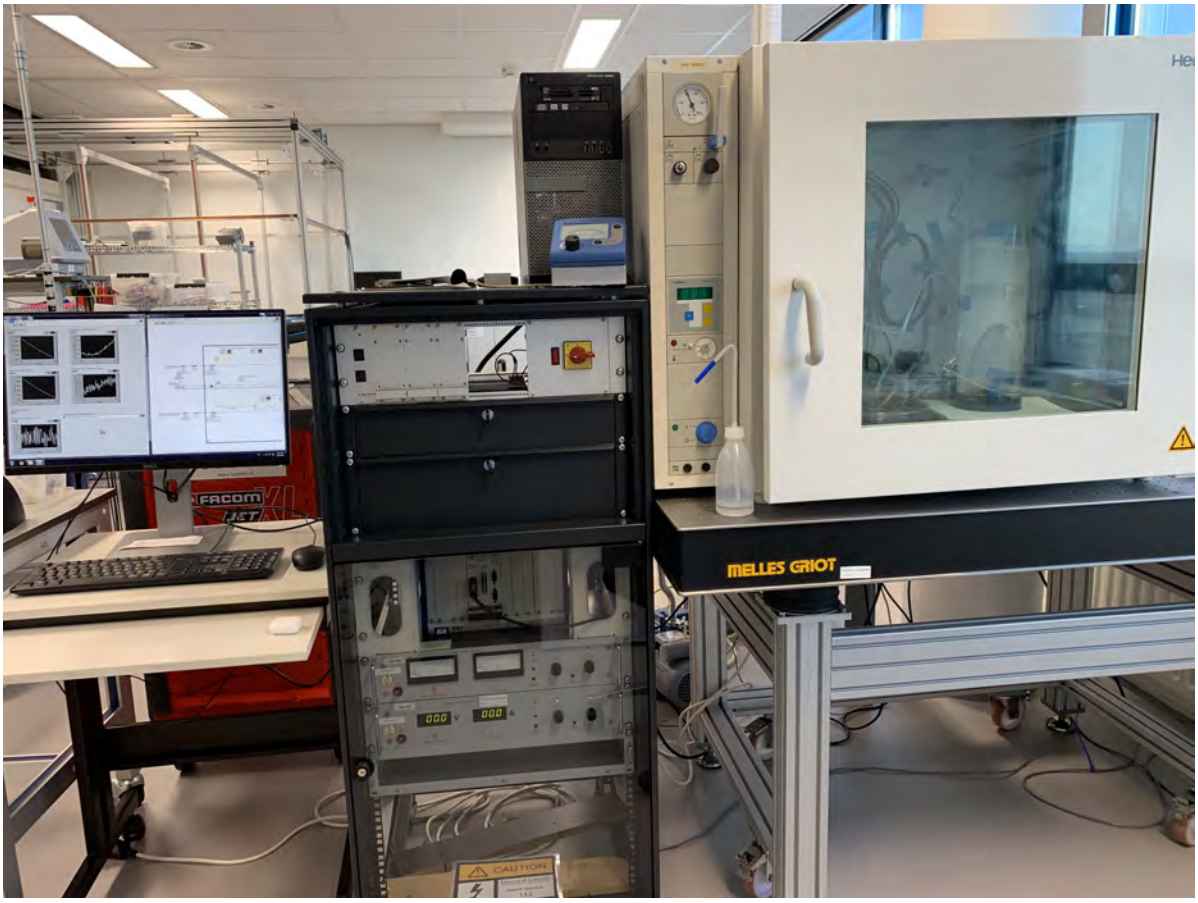

Figure 6.10: Overview of total experiment with the mini moon in the vacuum chamber on the right, the power supply in the middle and the computer registering the temperatures and pressures on the left

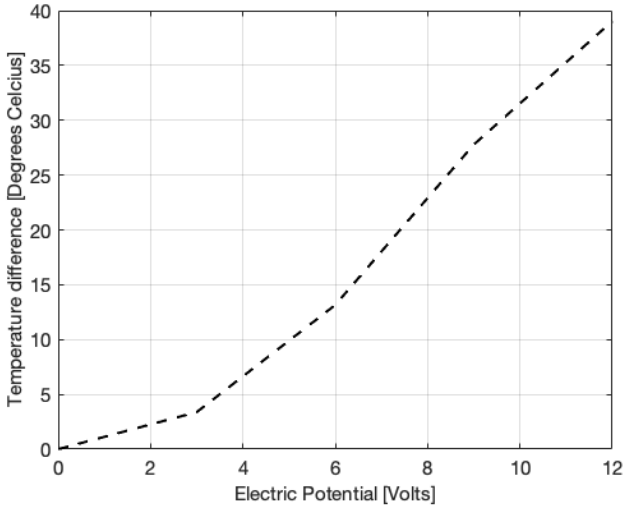

Figure 6.11: Temperature difference between the top of the cap and the room temperature for different voltages through the heatingfoil

Since the cap is made of a badly conducting material, putting water and ice on top of the cap reduces the amount of heat being transferred from the heatingfoil to the water in the reservoir. Figure 6.13 shows the redesigned set-up with a heating foil in the bottom cap. The temperature difference between the ice and heated water causes condensation on the see-through tube before starting the run.

The results from the last run are shown in Figure 6.14. The top graph shows the temperature of the vent (red) and reservoir (blue) on the y-axis and the time in seconds on the x-axis. The bottom graph shows the pressure at the vent (red) and reservoir (blue) on the y-axis and the time on the x-axis. The triple point temperature and pressure are shown in black dashed lines. The required vent pressure is shown in dotted black lines.

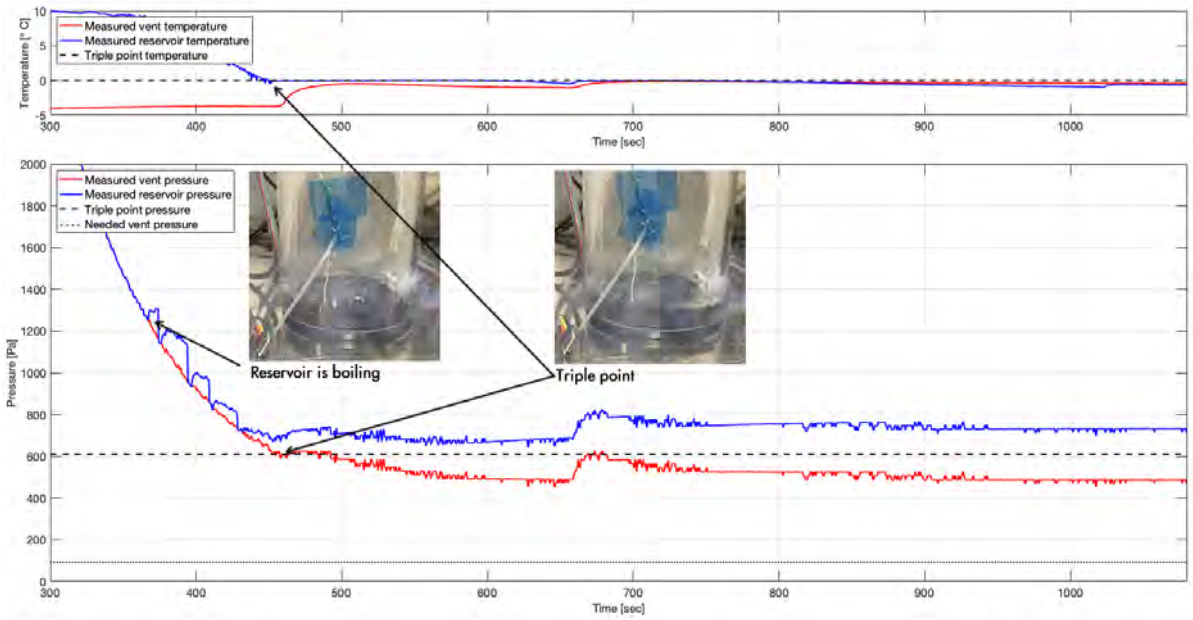

Figure 6.14: Results from mini moon experiment with the temperature and pressure at the vent in red, the temperature and pressure in the reservoir in blue, the triple point temperature and pressure in dashed black lines and the required vent pressure in dotted black

It can be seen that the temperature in the reservoir started dropping when the liquid started boiling. Large vapour bubbles caused temporary relative increases in pressure in the reservoir. The pressures of the reservoir and vent remained otherwise the same until the triple point was reached. Around the triple point an increase in pressure was detected in the reservoir compared to the vent due to the continuous boiling of the liquid. At the same time, a temperature increase was detected at the vent. This temperature increase would suggest the presence of a continuous plume 'hitting' the thermocouple at the vent. The heatingfoil was able to keep the temperature of the liquid reservoir around the triple point temperature. But it took the maximum possible heat (12 volts) to keep such temperature. It kept the reservoir just liquid until the entire reservoir was boiled away after about 23 minutes (Figure 6.14 is only an excerpt of the total run). At around 650 seconds, there was a large bubble of vapour 'exploding' causing the pressure and temperature to spike. The second challenge revealed was that the large amounts of vapour that were created by vaporisation and sublimation made it not possible to reach the desired pressure in the vacuum chamber. The pump was not able to get the pressure much lower than about 500 Pa. To get a supersonic plume, the required pressure at the vent needed to be around 100 Pa. The set-up was not designed to measure the actual plume velocity, but based on the available temperature difference data and equation 6.6, the estimated velocity of the plume was somewhere between Mach 0.12 and 0.26 (with the low pressures and densities this would suggest a velocity of an estimated 49 to 106 m/s). But since the temperature of the reservoir was measured in the water and not the actual gas, these velocities should be taken with a grain of salt.

6.7. CONCLUSION

The results of the experiments done with the smaller version have shown that a laboratory set-up of an icy moon plume is possible. Some practical design features have been detected by doing these smaller experiments. Firstly, the moulds should be made out of metal to be easily removable from the ice. And secondly, the water reservoir should be heated to prevent freezing (to efficiently heat the reservoir, a waterproof heater should be placed in the reservoir and not insulated below). Though with the equipement available for this study at the Delft University of Technology it was not possible to lower the pressure enough to get a supersonic plume, the experiment proved the overal concept for a larger design with the better facilities available in Aachen.

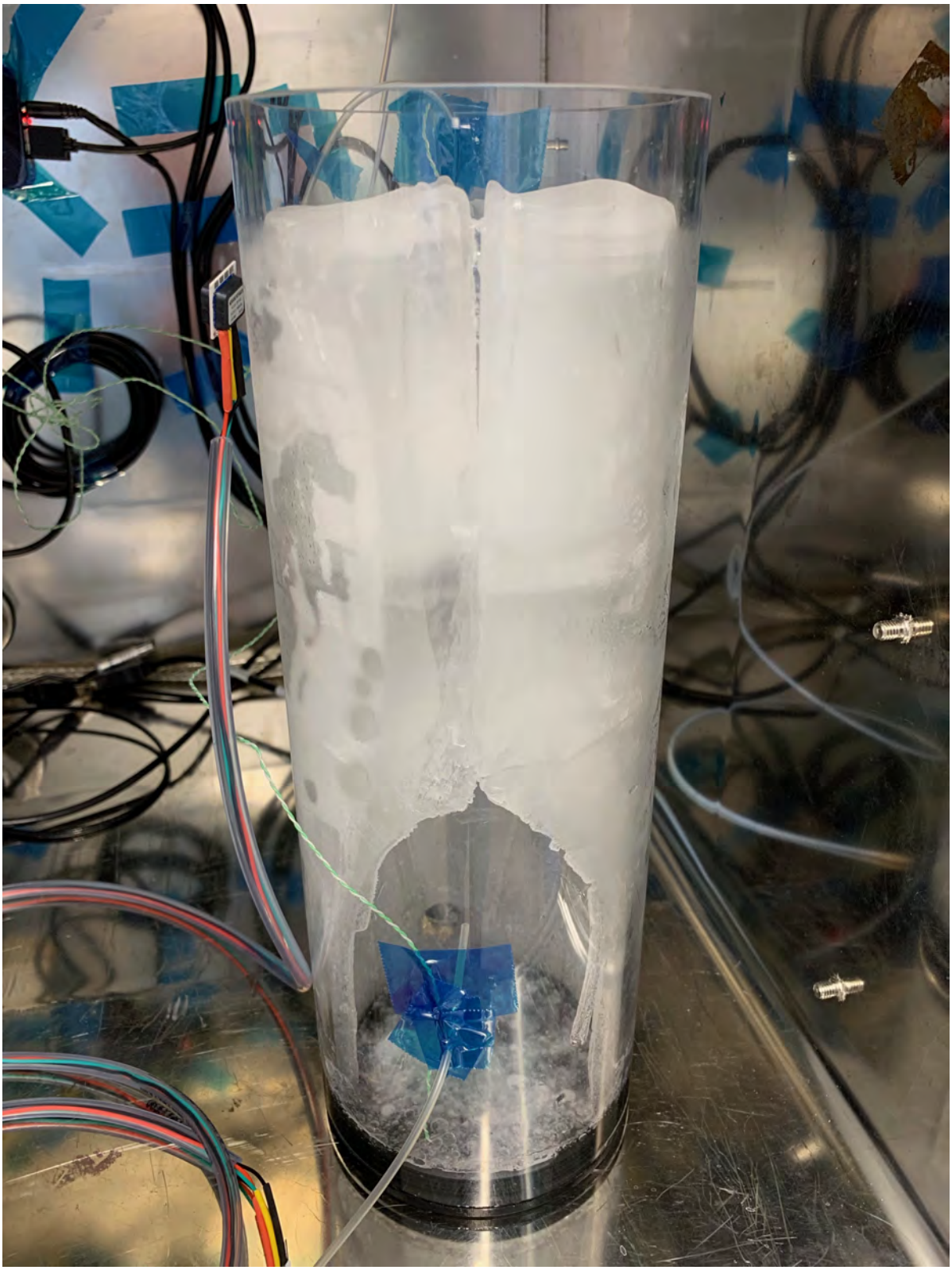

Figure 6.12: Mini moon without heating after a failed run with a frozen reservoir

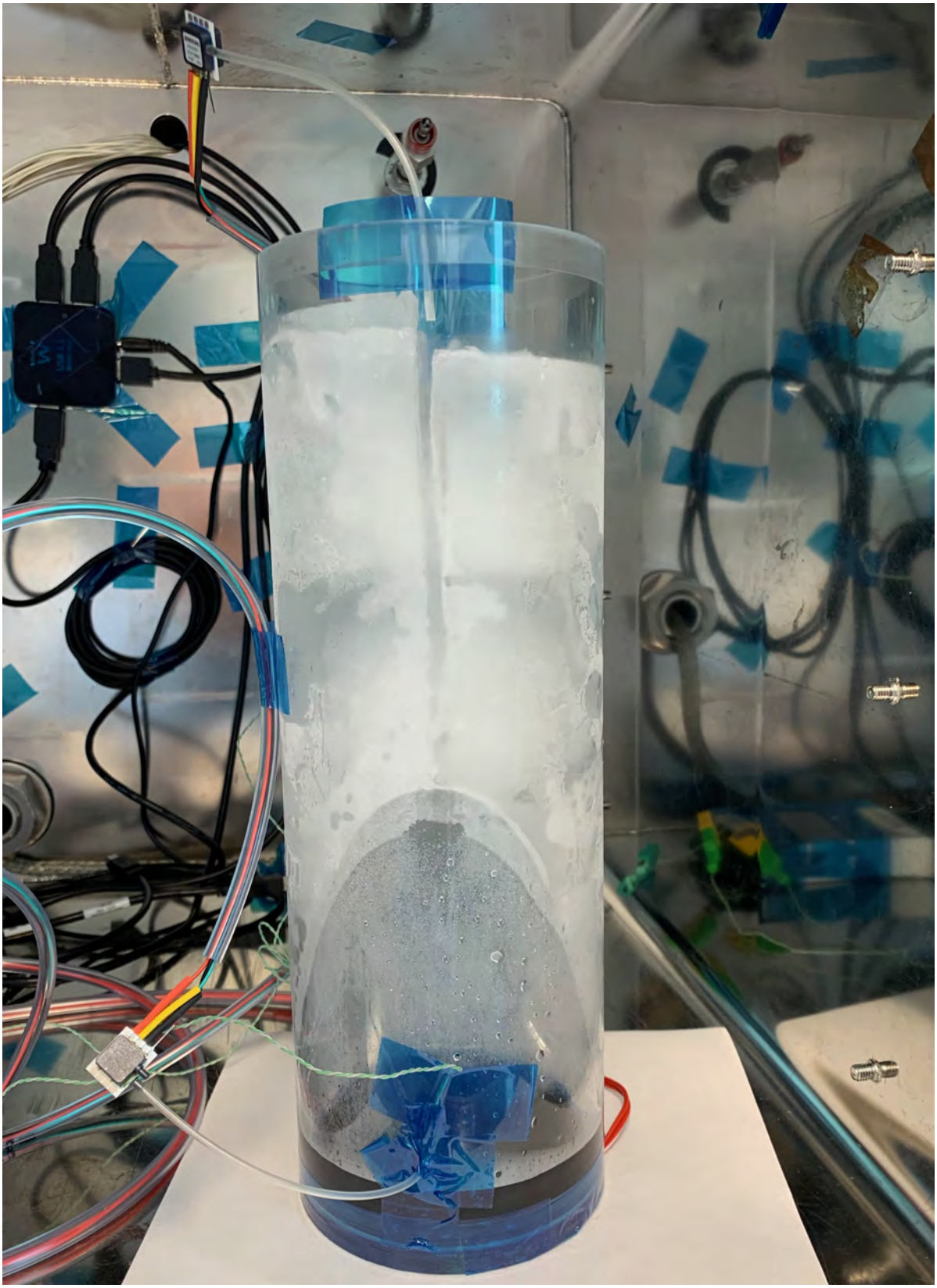

Figure 6.13: Mini moon with heatingfoil before a run

7

Final Design

With the theoretical knowledge of the established relations and the practical knowledge gained by the smaller version experiment, the final design can now be assembled and proposed. The final design and its considerations are summarised in Section 7.1, the preparation of the experiment is explained in Section 7.2 and the measurements are discussed in Section 7.3.

7.1. The design

The relations derived in Section 6.3 are valid for every size of the design and therefore will not change from the small design to the final design. The proof-of-concept model designed based on these relations and build in Section 6.5 has given a lot of practical knowledge that is incorporated in the final design. These points are listed below.

7.1.1. Mould material

The non-conductive material of which the small mould parts were constructed proved difficult to remove from the ice. The solution presented in Chapter 6 was to cover it in a layer of plastic to prevent the ice growing directly onto the mould parts. This did form irregularities in the ice structure due to wrinkles in the plastic layer. Therefore it is recommended to construct the mould parts from a conductive material like most metals. The ice can be grown directly onto the mould parts and when the mould parts need to be removed they can be flash heated, melting a tiny layer around the moulds making them removable.

7.1.2. Temperature control

During the small version experiments it was discovered that the temperature of the liquid in the reservoir drops below the freezing temperature too fast. This froze the entire reservoir and therefore stoped the experiment. The temperature of the liquid needs to be controlled by a heating element inside the liquid reservoir. This simulates the natural heating phenomenon of Enceladus' ocean.

7.1.3. Freezing of the channel opening

It was expected that a negative side effect of the plume could be that the vapour would freeze the channel closed. This was not discovered during experiments with the small model. Comparing the throat and vent openings before and after the experiment did not reveal any measurable differences in opening areas. Whether this will be the case for a larger scale experiment is unknown. But the longer the channel height (distance from reservoir to vent) the higher the chance that vapour or ice grains will freeze onto the channel walls [62]. Though since the size of the larger proposed experiment is still only one meter in length, it is doubtful that the channel will experience any measurable decreased opening.

7.1.4. Minimal ice thickness

The minimal ice thickness located between the small end of the crevasse and the tube was set on 10 mm and the other size was left open to make the reservoir and channel visible during the experiment. This 10 mm proved to be too thin and easily breakable, especially since the ice was only connected at one side. The

set-up in Aachen does not have a see-through tank, therefore it is not necessary to have an opening at the sides of the crevasse. In fact, to have better experimental results, it is advisable to have all sides covered by ice (especially for grain growth experiments where the wall material plays a role). Therefore, for the redesigned larger experiment, both sides of the crevasse are closed and the wall thickness is increased to 20 mm. With the maximal diameter of 290 mm, this leaves a reservoir diameter and channel length of 250 mm and based on the relations of equation 6.16 a throat width of 10.8 mm.

7.1.5. CHANNEL DEPTH

The small model had a channel and reservoir of equal heights. For different versions of the experiment, different ratios can be preferred. For example, experiments to study grain growth might prefer a long channel and a small reservoir to test the influence of collisions with the channel walls on the size of the grains [6] (see Section 10.3). But experiments that study the influence of the size of the boiling chamber (reservoir volume) might prefer a larger reservoir and a smaller channel so the reservoir can be filled up to different heights with the evaporating liquid [36] (see Section 10). Therefore, based on the scientific purposes for the general design, the heights of the reservoir and channel are kept equal. Since the established relations only put restrictions on the horizontal dimensions and not on the vertical dimensions, different versions of the same design can be used when only the height ratio of the reservoir and channel are altered. On a time note, having a larger reservoir means that more liquid can be placed in the reservoir which means that the experiment can be sustained for longer periods of time. For example, a reservoir filled with 0.5 L of liquid can sustain a supersonic plume for 23 minutes while a reservoir filled with 1.0 L of liquid can sustain a supersonic plume for twice as long. On a cost note, having a smaller reservoir means less volume of 3D printed or machined material which will save on the costs of the moulds.

7.1.6. EXHAUST VELOCITY

As explained in Section 6.5 for practical reasons a Mach number of 1.83 was chosen that influenced the throat to vent ratio. This Mach number and the resultant ratio of 1.5 is still proposed for the larger design for the same practical reasons as before. (Only Mach numbers between 1.00 and 2.00 are possible. For unforeseen extra experimental limitations it is prudent not to be too close to the limits. And a Mach number of 1.83 results in a practical throat to vent area ratio of 1.5.) Since only the top mould part influences the exhaust velocity, using different top mould pieces would allow for different exhaust velocities. Also, the top part of the mould is cheaper (see Chapter 8). Table 7.1 shows some of the possible reachable Mach numbers and the design specifications for the top mould part based on equations 6.6 till 6.5.

Table 7.1: Modular design specifications for the top mould part based on a 250 mm reservoir diameter

Mach number [-]	1.00	1.10	1.20	1.30	1.40	1.50	1.60	1.70	1.83	1.90	2.00
Area ratio [-]	1.00	1.01	1.03	1.07	1.12	1.18	1.26	1.36	1.50	1.60	1.74
Vent width [mm]	10.8	10.9	11.2	11.6	12.1	12.8	13.7	14.7	16.2	17.3	18.9
Required vent pressure [Pa]	291	259	229	200	174	151	130	112	92.3	82.1	70.0
Vent temperature [K]	234	228	221	213	206	199	192	185	176	171	164
Plume velocity [m/s]	379	411	442	471	498	525	549	573	600	616	635

7.1.7. SUMMARY

The final design based on the small design proposed in Chapter 6 together with the proposed alterations of the previous sections results in the design shown in Figure 7.1. The diameter of the crevasse (and therefore the length of the throat and vent) are 250 mm. The design Mach number is 1.83 resulting in an area ratio between throat and vent of 1.50. The width of the throat is 10.8 mm and the width of the vent is 16.2 mm. The hight of the reservoir and channel are 500 mm. On the bottom of the bottom mould part and on the top of the top mould part a larger extension is placed that makes sure the mould parts are placed at the precise middle of the test cylinder when freezing the ice.

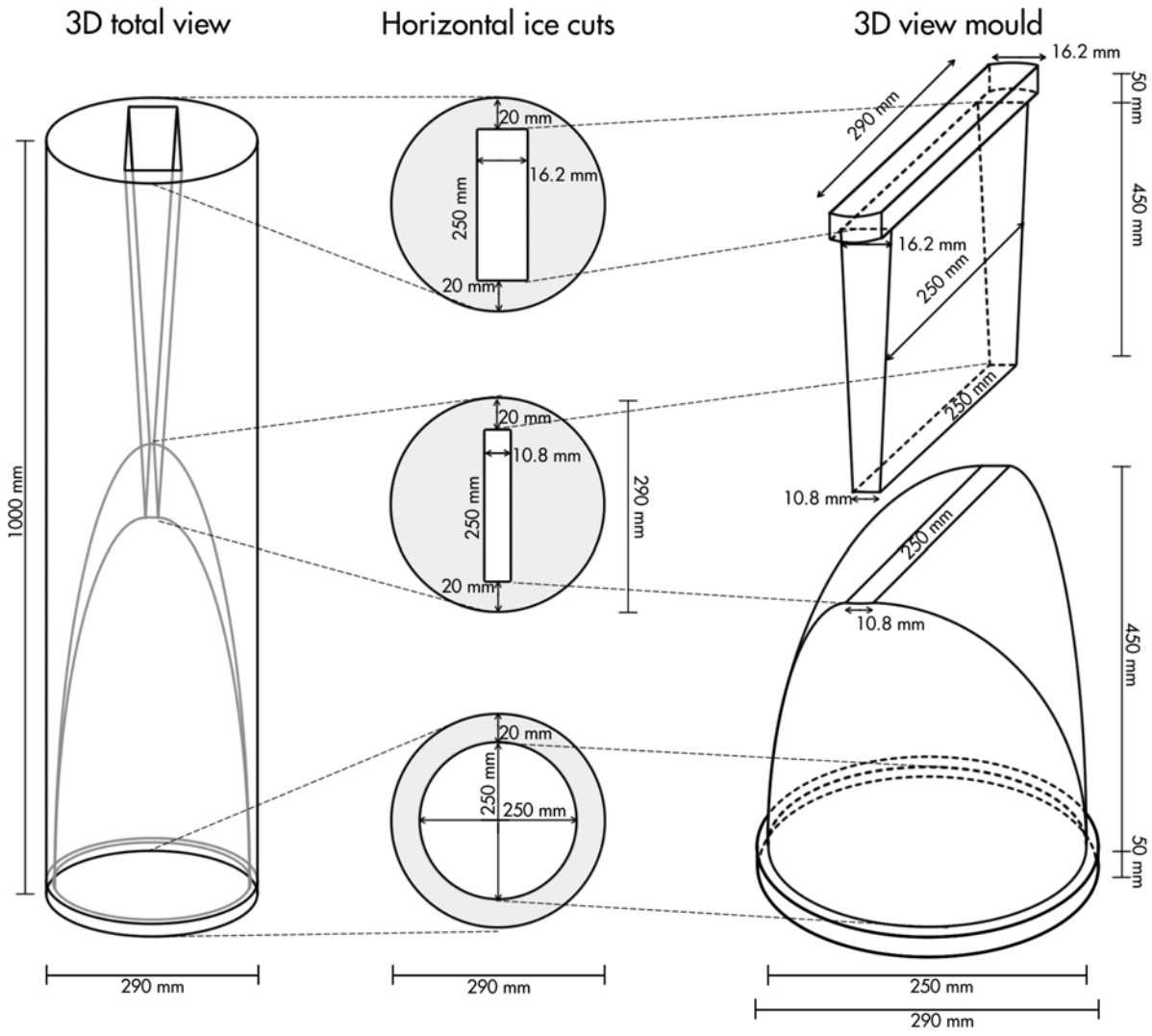

Figure 7.1: Design specifications of the large model

7.2. PREPARING THE EXPERIMENT

The final design is three times larger as the small version used in Chapter 6. The small version has an approximate volume of 2,356 cm^3 which is filled with ice weighs about 2.2 kg. In contrast, the final design will have an approximate volume of 70,686 cm^3 and when filled with ice it weighs up to about 65 kg. Although approximated, it is obvious that this is not practical to operate by hand. The use of the final design will have to be prepared. Figure 7.2 shows how the plume crevasse is made, the mould parts are removed and finally placed in the vacuum chamber.

(A) The two mould parts are placed in the refrigerator, liquid water is poured around the mould parts and the mould and water is frozen.

(B) The sides of the ice block are flash heated so a small part of the outer layer melts making it easier to remove the ice block with mould parts from the refrigerator. The ice block is then lifted out of the refrigerator with a crane.

(C) While hanging from the crane, the sides of the bottom mould part is flash heated and the bottom mould part is removed.

(D) The ice block with top mould part is placed in the test cylinder.

(E) The top mould part is flash heated to make it easier to remove and then lifted out of the ice block leaving just the ice with the crevasse and reservoir openings in it.

(F) The test cylinder with the ice block are lifted with the crane

(G) The test cylinder with the ice block are placed inside the vacuum chamber.

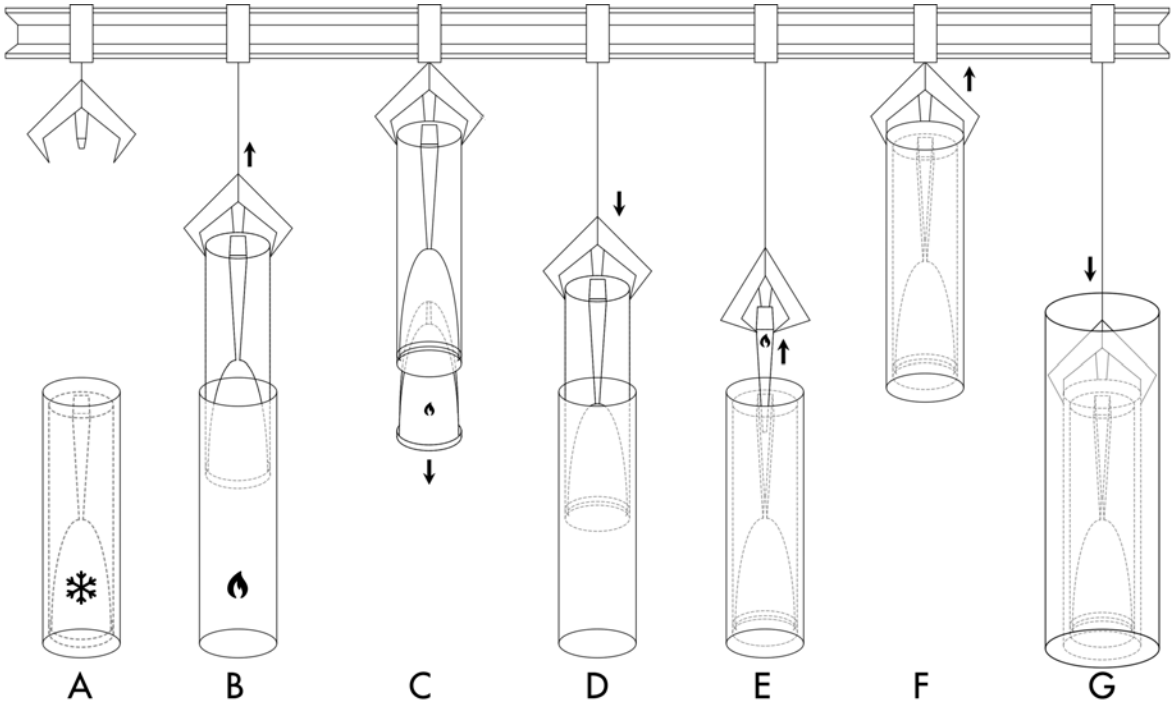

Figure 7.2: Practical experiment preparation. A: freeze ice in refrigerator. B: flash heat sides and remove ice from refrigerator. C: flash heat bottom mould and remove from ice block. D: place ice block in test cylinder. E: flash heat top mould part and remove from ice block. F: lift test cylinder with ice block. G: place test cylinder with ice block in vacuum chamber

After the ice block is finished and the mould parts are removed, the reservoir on the bottom still needs to be accessed. Not all sensors that may be used will be able to withstand being frozen or in liquid for long periods of time and therefore need to be added after the ice block is ready. Next to that, the liquid water needs to be poured in to the reservoir. If the liquid water (which have a high temperature than the ice) is poured through the crevasse, it may melt the walls and therefore influence the geometry. Therefore a reservoir access point is needed here as well. The solution proposed here is to freeze in tubes in the ice which connect to the reservoir mould and open at the top. These tube remains in the ice during the experiment and do not have to be removed. When the bottom mould is removed, there are channels which open at the top and reservoir through which first water can be poured and then sensors can be lowered. The tubes should be closed before the experiment starts to prevent loss of pressure through this tube. This part of the preparation should be done at Figure 7.2 step A and is shown in more detail in Figure 7.3. The tubes shown here are examples of the possibilities. Having an easy connection to the reservoir is very beneficial for filling the reservoir and placing sensors. Another possibility is to connect a tube with the throat for placing sensors where the subsonic to sonic transition takes place. Both are shown in Figure 7.3. Another option is to fill the test cilinder with water at step D before placing the ice block instead of filling the reservoir through tubes.

7.3. MEASUREMENTS

To perform the measurements several sensors are needed. To perform the basic experiment, at least temperature and pressure sensors are required. In the sections below the temperature and pressure sensors available in Aachen are discussed. For more detailed experiments that require other measurements like velocity, dust analysers or mass spectrometry, instruments can be added but are not discussed here.

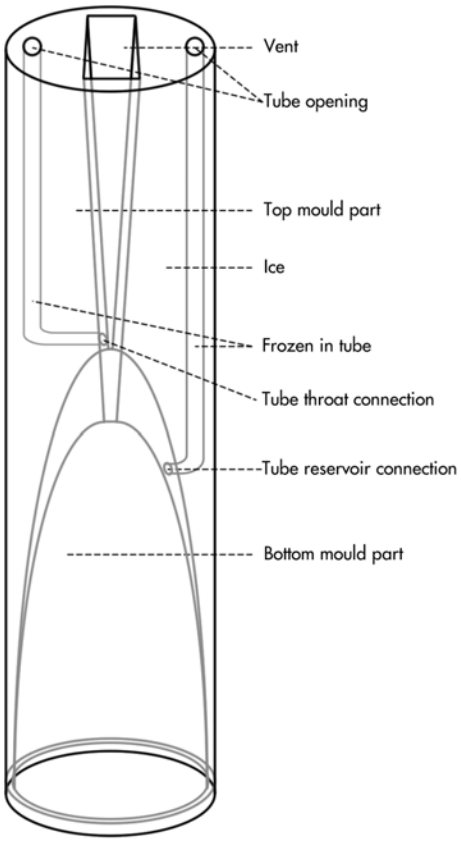

Figure 7.3: Practical experiment preparation 2. A more detailed version of Figure 7.2 A, in which is shown that the mould parts are frozen in together with tubes that will connect the reservoir and throat with the top to have easy access to the reservoir and throat

7.3.1. PRESSURE MEASUREMENTS

Just like the set-up in Delft, the vacuum chamber in Aachen contains an absolute pressure sensor and would require either the use of relative pressure sensors that measure the difference between the pressure in the chamber and local pressures in the reservoir and throat (the pressure at the vent is expected to be equal to the absolute pressure in the chamber, but a relative pressure sensor can be placed there as well). The relative pressure sensors used and available in Aachen are DLVR-10D chips. These chips can measure a pressure difference up to 30,000 Pa[1]. Since the expected different between reservoir and vent is only a few hundred Pa, these sensors are more than sufficient.

7.3.2. TEMPERATURE MEASUREMENTS

The available temperature sensors used in current experiments in the vacuum chamber in Aachen are the PT1000 and DS18S20 sensors. The PT10000 sensor has a measuring range of $-40°C$ to $500°C$ and the DS18S20 sensor has a digital output with a measuring range of $-55°C$ to $125°C$[2]. To make the sensors water resistant they are covered by a thin glass fiber hose and drained in resin. Looking at the expected vent temperatures for supersonic plumes in Table 7.1 a minimum measurable temperature of $-39°C$ to $-109°C$ are needed ($-97°C$ for the proposed design Mach number of 1.83). The current sensors are therefore suitable for measuring the temperature in the reservoir ($0.01°C$) and throat ($-39°C$), but a different sensor is needed to measure the temperature at vent if higher Mach numbers are expected at the vent.

[1] https://nl.mouser.com, last visited on 24-01-2019
[2] https://nl.farnell.com, last visited on 24-01-2019

8

COST

This chapter will list the cost of every part of the large scale experiment designed for the facilities in Aachen in the previous chapters. There are one-time-only costs which include the purchase of the mould parts in Section 8.1 and the price of the required sensors in Section 8.2 and there are operating costs that will have to be covered every time the experiment is performed. This is shown in Section 8.3. A summation of the one-time expenses and operating expenses is given in Section 8.4.

8.1. MOULD PARTS

The design of the mould as proposed in Chapter 8 requires either machining or 3D printing. The material choice based on heat conductivity required a form of metal. Materialise[1] in Leuven (Belgium) has the ability to 3D print the mould parts. They offer three types of metal: Aluminum ($AlSi_{10}Mg$), Titanium ($TiAl_6V_4$) and Stainless Steel (316L or 1.4404), but only Aluminium can be printed in blocks large enough to fit the design from this study. Therefore for this cost estimate, Aluminium is used. The design as proposed in this study consists out of two mould pieces, a top part (that will hollow out the channel) and a bottom part (that will hollow out the reservoir). The costs of both parts are listed in Table 8.1. All prices are listed without VAT.

Table 8.1: Costs 3D printing metal model parts

Part	Cost
Top (channel)	€1,742.37
Bottom (reservoir)	€13,982.70
Total	€15,725.07

For the smaller experiment done in Chapter 6 3D printing was chosen to create the mould parts out of plastic. 3D printing metal moulds three times that size is much more costly as can be seen from Table 8.1. Another method of creating the metal mould parts is machining them from existing blocks of metal. The DEMO department estimates the total price for machining the metal mould pieces between €7,000 and €10,000 based on the large blocks of metal and the man-hours needed.

8.2. SENSORS AND OTHER EQUIPEMENT

Next to the mould parts, there are the sensors to be purchased. This is again a one-time-expense. For simplicity, the bare minimum of sensors are listed here (more sensors can always be added along the channel). The temperature and pressure needs to be known in the reservoir, throat and vent locations therefore requiring at least three temperature sensors and three pressure sensors. The vacuum chamber contains an absolute pressure sensor already, therefore the three pressure sensors required can be relative pressure sensors. At the moment of writing the temperature sensors used in the vacuum chamber in Aachen are DS18S20 and for the

[1] https://www.materialise.com, last visited on 17-01-19

relative pressure measurements DLVR-10D sensors are used. As discovered in Chapter 6, the reservoir needs to be heated to keep the liquid water from freezing. This can be done by heating foil on the outside of the metal cylinder or by so called aquarium heaters that are water resistant and can therefore be placed inside the reservoir. Since it is more energy efficient to have the heat source inside the liquid water reservoir and in this bigger version of the experiment there is room to put a heat source inside the reservoir, the preference is given to the use of such an aquarium heater. Table 8.2 shows the cost per sensor/equipement based on the prices of Mouser[2] and the cost of an aquarium heater based on the price of Conrad[3].

Table 8.2: Costs sensors and other equipement

Part	Cost	Minimal needed quantity
Temperature DS18S20 sensor	€2.86	3
Pressure DS18S20 sensor	€40.08	3
Aquarium heater	€49.99	1
Total	€178.81	

8.3. VACUUM CHAMBER OPERATING COSTS

The operating costs of the vacuum chamber in Aachen are separated into two parts, the growing of the ice block and the usage of the vacuum chamber itself. These costs shown here are an estimate of the current operating costs as known at the FH University of Applied Physics Aachen. If this project is undertaken at a different location, these costs will vary. The costs of growing the ice are listed in Table 8.3.

Table 8.3: Costs growing ice

Part	Cost
Distilled water (80 L)	€35.00
Coolant refill (0.1 L)	€13.00
Degassing membrane wear-out	€17.00
Energy	€190.00
Total	€255.00

The operating costs of the vacuum chamber itself per hour are listed in Table 8.4. Based on previous experiments done in this vacuum chamber, an experiment can run as long as 6 hours. This would imply operating cost per experiment to be €90.00 The experiment preparation can, if the ice block is ready, be done in about 10 minutes. This list does not include labour hours.

Table 8.4: Costs operating vacuum chamber per hour

Part	Cost per hour
Vacuum pump maintenance	€2.00
Vacuum pump energy	€6.00
Vacuum pump cooling water	€5.00
Vacuum grease to seal chamber flange	€2.00
Total	€15.00

Adding both operating costs together comes down to a cost per experiment run of about €345.00. The most influencing factor is the energy cost needed to freeze the entire ice sculpture. It is here assumed that the

[2] https://nl.mouser.com, last visited on 17-01-19
[3] https://www.conrad.nl, last visited on 17-01-19

entire ice block is no longer usable after one run and has to be regrown for a new run. And indeed there will be deformations due to the experiment. But it might be possible to re-use (parts of) the ice for the next run which will decrease the energy cost and time needed to regrow the ice.

8.4. CONCLUDING THE TOTAL COSTS

The previous sections give the one-time expenses and the operating expenses. The summation of these expenses are given in Table 8.5.

Table 8.5: Total cost of Aachen laboratory icy-moon plume simulator

Estimated minimum one-time expenses (moulds, sensors and heater)	€7,178.81
Estimated cost per experiment run (electricity, coolant and water)	€345.00

9

VERIFICATION AND VALIDATION

During the design phase of the laboratory set-up a number of physical relations have been used and combined that together resulted in a model. These individual relations that make up the model are verified individually in Section 9.1. Section 9.2 verifies the physical requirements set in Chapter 4. The final section of this chapter contains the validation of the requirements set by the FH University of Applied physics in Aachen listed in Chapter 4.

9.1. MODEL VERIFICATION

The verification consists out of two parts. The verification of constructed model for the design and the verification of the physical requirements on the design. This section lists the model verification in which parts of the model and the total model itself are compared to literature and hand calculations.

9.1.1. AMMONIA CONCENTRATION

The water and 25% aqueous ammonia volumes needed to create the required ammonia concentrations calculated in this study in Table 5.1 are verified with a Solution Dilution Calculator[1] and shown in Table 9.1.

Table 9.1: Verification of relation that provides desired ammonia concentrations

Desired ammonia concentration	0%	1%	2%	3%	4%	5%
25% aqueous ammonia volume from Solution Dilution Calculator [ml]	0	0.4	0.8	1.2	1.6	2.0
25% aqueous ammonia volume from this study [ml]	0	0.4	0.8	1.2	1.6	2.0
Difference in ammonia concentration volume [ml]	0	0	0	0	0	0
Water volume from Solution Dilution Calculator [ml]	10	9.6	9.2	8.8	8.4	8.0
Water volume from this study [ml]	10	9.6	9.2	8.8	8.4	8.0
Difference in water volume [ml]	0	0	0	0	0	0

It can be seen that there is no difference between the solution dilution calculator and the concentrations generated by this study thereby verifying this part of the model/calculation.

9.1.2. TEMPERATURE RATIO - MACH NUMBER RELATION

The temperature ratio in a nozzle depending on Mach numbers relation as given in Equation 6.6 and of which the results are shown in the second graphs of Figure 6.6 are verified with Anderson [37] Appendix A. Note that Anderson [37] appendix A is based on air and not on water vapour. This requires different values for the specific heat constant and gas constant then have been used in this study. The values displayed here are therefore not corresponding with the values in earlier chapters. This is purely to verify these lines of code in

[1] https://www.sigmaaldrich.com/chemistry/stockroom-reagents/learning-center/technical-library/solution-dilution-calculator.html, last accessed on 26-12-18

the model. The specific heat ratio of air is $\gamma = 1.4$ while for water vapour it is $\gamma = 1.331$. The gas constant for air is $R = 287.05 \frac{J}{Kg \cdot K}$ while the gas constant for water vapour is $R = 461.52 \frac{J}{Kg \cdot K}$. Table 9.2 shows the values obtained from Anderson [37], the values obtained from the model made during this study and the differences between those two sources.

Table 9.2: Verification of temperature ratio - Mach number relation

Mach number [-]	1.00	1.50	1.60	1.70	1.80	1.86	1.90	2.00	2.10
Temperature ratio from this study [-]	1.20	1.45	1.51	1.58	1.65	1.69	1.72	1.80	1.88
Temperature ratio from Anderson [37] [-]	1.20	1.45	1.51	1.58	1.65	1.69	1.72	1.80	1.88
Difference [-]	0	0	0	0	0	0	0	0	0

It can be seen that there is no differences between the values obtained from this study's model and the values provided by Anderson [37], thereby verifying this portion of the total model.

9.1.3. PRESSURE RATIO - MACH NUMBER RELATION

The pressure ratio in a nozzle depending on Mach numbers relation as given in Equation 6.7 and of which the results are shown in the bottom graphs of Figure 6.6 are verified with Anderson [37] Appendix A. Table 9.3 shows the values obtained from Anderson [37], the values obtained from the model made during this study and the differences between those two sources.

Table 9.3: Verification of pressure ratio - Mach number relation

Mach number [-]	1.00	1.50	1.60	1.70	1.80	1.86	1.90	2.00	2.10
Pressure ratio from this study [-]	1.89	3.67	4.25	4.94	5.75	6.30	6.70	7.82	9.14
Pressure ratio from Anderson [37] [-]	1.89	3.67	4.25	4.94	5.75	6.30	6.70	7.82	9.15
Difference [-]	0	0	0	0	0	0	0	0	0.01

It can be seen that there is almost no differences between the values obtained from this study's model and the values provided by Anderson [37], thereby verifying this portion of the model. Only the last value has a 0.01 discrepancy which is caused by a rounding error between the model and Anderson [37].

9.1.4. AREA RATIO - MACH NUMBER RELATION

The area ratio of the vent and throat of a nozzle depending on Mach numbers relation as given in Equation 6.12 and of which the results are shown in the top graphs of Figure 6.6 are verified with Anderson [37] Appendix A. Table 9.4 shows the values obtained from Anderson [37], the values obtained from the model made during this study and the differences between those two sources.

Table 9.4: Verification of nozzle area ratio - Mach number relation

Mach number [-]	1.00	1.50	1.60	1.70	1.80	1.86	1.90	2.00	2.10
Area ratio from this study [-]	1.00	1.18	1.25	1.34	1.44	1.51	1.56	1.69	1.84
Area ratio from Anderson [37] [-]	1.00	1.18	1.25	1.34	1.44	1.51	1.56	1.69	1.84
Difference [-]	0	0	0	0	0	0	0	0	0

It can be seen that there is no differences between the values obtained from this study's model and the values provided by Anderson [37], thereby verifying this portion of the total model.

9.1.5. SPEED OF SOUND

The speed of sound depending on temperature, gas constant and specific heat ratio and velocity depending on speed of sound and Mach number as combined in Equation 6.5 and shown in the third graphs of Figure

6.6 are verified with a standard atmosphere table given by Engineering Toolbox[2] and with hand calculations and are shown in Table 9.5. It should be noted that this part of the verification is again done with air as gas and not water vapour. The values obtained here are therefore again different from the values for water vapour used in this study.

Table 9.5: Verification of speed of sound - temperature relation including Mach number and stream velocity

Temperature [$°C$]	-40	0.0	5.0	10	15	20	25	30	40
Mach number [-]	1.00	1.50	1.60	1.70	1.80	1.86	1.90	2.0	2.10
Speed of sound from this study [m/s]	306.1	331.3	334.3	337.3	340.3	343.2	346.1	349.0	354.7
" from Engineering Toolbox [m/s]	306.2	331.4	334.4	337.4	340.4	343.3	346.3	349.1	354.7
Difference [m/s]	0.1	0.1	0.1	0.1	0.1	0.1	0.2	0.1	0
Velocity from this study [m/s]	306.1	497.0	534.9	573.5	612.5	638.4	657.7	698.1	745.0
Velocity from hand calculations [m/s]	306.1	497.0	534.9	573.5	612.5	638.4	657.7	698.1	745.0
Difference [m/s]	0	0	0	0	0	0	0	0	0

It can be seen that there is very little difference between the speed of sound found in Engineering Toolbox and the speed of sound obtained by the model. The differences are most likely due to rounding errors in both the gas constant and the speed of sound. There are no differences between the hand calculated velocities and the velocities obtained by the model. This verifies this portion of the model.

9.1.6. MASS FLOW OF A CHOKED NOZZLE

The mass flow through a choked nozzle calculations as shown in Equation 6.13 are verified by hand calculations and one case found in Anderson [37]. Not all cases use water vapour and therefore all the different values are listed together with the resultant mass flow and the differences in Table 9.6. The first column is the case presented in Anderson [37], the second column is sea-level air at 0 degrees Celcius and the third column is at the triple point of water.

Table 9.6: Verification of mass flow through choked nozzle calculations

Temperature [K]	3500.0	273.15	273.16
Pressure [Pa]	$3.030 \cdot 10^6$	$1.0133 \cdot 10^6$	611.7
Specific heat ratio (γ) [-]	1.22	1.40	1.33
Gas constant (R) [J/kg/K]	520	287	462
Throat area [m^2]	0.4	2.2	10
Mass flow from Anderson [37] [kg/s]	586.4	-	-
Mass flow from hand calculation [kg/s]	586.1	545.1	11.59
Mass flow from this study [kg/s]	586.1	545.1	11.59
Difference [%]	$5.11 \cdot 10^{-2}$	0	0

It can be seen that the difference between this study's mass flows and the one case presented in Anderson [37] is only 0.005 %. Anderson [37] already specified that "a larger cumulative roundoff error" is playing a part due to the fact that the author is using a handheld calculator with less significant digits than computer software would use. There is no difference between the other hand calculations and the model's results thereby verifying this part of the model.

9.1.7. HERTZ, KNUDSEN & LANGMUIR'S EVAPORATION

The mass flow generated by evaporation due to the pressure difference between the vapour pressure of the liquid and the local pressure as shown in Equation 6.15 is verified by hand calculations in Table 9.7. The rest of the values used are those for pure water at the triple point with a sticking coefficient of 1.

[2] https://www.engineeringtoolbox.com/air-speed-sound-d_603.html, last accessed on 24-12-18

Table 9.7: Verification of Hertz, Knudsen & Langmuir's evaporation calculations

Pressure difference [Pa]	0	100	200	300	400	500	600	700	800
Evaporation mass flow from this study [g/s]	0	0.88	1.76	2.65	3.53	4.41	5.29	6.18	7.06
Evaporation mass flow from hand calculations [g/s]	0	0.88	1.76	2.65	3.53	4.41	5.29	6.18	7.06
Difference [g/s]	0	0	0	0	0	0	0	0	0

It can be seen that the differences between the hand calculations and the model in this study are 0, thereby validating this part of the model.

9.1.8. EVAPORATION - THROAT AREA RELATION

The combined relation between generated mass flow and choked mass flow of Equation 6.16 depending on pressure difference in the reservoir and reservoir area that results in a maximum throat area is verified in Table 9.8. The rest of the values are the physical constants set for pure water.

Table 9.8: Verification of final throat area relation depending on evaporation and choked mass flow

Reservoir pressure difference [Pa]	0	100	200	300	400	500
Reservoir diameter [m]	0.05	0.10	0.20	0.50	1.00	2.00
Throat area from this study [m^2]	0	$9.10 \cdot 10^{-4}$	$9.05 \cdot 10^{-3}$	0.11	0.88	8.34
Throat area from hand calculations [m^2]	0	$9.10 \cdot 10^{-4}$	$9.05 \cdot 10^{-3}$	0.11	0.88	8.34
Difference [m^2]	0	0	0	0	0	0

It can be seen that there is no difference between the hand calculations and the results from the model thereby verifying this last step of the model.

9.1.9. VERIFICATION WITH EXISTING MODEL

Yeoh *et al.* [2] published a table in which the conditions of the vent were listed generated by their model. The same parameters are generated by the model from this study and compared in Table 9.9 as an additional verification. It can be seen that the differences between Yeoh *et al.* [2] and the model used in this study are small.

Table 9.9: Resultant values from the model for temperature, pressure and vent-throat area ratio for Mach 3 and Mach 5

Case	Mach 3			Mach 5		
Source	This study	Yeoh *et al.* [2]	Difference	This study	Yeoh *et al.* [2]	Difference
Temperature [K]	110	110	0	53	53	0
Pressure [Pa]	15.6	15.8	0.2	0.9	0.9	0
Vent-throat area ratio [-]	4.8	4.8	0	37.1	36.6	0.5
Velocity [m/s]	779	780	1	904	902	2

9.2. VERIFICATION OF REQUIREMENTS

This section lists again the physical requirements set in Chapter 4 and verifies them in Table 9.10.

Table 9.10: Verification of physical requirements

Requirement	Description	Compliance	Notes
Res-1.	The design shall mimic Enceladus' liquid ocean content.	✓	Ammonia and sodium-chloride are investigated but have little effect.
Res-2.	The design shall mimic Enceladus' ocean temperature.	✓	Triple point temperature of water is used.
Res-3.	The design shall mimic Enceladus' ocean pressure.	✓	Triple point pressure of water is used.
Res-4.	The design shall mimic Enceladus' ice layer.	✓	The crevasse and reservoir walls are constructed out of water-ice.
Res-5.	The design shall mimic Enceladus' surface geometry.	✓	The throat and vent are long rectangular slits.
Res-6.	The set-up shall be able to produce a supersonic plume via a converging diverging nozzle structure.	≈	A converging-diverging nozzle structure is used, but the design is not yet proven to produce a supersonic plume.

9.3. VALIDATION

This section lists again the requirements set by the FH University of Applied Physics in Aachen listed in Chapter 4 and validates them in Table 9.11.

Table 9.11: Validation of FH University of Applied Physics Aachen requirements

Requirement	Description	Compliance	Notes
Req-1.	The set-up shall fit inside the existing test cilinder and therefore shall have a diameter of 29 cm and a height of 100 cm.	✓	The set-up is exactly 29 cm in diameter and 100 cm in height.
Req-2.	The design shall not need a vacuum chamber pressure lower than 70 Pa.	✓	The minimal pressure needed is 92.3 Pa.
Req-3.	The set-up shall be removable from the vacuum chamber.	✓	The set-up can be hoisted in and out of the vacuum chamber and defrosted to remove from the test cilinder.
Req-4.	The set-up shall be designed to use freezing equipement present in Aachen.	✓	The size of the set-up fits in the freezing equipement already present.
Req-5.	The set-up shall be reusable.	✓	The moulds can be reused after every run.
Req-6.	The experiment shall be repeatable.	✓	The use of moulds makes it possible to precisely create and recreate the ice structure for every run.

10

APPLICATIONS AND RECOMMENDATIONS

The icy moon plume model designed in this study has a number of practical uses of which the foremost is to recreate a simpler (slower with smaller mass-flow) version of Enceladus' observed plumes (Section 10.1). But this study can function as the start of a larger range of experiments that could gain more insight in the physics and chemistry of icy moon plumes and everything that is connected with those plumes. It can function as a test facility for future landers with their mission located around plumes (Section 10.2), study grain growth (Section 10.3), study the effect of the boiling chamber volume 10.4, study the Europa plume sightings or test current hypotheses on larger organic molecules observed around Enceladus (Section 10.6). A final recommendation is to attempt to form a plume without a liquid ocean. Which is proposed in Section 10.7.

10.1. PLUME RECREATION

The model build during this study is meant to reproduce a plume from evaporating liquid water through a crevasse following aerodynamics. A small version of such an experiment is already performed in Chapter 6 and a large version is proposed in Chapter 7. But there are limitations. The observed mass flow and exhaust velocity on Enceladus are many times larger than the proposed mass flows and exhaust velocities in this study, even for the larger design. A mass flow of several kilograms per second is obviously not very practical to reproduce in a lab and for a prove of concept it is not necessary. But for possible future experimentations on Enceladus' E-ring it might be useful to have a larger mass flow then proposed here. Another practical limitation is the exhaust velocity. The vacuum-pumps available are not able to generate the needed pressure difference needed to obtain the observed exhaust velocity of Enceladus with the gas balast of the plume. If for a future experiment the exhaust velocity will be a crucial factor, a more efficient vacuum pump needs to be used. And finally, in Chapter 5 it was determined that the chemical differences of ammonia and natrium-chloride that influence the triple point of pure water were negligible for the designs proposed in this study. Although ammonia and natrium-chloride are among the most abundant observed in Enceladus' plumes, there are many more trace elements that have not been investigated in this study. The ocean content is a rather larger subject which can be a study on its own, but for a more precise recreation of the Enceladus plume, ocean and ices, the effect of all the observed elements on the triple point is recommended. This is related to the study of macromolecular organic molecules proposed in Section 10.6. In this study, the final experiments have been preformed with pure water. For other icy moon plumes (like Europa for example) a completely different ocean content needs to be studied and the effects on the triple point of pure water.

10.2. TEST ENVIRONMENT FOR LANDERS

The discovery of icy moon plumes has been relatively new and at the moment of writing there have not been any landings in or close to a plume to further investigate the phenomenon. It can be imagined that there will be future missions with just this goal. Landers can be designed to land in the plume crevasse or close to the vent and might even dig around. Since there are no such phenomena on Earth, testing these kind of landers is limited to crevasses in places like Antartica. These conditions are not the exact same as expected on icy moons. As mentioned in the previous section, such a laboratory set-up will not be an exact replica but having a laboratory test facility that recreates such a small version of an icy moon plume is the next best location to test future landers before sending them into outer space. An example of such a test is to test the Ice-Mole

(mentioned in Chapter 4). The biggest limitation here is the size of the set-up. The simulated surface is only about 30 cm in diameter which can only support small landers. This would either require a miniaturised version of the lander or a larger scale of the set-up. The models created in this study can be scaled up to obtain the dimensions for larger set-ups, but this would require larger versions of the equipement as well.

10.3. STUDY GRAIN GROWTH

Next to the vapour expelled by the Enceladus plumes, grains have also been observed by Cassini (as mentioned in Chapter 2.2). The three observed grain types (water rich, salt rich and organic rich) have been found in different locations and in different sizes around the Enceladus plumes. This laboratory set-up can be used simulate grain growth. It is doubtful that grains will be grown on their own in the relatively small designs proposed in this study. But the growth of grains can be studied when smaller nucleation particles of known size and composition are placed in the reservoir. The grains expelled by the laboratory plume can then be studied for their size and composition which will give insight on the growth process. For the earlier experiments proposed in this chapter, the chemical composition of the ice walls and ocean have not been of vital importance, therefore pure water could be used. But to have the best results for grain growth, the ocean and ice walls have to resemble the Enceladus ice and ocean as close as possible. As proposed by Schmidt *et al.* [6] and explained in Chapter 2.2, grain growth is partially stimulated by collisions with the walls of the crevasse during voyage from the ocean to the surface. Therefore the grains take on particles from the walls. It is therefore recommended to recreate the ice and ocean from the same liquid as the observed Enceladus plume content and therefore first perform the study proposed in Section 10.1 before studying grain growth. As mentioned above, grains grow from collisions with the walls. The designs proposed in this study have completely straight walls with the desired throat-to-vent ratio. Schmidt *et al.* [6] proposed that having very irregular walls allow for more collisions and therefore increase the grain growth. As explained in Chapter 6, naturally formed crevasses on Earth also have very irregular shaped walls. It is therefore recommended to alter the design proposed in this study to have irregular shaped walls instead of straight channels, but with the minimum and maximum openings set by the throat-to-vent ratio. It is also recommended to perform a study on the effect of the length of the channel on the grain growth. It can be imagined that a longer channel will have more grain-wall collisions and therefore larger grains even though the exit velocity is the same.

10.4. STUDY BOILING CHAMBER VOLUME

It is not entirely clear whether there are large vapour chambers present between Enceladus' ice sheet and the liquid ocean or if the ocean rises all the way to the throat of the cracks. Ingersoll and Nakajima [36] modelled these different possibilities. A next step would be to use the design proposed in this study and fill the reservoir to different levels thereby reducing the vapour chamber volume. This experiment requires the exact opposite of the design as proposed in Section 10.3: a smaller channel and a larger reservoir. The design proposed in this study has divided the length of the test chamber equally over the reservoir and channel. But a dedicated design based on the same relations presented in this study can be constructed.

10.5. STUDY EUROPA PLUME SIGHTINGS

Huybrighs [63] proposed the presence of plumes on Europa as an explanation for a reduced charged particle flux during Galileo's E12 flyby's of Europa. Vapour expelled from such an Europa plume would mix with the charge particles around Europa, which would change the local flux. A real-life recreation of a Europa plume set in an environment with artificially produced charged particles could be used to recreate the measurements from Galileo to confirm the presence of an Europa plume during that flyby. The design proposed in this study is mostly based on Enceladus' plumes but can be adapted to form Europa plumes when the content of Europa's ocean is used as a starting point for the design. The developed relations in this study are still valid. Such an experiment would however require a different layout of the vacuum chamber. Until now, every measurement stopped not too far from the surface. This experiment would require a large (low pressure) space above the vent where the plume can propagate through simulated space and mix with charge particles. To form this charged particle environment would also require an ionisation source that would be able to create these charged particles in a low pressure environment.

10.6. STUDY MACROMOLECULAR ORGANIC MOLECULE BEHAVIOUR

Postberg *et al.* [4] showed evidence that Cassini had picked up traces of macromolecular organic molecules even though the instruments of Cassini were initially not designed to observe these larger molecules. Nevertheless, the signs are there. In this same study it was proposed that these organic molecules exist in Enceladus' ocean and are transported into space with the plumes (as explained in Chapter 2). The Enceladus environment and the science equipement on Cassini will inflict damage to the organic molecules and fragment them. The fragmentation of molecules in a mass spectrometer is known, but the fragmentation of a plume is not. This set-up can assist in determining what an icy moon plume does to organic molecules and with the data obtained from Cassini, the original molecules might possibly be reverse engineered. Such an experiment would entail placing organic molecules (possibly even bacteria) inside the reservoir and determine what fragments are measured above the vent, matching these with Cassini's observations. For this version of the experiment to be as successful as possible, the exact content of the ice and liquid of the design need to match Enceladus' specifications as close as possible and therefore require the study proposed in Section 10.1. Since the plumes generated by such a laboratory set-up are not a perfect representation of the real versions, the organic molecules will not fragment the exact same as on Enceladus. However, this will allow to study and understand processes at play, and extrapolate to conditions close to Enceladus. It is recommended to perform a study on the effect of the reduced Enceladus gravity compared to Earth on the plume as well as a study on the effect of the length of the channel on the plume since both will have an effect on the fragmentation.

10.7. PLUME WITHOUT A LIQUID OCEAN

Though throughout this study the basis has been that the plume was formed by a subsurface liquid ocean and a channel leading from this ocean to the surface, it might be worth investigating if a plume can be formed without a connection to a liquid reservoir. This would assume that the needed mass flow is generated by sublimation of ice instead of evaporation of water. Although similar, such an experiment would require a redesign of the model proposed in this study. The model in this study developed a relation between evaporation and throat area. A relation between sublimation and throat area will be needed.

11

CONCLUSION

The goal of this study was to develop a design for a laboratory set-up that would be able to recreate an icy moon plume. This set-up was designed for the facilities already available at the FH Aachen University of Applied Sciences. Two icy moons with plumes were considered: Europa and Enceladus. Since Cassini provided more information on Enceladus' plumes than the information gained by telescope observations on Europa, the design focussed on Enceladus.

The design of such an Enceladus plume recreation was based on two influencing factors, the subsurface ocean and the surface ice sheet. It was hereby assumed that the plumes are caused by a crack in the surface ice leading all the way to the liquid ocean. Therefore, the mass expelled by the plume comes mostly from ocean evaporation and not from ice sublimation (at least not the largest part). The fact that this plume mechanism required a liquid ocean set limits on the temperature and pressure. The lowest temperature and pressure at which pure water can remain liquid is at $0.01^{\circ}C$ and 612 Pa. This is also the triple point of water where water can exist in liquid, solid and vapour phase as the same time. The content of Enceladus' ocean has a very minor influence on the triple point. Experiments done with low concentrations of ammonia water and similar experiments taken from literature with low sodium-chloride water concentrations showed that the triple point only varied a few degrees in temperature and a few tens of pascals in pressure. On the grand scale, the difference between a design based on pure water and small concentrations of ammonia or sodium chloride water proved to be negligible. But since this study only did preliminary tests on the ocean content's influence, the true effect of Enceladus' total ocean content on the plume requires more study.

The second influencing factor on the plume, the ice layer, drove the design. To mimic Cassini's observed plume exhaust velocity, the crack in the ice layer leading from the ocean to the surface was expected to resemble a supersonic nozzle like structure. This converging-diverging geometry allowed for the supersonic acceleration Cassini observed. Ocean water vaporised due to the low pressure and accelerated from almost no velocity to sonic velocity (Mach 1) in throat and supersonic velocity at the vent. This required a relation between the mass flow generated by evaporation and the mass flow needed in the throat and vent. This relation gave the design area's of the reservoir, throat area and vent area based on the area of the set area of the reservoir, the design Mach number and the physical characteristics of the ocean content. A smaller version of the experiment was designed, build and performed at Delft University of Technology to prove the concept and tackle practical issues before making the proposal for the larger version. The mould parts designed to create the reservoir and channel openings in the ice were made from a non-conducting material making them hard to remove when frozen. Therefore, the final design proposition included metal mould parts. Earlier versions of the smaller experiment performed in Delft proved that the reservoir froze soon after the triple point was reached. A redesign of the set-up included a heating element to keep the reservoir above freezing temperature. Although the small model proved the concept can work, the pressure obtained in vacuum chamber in Delft was not low enough to generate a pressure difference between reservoir and vent that allowed for the supersonic plume the set-up was designed for.

With this design for the set-up for the facilities in Aachen, it will be possible to first of all study if the current hypotheses on the Enceladus plume mechanism are correct. But in the future it will also be possible to study more detailed aspects of the Enceladus plume. Reverse engineering grain growth and macromolecular organic molecules will give insight on the ocean content and ice wall contribution. Varying the channel length, reservoir volume and content will show if other mechanisms can also form plumes. Lastly, the set-up could serve as a test environment for future landers.

BIBLIOGRAPHY

[1] M. Nakajima and A. P. Ingersoll, *Controlled boiling on enceladus. 1. model of the vapor-driven jets,* Icarus **272**, 309 (2016).

[2] S. K. Yeoh, T. A. Chapman, D. B. Goldstein, P. L. Varghese, and L. M. Trafton, *On understanding the physics of the enceladus south polar plume via numerical simulation,* Icarus **253**, 205 (2015).

[3] J. H. Roberts and F. Nimmo, *Near-surface heating on enceladus and the south polar thermal anomaly,* Geophysical Research Letters **35** (2008).

[4] F. Postberg, N. Khawaja, B. Abel, G. Choblet, C. r. Glein, M. S. Gudipati, B. L. Henderson, H.-W. Hsu, S. Kempf, F. Klenner, G. Moragas-Klostermeyer, B. Magee, L. Nölle, M. Perry, rené reviol, J. Schmidt, ralf Srama andFerdinand Stolz, G. tobie, M. trieloff, and J. H. Waite, *Macromolecular organic compounds from the depths of enceladus,* Nature **558**, 564 (2018).

[5] S. K. Yeoh, Z. Li, D. B. Goldstein, P. L. Varghese, D. A. Levin, and L. M. Trafton, *Constraining the enceladus plume using numerical simulation and cassini data,* Icarus **281**, 357 (2016).

[6] J. Schmidt, N. Brilliantov, F. Spahn, and S. Kempf, *Slow dust in enceladus' plume from condensation and wall collisions on tiger stripe fractures,* Nature **451**, 685 (2008).

[7] N. Khawaja, F. Postberg, F. Klenner, R. Reviol, L. Nölle, and R. Srama, *Organic compounds in ice grains from the sub-surface ocean of enceladus,* in *Extreme Habitable Worlds*, 51 (ESLAB, 2017).

[8] E. Adelstein, A. Trana, C. M. Saez, A. Shteinberg, and M. Manga, *Geyser preplay and eruption in a laboratory model with a bubble trap,* Journal of Volcanology and Geothermal Research **285**, 129 (2014).

[9] A. Toramaru and K. Maeda, *Mass and style of eruptions in experimental geysers,* Journal of Volcanology and Geothermal Research Volume 257, 1 May 2013, Pages 227-239 Journal of Volcanology and Geothermal Research Volume 257, 1 May 2013, Pages 227-239 Journal of Volcanology and Geothermal Research **257**, 227 (2013).

[10] A. Namiki, Y. Ueno, S. Hurwitz, M. Manga, C. Munoz-Saez, and F. Murphy, *An experimental study of the role of subsurface plumbing on geothermal discharge,* Geochemistry, Geophysics, Geosystems **17**, 3691 (2016).

[11] J. S. Kargel, *Ammonia-water volcanism on icy satellites: Phase relations at 1 atmosphere,* Icarus **100**, 556 (1992).

[12] M. L. Johnson and M. Nicol, *The ammonia-water phase diagram and its implications for icy satellites,* Journal of Geophysical Research **92**, 6339 (1987).

[13] J. J. Lissauer and I. de Pater, *Fundamental Planetary Science,* 3rd ed. (Cambridge University Press, 2013).

[14] J. H. Waite, W. S. Lewis, B. A. Magee, J. I. Lunine, W. B. McKinnon, C. R. Glein, O. Mousis, D. T. Young, T. Brockwell, J. Westlake, M.-J. Nguyen, B. D. Teolis, H. B. Niemann, R. L. McNutt, M. Perry, and W.-H. Ip, *Liquid water on enceladus from observations of ammonia and 40ar in the plume,* Nature **460**, 487 (2009).

[15] J. R. Spencer, J. C. Pearl, M. Segura, F. M. Flasar, A. Mamoutkine, P. Romani, B. J. Buratti, A. R. Hendrix, L. J. Spilker, and R. M. C. Lopes, *Cassini encounters enceladus: Background and the discovery of a south polar hot spot,* Science **311**, 1401 (2006).

[16] L. Roth, J. Saur, K. D. Retherford, D. F. Strobel, P. D. Feldman, M. A. McGrath, and F. Nimmo, *Transient water vapor at europa's south pole,* Science **343**, 171 (2014).

[17] J. R. Gruesbeck, D. J. Gershman, J. R. Espley, and J. E. P. Connerney, *The interplanetary magnetic field observed by juno enroute to jupiter,* Geophysical Research Letters **44**, 5936 (2017).

[18] E. S. Belenkaya, S. H. Cowley, I. I. Alexeev, V. V. Kalegaev, I. A. Pensionerov, M. S. Blokhina, and D. A. Parunakian, *Open and partially closed models of the solar wind interaction with outer planet magnetospheres: the case of saturn,* Annales Geophysicae **35**, 1293 (2017).

[19] T. Armstrong, S. Taherion, J. Manweiler, S. Krimigis, C. Paranicas, D. Mitchell, and N. Krupp, *Energeticionstrappedinsaturn'sinnermagnetosphere,* PlanetaryandSpaceScience **57**, 1723 (2009).

[20] H. Hsu, F. Postberg, Y. Sekine, T. Shibuya, S. Kempf, M. Horányi, A. Juhász, N. Altobelli, K. Suzuki, Y. Masaki, T. Kuwatani, S. Tachibana, S. Sirono, G. Moragas-Klostermeyer, and R. Srama, *Ongoing hydrothermal activities within enceladus,* Nature **519**, 207 (2015).

[21] M. Beuthe, A. Rivoldini, and A. Trinh, *Enceladus's and dione's floating ice shells supported by minimum stress isostasy,* Geophysical Research Letters **43**, 10088 (2016).

[22] O. Cadek, G. Tobie, T. V. Hoolst, M. Massé, G. Choblet, A. Lefèvre, G. Mitri, R.-M. Baland, M. Behounková, O. Bourgeois, and A. Trinh, *Enceladus's internal ocean and ice shell constrained from cassini gravity, shape, and libration data,* Geophysical Research Letters **43**, 5653 (2016).

[23] R. H. Brown, R. N. Clark, B. J. Buratti, D. P. Cruikshank, J. W. Barnes, R. M. E. Mastrapa, J. Bauer, S. Newman, T. Momary, K. H. Baines, G. Bellucci, F. Capaccioni, P. Cerroni, M. Combes, A. Coradini, P. Drossart, V. Formisano, R. Jaumann, Y. Langevin, D. L. Matson, T. B. McCord, R. M. Nelson, P. D. Nicholson, B. Sicardy, and C. Sotin, *Composition and physical properties of enceladus' surface,* Science **311**, 1425 (2006).

[24] W. M. Grundy, M. W. Buie, J. A. Stansberry, and J. R. Spencer, *Near-infrared spectra of icy outer solar system surfaces: Remote determination of h2o ice temperatures,* Icarus **142**, 536 (1999).

[25] V. F. Petrenko and R. W. Whitworth, *Physics of Ice* (Oxford: Oxford University Press, 1999).

[26] S. Vance, M. Bouffard, M. Choukroun, and C. Sotin, *Ganymede's internal structure including thermodynamics of magnesium sulfate oceand in contact with ice,* Planetary and Space Science **96**, 62 (2014).

[27] R. M. Mastrapa and R. H. Brown, *Ion irradiation of crystalline h2o–ice: Effect on the 1.65-μm band,* Icarus **183**, 207 (2006).

[28] A. Coustenis, T. Tokano, M. Burger, T. Cassidy, R. Lopes, R. Lorenz, K. Retherford, and G. Schubert, *Atmospheric/exospheric characteristics of icy satellites,* Space Science Reviews **153**, 155 (2010).

[29] J. H. Waite, M. R. Combi, W.-H. Ip, T. E. Cravens, R. L. McNutt, W. Kasprzak, R. Yelle, J. Luhmann, H. Niemann, D. Gell, B. Magee, G. Fletcher, J. Lunine, and W.-L. Tseng, *Cassini ion and neutral mass spectrometer: Enceladus plume composition and structure,* Science **311**, 1419 (2005).

[30] E. Drabek-Maunder, J. Greaves, H. J. Fraser, D. L. Clements, and L.-N. Alconcel, *Ground-based detection of a cloud of methanol from enceladus: when is a biomarker not a biomarker?* International Journal of Astrobiology (2017).

[31] M. H. Burger, E. C. S. Jr., R. E. Johnson, H. T. Smith, O. J. Tucker, and V. I. Shematovich, *Understanding the escape of water from enceladus,* Journal of Geophysical Research **112** (2007).

[32] F. Tian, A. Stewart, O. B. Toon, K. W. Larsen, and L. W. Esposito, *Monte carlo simulations of the water vapor plumes on enceladus,* Icarus **188**, 154 (2007).

[33] Y. Dong, T. W. Hill, B. D. Teolis, B. A. Magee, and J. H. Waite, *The water vapor plumes of enceladus,* Journal of Geophysical Research **116** (2011).

[34] O. J. Tucker, M. R. Combi, and V. M. Tenishev, *2d models of gas flow and ice grain acceleration in enceladus' vents using dsmc methods,* Icarus **257**, 362 (2015).

[35] J. Saur, N. Schilling, F. Neubauer, D. Strobel, S. Simon, M. Dougherty, C. Russell, and R. Pappalardo, *Evidence for temporal variability of enceladus' gas jets: Modeling of cassini observations,* Geophysical Research Letters **35** (2008).

[36] A. P. Ingersoll and M. Nakajima, *Controlled boiling on enceladus. 2. model of the liquid-filled cracks,* Icarus **272**, 319 (2016).

[37] J. D. Anderson, *Fundamentals of Aerodynamics*, 5th ed. (McGraw-Hill, 2011).

[38] Y. Dong, T. W. Hill, and S.-Y. Ye, *Characteristics of ice grains in the enceladus plume from cassini observations,* Journal of Geophysical Research: Space Physics **120**, 915 (2015).

[39] L. Anderson, J. Anderegg, and J. Lawler, *Model geysers,* Nature **65**, 247 (1902).

[40] R. T. Pappalardo, W. B. McKinnon, and K. K. Khurana, *Europa* (University of Arizona Press, 2009).

[41] A. Vorburger and P. Wurz, *Europa's ice-related atmosphere: The sputter contribution,* Icarus **311**, 135 (2018).

[42] E. Congiu, H. Chaabouni, C. Laffon, P. Parent, S. Baouche, and F. Dulieu, *Efficient surface formation route of interstellar hydroxylamine through no hydrogenation. i. the submonolayer regime on interstellar relevant substrates,* The Journal of Chemical Physics **137** (2012).

[43] M. Accolla, E. Congiu, G. Manicò, F. Dulieu, H. Chaabouni, J. L. Lemaire, and V. Pirronello, *Morphology of the solid water synthesized through the pathway d + o2 studied by the sensitive tpd technique,* Monthly Notices of the Royal Astronomical Society **429**, 3200 (2013).

[44] J. Lemaire, G. Vidaly, S. Baouche, M. Chehrouri, H. Chaabouni, and H. Mokrane, *Competing mechanisms of molecular hydrogen formation in conditions relevant to the interstellar medium,* The Astrophysical Journal Letters **725** (2010).

[45] Z. Dohnálek, G. A. Kimmel, P. Ayotte, R. S. Smith, and B. D. Kay, *The deposition angle-dependent density of amorphous solid water films,* Journal of Chemical Physics **118**, 364 (2003).

[46] T. L. Hudson, O. Aharonson, and N. Schorghofer, *Laboratory experiments and models of diffusive emplacement of ground ice on mars,* Journal of Geophysical Research **114** (2009).

[47] M. Siegler, O. Aharonson, E. Carey, M. Choukroun, T. Hudson, N. Schorghofer, and S. Xu, *Measurements of thermal properties of icy mars regolith analogs,* Journal of Geophysical Research **117** (2012).

[48] F. F. Rupert, *The solid hydrates of ammonia,* Journal of American Chemical Society **31**, 866 (1909).

[49] T. Spohn and G. Schubert, *Oceans in the ice galilean satellites of jupiter?* Icarus **161**, 456 (2003).

[50] O. Grasset and C. Sotin, *The cooling rate of a liquid shell in titan's interior,* Icarus **123**, 101 (1996).

[51] J. Leliwa-Kopystyński, M. Maruyama, and T. Nakajima, *The water-ammonia phase diagram up to 300 mpa: Application to icy satellites,* Icarus **159**, 518 (2002).

[52] F. Postberg, J. Schmidt, J. Hillier, S. Kempf, and R. Srama, *A salt-water reservoir as the source of a compositionally stratified plume on enceladus,* Nature **474** (2015).

[53] M. W. Zemansky and R. H. Dittman, *Heat and Thermodynamics*, 7th ed. (McGraw-Hill, 1997).

[54] K. M. Cuffey and W. S. B. Paterson, *The Physics of Glaciers*, 4th ed. (Elsevier, Inc., 2010).

[55] N. Doyle, ed., *Glaciers* (Nova Science Publishers, Incorporated, 2016).

[56] R. L. Hooke, *Principles of Glacier Mechanics*, 2nd ed. (Cambridge University Press, 2005).

[57] C. Porco, D. DiNino, and F. Nimmo, *How the geysers, tidal stresses, and thermal emission across the south polar terrain of enceladus are related,* The Astronomical Journal **148** (2014).

[58] F. Nimmo, C. Porco, and C. Mitchell, *Tidally modulated eruptions on enceladus: Cassini iss observations and models,* The Astronomical Journal **148** (2014).

[59] F. M. White, *Fluid mechanics*, 7th ed. (McGraw Hill, 2011).

[60] P. Reiss, *A combined model of heat and mass transfer for the in situ extraction of volatile water from lunar regolith,* Icarus **306**, 1 (2018).

[61] W. Wang, Q. C. Guo, W. Lu, Y. Feng, and W. Na, *A generalized simple model for predicting frost growth on cold flat plate,* International Journal of Refrigeration **35**, 475 (2012).

[62] P. H. Oosthuizen and W. E. Carscallen, *Introduction to Compressible Fluid Flow*, 2nd ed. (Taylor & Francis, 2013).

[63] H. Huybrighs, *A search for signatures of Europa's atmosphere and plumes in Galileo charged particle data*, Ph.D. thesis, Technischen Universität Carolo-Wilhelmina zu Braunschweig (2018).